TRACER GAS MAPPING OF BEVERAGE CART WAKE IN A TWIN AISLE AIRCRAFT
CABIN SIMULATION CHAMBER

by

ANDREW TRISTAN TRUPKA

B.S., Kansas State University, 2009

A THESIS

submitted in partial fulfillment of the requirements for the degree

MASTER OF SCIENCE

Department of Mechanical and Nuclear Engineering
College of Engineering

KANSAS STATE UNIVERSITY
Manhattan, Kansas

2011

Approved by: Approved by:

Co-Major Professor   Co-Major Professor
Dr. Mohammad H. Hosni   Dr. Mohammad H. Hosni

Copyright

ANDREW TRISTAN TRUPKA

2011

Abstract

In 2010, over 786 million passengers flew on commercial flights in the United States according to the Bureau of Transportation Statistics (2011). With the average flight length over 1300 miles for domestic flights, this amounts to billions of hours spent aboard airliners by passengers each year. During these flights, diseases and other harmful contaminates, some malicious, can spread throughout aircraft cabins, harming passengers. Aircraft ventilation systems are designed to remove these harmful contaminates as quickly as possible to minimize spread in cabin air. Disruptions to the design airflow pattern can hinder the effectiveness of contamination removal efforts. A common form of this airflow disruption is longitudinal air movement through cabin aisles. To examine the effect of contaminate transport down aircraft aisles by a moving body, a motorized beverage cart is past by a contamination source as it traverses the length of the cabin aisle.

An experimental study is performed in a mockup Boeing 767 cabin section consisting of eleven rows with seven seats per row. Carbon Dioxide (CO_2) tracer gas is injected at a constant flow rate at a location of interest until concentrations in the cabin reach steady state. Ventilation equipment and flow rates representative of an actual aircraft are used for all experiments. Seats in the mockup are occupied by thermal manikins to simulate passenger heat load. A motorized beverage cart traverses the length of the cabin aisle passing by the injection location. The concentrations of tracer gas displaced by the cart are measured at locations throughout the cabin. Comparing these measurements to baseline readings taken with no cart movement, a map of the degree to which contaminant transport is affected by the beverage cart is calculated.

The cabin mockup is supplied by 100% outdoor air through actual Boeing supply ductwork and linear diffusers along the cabin length above the aisles. The CO_2 level is measured in the inlet air, measurement locations in the cabin, and exhaust air using nondispersive infrared (NDIR) sensors. Measured results are reported for all (54) seat locations downstream of the cart traverse/injection location for an injection location near the rear of the cabin. Analogous measurements are also conducted examining the effect of variations in cart speed and modified injection location.

It was found the beverage cart movement had an effect of up to a 35% increase in tracer gas concentration relative to the local steady state concentration for several seat locations adjacent to the aisle. This increased concentration continued for only a few minutes in all cases, but was generally less than the steady state exposure one row closer to the injection location. Moving in the lateral direction away from the aisle, the variance in tracer gas concentration due to the cart movement diminished quickly. The significance of increased concentration for such short periods of time in comparison to the length of actual commercial flights may require further biological analysis. The data showed general tracer gas concentration increases due to cart movement in a small section of the cabin mockup which could warrant further analysis, but increases were generally insignificant when considering entire flight contamination exposure levels.

Table of Contents

List of Figures

List of Tables

Acknowledgements

I would like to thank my friends and family for their continued support throughout the pursuit of my educational endeavors. Their support has made my research and this thesis possible. I would also like to thank professors who have directed through my graduate degree program. In particular, the guidance of Dr. Hosni, Dr. Jones, and Dr. Fenton has helped shape my research and its presentation in this thesis.

Chapter 1 - Introduction

Aircraft air quality standards are an issue which affects the health of the world on a daily basis. Not only are there concerns regarding contagious disease transmission during flights, there is also the possibility of intentional dispersal of biological or other types of agents by passengers with malicious intent. To eliminate risks posed to flyers, aircraft ventilation systems need to be able to properly eradicate these air contaminants quickly.

To address air quality concerns, the Air Transportation Center of Excellence for Airliner Cabin Environmental Research (ACER) team was formed, in part, to investigate transport phenomena in aircraft cabins. The scope of the ACER project includes ozone and pesticide sampling and prediction, prediction and sampling of combustion products in cabin air, need and location of air quality sensors, delivery of decontaminating agents, as well as the prediction of transmission paths for respirable diseases (Air Transportation Center of Excellence (CoE) for Airliner Cabin Environment Research (ACER), 2007). Experimental research is required to verify and aide development of computational fluid dynamic (CFD) models which can accurately predict the airflow patterns seen in real-world aircraft. In the particular twin aisle cabin mockup used in this study, experimental work has already been completed examining general dispersion of tracer gas and particulates (Lebbin, 2006), longitudinal particulate dispersion (Beneke, 2010), and optimal particulate sensor location (Shehadi, 2010).

A major concern with CFD models is the ability to predict air movement throughout the aircraft cabin when the design airflow pattern is disturbed by moving objects. The research at hand delves into this matter by monitoring the effects of a moving beverage cart on a gaseous contaminate. To simulate the gaseous contaminate, carbon dioxide tracer gas is injected at a location of interest in the cabin. The tracer gas concentration is then monitored throughout the cabin before, during and after a beverage cart traverses along a cabin aisle, passing near the injection location.

Chapter 2 - Background and Literature Review

With so many passengers traveling via commercial airliners each day, and thus being together in a confined space for an extended period of time, the quality of the air the passengers are sharing becomes a major health concern. Contaminates in the cabin air encompass particulate, chemical, and biological forms. Any of these contaminates could arise from unclean outside air, equipment malfunction (engine oil in bleed air used for cabin pressurization), malicious intent, or emanate naturally from infected passengers. To safeguard passengers, regulations have been made to control contamination levels.

2.1 Aircraft Air Quality Standards

The Federal Aviation Administration (FAA) regulates air quality standards for flights in the United States. These standards encompass many aspects of cabin air including temperature and pressure, as well as specific contaminate levels (Zhang & Sun, 2005). It addition, other factors, such as relative humidity of cabin air and unregulated contaminate levels, are important to passenger safety and comfort.

2.1.1 Temperature, Pressure, and Humidity

According the FAA standards, the temperature of the aircraft cabin must remain in the range 67-73 °F (19.5-23 °C). Additionally, the temperature cannot vary more than 5 °F (2.8 °C) between zones of the cabin (O'Donnell A., 1991).

Section 25.841 of the FAA's Code of Federal Regulations requires a minimum cabin pressure equivalent to atmospheric pressure at 8000 ft altitude (2440 m). Additionally, in the event of any foreseeable equipment failure, the minimum altitude pressure is 15,000 ft (4570 m). This 8,000 ft altitude pressure is equivalent to 75.2kPa.

A common complaint air travelers have is the dryness of the cabin air. This can be attributed to several factors regarding the aircraft air handling system, but is primarily a function of the drier air at altitude due to the temperature gradient present throughout the Earth's atmosphere

(Shehadi, 2010). Airlines prefer low humidity levels to prevent corrosion and the growth of bacteria on cabin surfaces.

2.1.2 Ventilation & Contaminates

Ventilation rates in aircraft are controlled by several factors including occupant and contamination levels. Section 25.831 of the FAA regulations requires crew compartments of the cabin to receive 10 cfm (5 L/s) of fresh air per person. The regulation also states "Crew and passenger compartment air must be free from harmful or hazardous gases or vapors," specifically limiting contamination levels to 50 ppm CO and CO_2 to 3% by volume. Section 25.832 limits the concentration of ozone to 0.25 ppm by volume, sea level equivalent, at any instant the aircraft is above 32,000 ft (9750 m) and 0.10 ppm average for any three hour interval above 27,000 ft (8230 m). Amendment 25-87 requires, in case of any probable failure, a ventilation rate of 0.55 lb/min (0.25 kg/min) fresh air per occupant. This is equal to about 10 cfm at 8,000 ft (ASHRAE, 2007).

It is important to note these ventilation standards only account for fresh (outside) air. Beginning in the 1980's, aircraft were equipped with recirculation systems to save energy used conditioning outside air. Many aircraft double the ventilation rate to 20 cfm (10 L/s) per person but only use 50% fresh air. This alleviates concerns with humidity levels dropping too low when using only outside air, but creates a new issue of cleaning air between cabin circulation cycles. Humidity can be controlled in this manner because the majority of humidity in cabin air emanates from passengers onboard. To handle air cleaning, HEPA and other specialty filters are installed in the air recirculation systems. (Lebbin, 2006)

2.2 Design Airflow

The design airflow pattern for a twin aisle aircraft is quite simple. Two linear slot diffusers run the length of the cabin above both periphery of the middle bank of seats. The air then circulates laterally across the cabin and exits through the cabin wall near the floor. Figure 2.1 shows a cross section of the flow pattern in the lateral direction. This pattern is continuous throughout the length of the cabin with little flow in the longitudinal direction. Longitudinal airflow is

3

minimized to localize any spread of odors or disease. Any contaminates emanating from an infected passenger, in theory, would only be shared within one row fore and aft of the passenger.
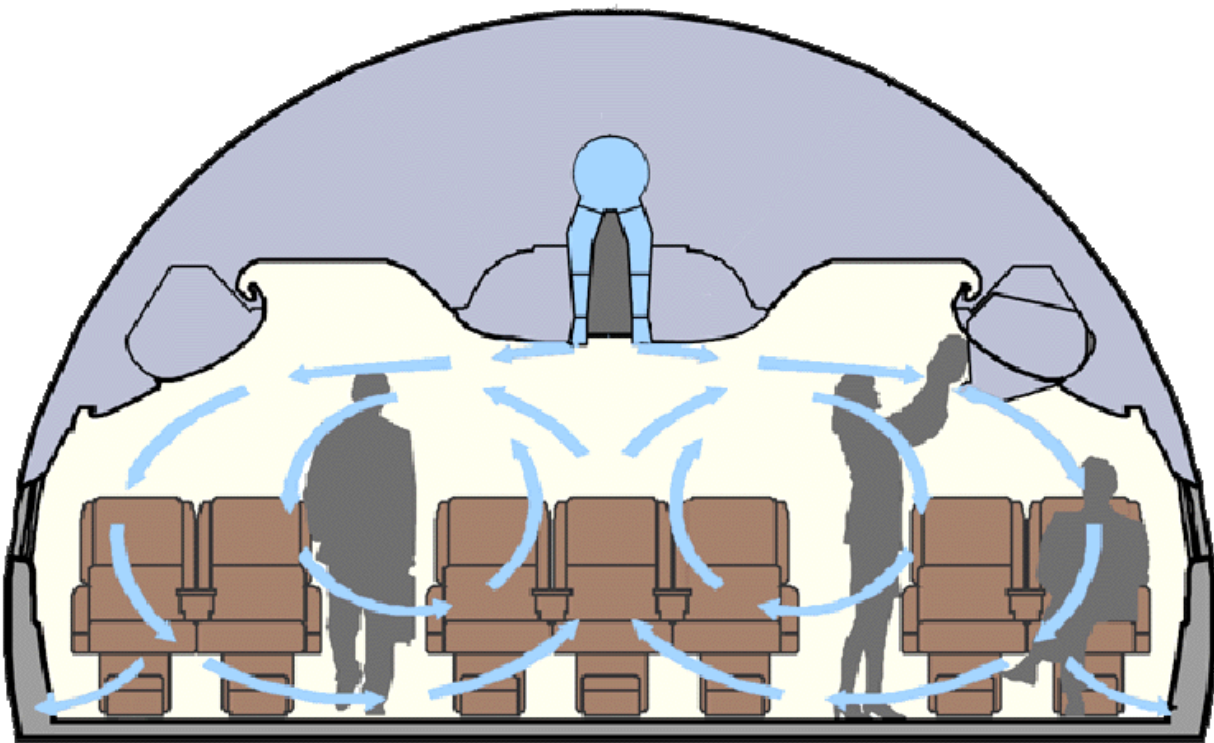
Figure 2.1 Design Airflow in Lateral Direction (Boeing)

2.3 Tracer Gas and Sampling Methods

To simulate the dispersion of a gaseous contaminate in the aircraft cabin, a tracer gas needed to be introduced and its concentration measured throughout the cabin during normal ventilation. An ideal tracer gas would be easy to measure accurately, nonhazardous, abundantly available, and mix well with the cabin supply air. Carbon dioxide (CO_2) was chosen as it exhibits these qualities reasonably well.

2.3.1 CO_2 as a Tracer Gas

Carbon dioxide is commonly used in tracing applications primarily because it is easy to detect due to its large molecule size. It is readily abundant on industrial levels and is, therefore, inexpensive. This brings rise to the first caveat; CO_2 is naturally present at measurable levels in

the Earth's atmosphere. Since atmospheric air is delivered to the cabin during testing, this natural occurring level needs to be measured and negated from any tracer gas readings. The background CO_2 level caused several issues throughout experimentation, which are further discussed in Appendix A.

An additional concern with using CO_2 as a tracer gas is that it is potentially harmful to humans in high enough concentrations. Exposure to concentrations of 7 to 10% CO_2 by volume can cause unconsciousness within a few minutes (United States Environmental Protection Agency, 2000). To alleviate safety concerns, a CellarSafe CS100 CO_2 detector/alarm was installed in the cabin mockup enclosure. If concentrations reach an unsafe level, an alarm sounds. Additionally, the alarm triggers a "GAS IN USE" warning light when concentrations of CO_2 reach levels higher than atmospheric. This warns all laboratory occupants that tracer gas experiments are underway and to use caution when in and around the aircraft cabin mockup.

2.3.2 NDIR Sensors

To measure the levels of tracer CO_2, non-dispersive infrared spectrometers were chosen for their relative low cost and stable measurements. NDIR sensors function on the Lambert-Beer law which states the absorption of infrared light by a gas is directly proportional to its concentration.

To apply this principle, NDIR sensors pass the gas sample through a chamber of known distance with a filtered light source on one end and light detector on the other. The infrared light first passes through a filter to ensure only a particular wavelength, corresponding to the molecule size of gas being sampled, is transmitted into the chamber. The infrared sensor detects the amount of light which passes completely through the chamber. Thus, the amount of light absorbed by the gas is known and the sample concentration can be found using the Lambert-Beer law. The molecule size of CO_2 allows this process to execute accurately for concentrations ranging from 100 ppm to 100%. (Lebbin, 2006)

In addition to working well with large CO_2 molecules, NDIR sensor output is highly linear with sample concentration. This allows instruments to be calibrated in-house using simple linear regression. NDIR sensors are also relatively stable over long periods of time in comparison to other gas concentration sampling methods. NDIR sensors come in an abundance of

measurement ranges so they can be fine-tuned to the application at hand to produce the most accurate results.

Chapter 3 - Experimental Setup

The aircraft cabin mockup is located in a laboratory facility in Manhattan, KS. The cabin mockup itself is completely enclosed in a 7.4 by 9.8 by 4.9 m enclosure so all inlet and exhaust air can be properly sampled for tracer gas work. Figure 3.1 shows the outer cabin enclosure with duct routing noted. The cabin floor is raised 1.2 m off the floor so equipment can be placed underneath.

Inside the outer enclosure on either side of the experimental chamber, there are hallways which allow access to the outside of the cabin walls as well as house equipment and instrumentation. This void, including hallways and areas above and below the mockup chamber, serve as an exhaust air plenum for the cabin. Once exhausted from the cabin mockup, air is pulled from the plenum through the fans, noted in Figure 3.1, to acquire an exit CO_2 concentration for mass balance purposes.

Figure 3.1 Cabin Mockup Enclosure (Beneke, 2010)

3.1 Airliner Cabin

The experimental cabin is a mockup of 11 rows of a Boeing 767 aircraft cabin. The twin aisle configuration houses seats in a 2-3-2 configuration for a total of 77 seats. Each seat is equipped with a Rubie's Costume Company model number 1724 inflatable manikin. Each manikin has 25 m of Omega TFCY-015 thermocouple wire connected to 115 V AC power affixed to it. Each manikin generates 102 watts of thermal energy or the equivalent thermal output of a seated adult at rest (ASHRAE, 2005). A non-heated manikin of identical model is attached to the moving beverage cart and used to simulate a flight attendant. Approximate dimensions of the standing manikin attached to the beverage cart are shown later in this section in Figure 3.9. Power to the manikins can be controlled manually, but safety measures, including a pressure switch in the supply ductwork and a thermostat attached to the rear wall of the cabin, are also installed. These will interrupt the power to the manikins via a relay if the supply airflow to the cabin is too low, or the temperature in the cabin becomes too high. Figure 3.2 shows the interior of the cabin with the beverage cart and service manikin in the background.

Figure 3.2 Cabin Mockup

The cabin mockup is constructed of plywood decking and formed sheet aluminum walls and ceiling. Figure 3.3 depicts the plywood ribs, which support the aluminum walls and ceiling. To simulate a real aircraft cabin ventilation system, the walls terminate about 180 mm above the floor to allow air to exhaust from the chamber. Also seen in the figure, but not used in this phase of experimentation, are water jackets used to control the temperature of the cabin walls.

Figure 3.3 Cabin Wall Supporting Ribs and Exhaust Gaps

3.1.1 Cabin Dimensions

Figure 3.4 shows dimensions of the aircraft cabin mockup in plan view including locations of hallways, doors, and cabin seats. Also noted are the locations of several pieces of equipment in the hallways surrounding the chamber. The seat "columns" (A – G) and "rows" (1 – 11) are used to refer to specific seat locations throughout this thesis.
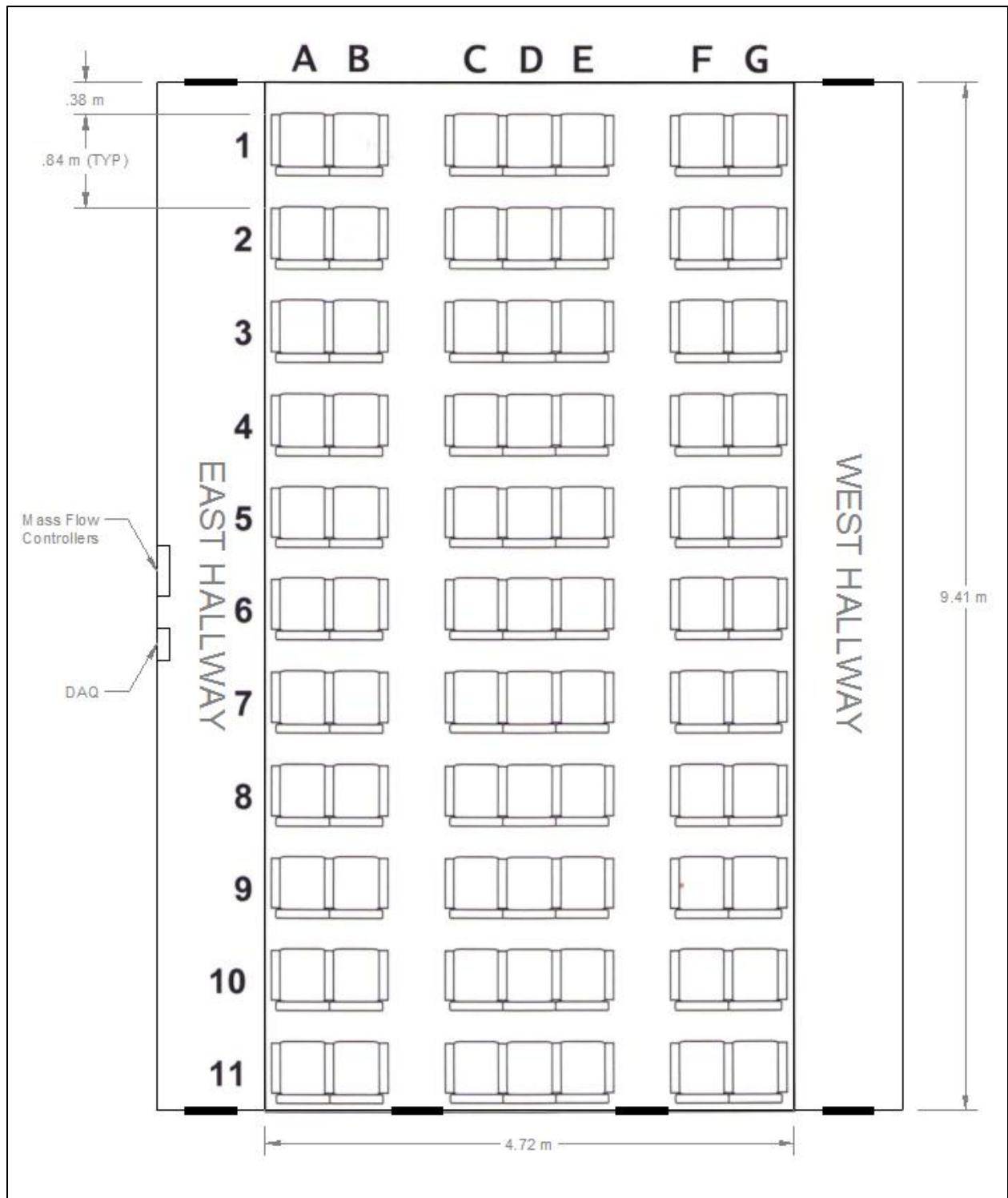
Figure 3.4 Cabin Plan View

Dimensions of the cabin cross section are shown in Figure 3.5. A more detailed mathematical model of the approximation of the cabin wall cross sectional shape can be found in (Lebbin, 2006).
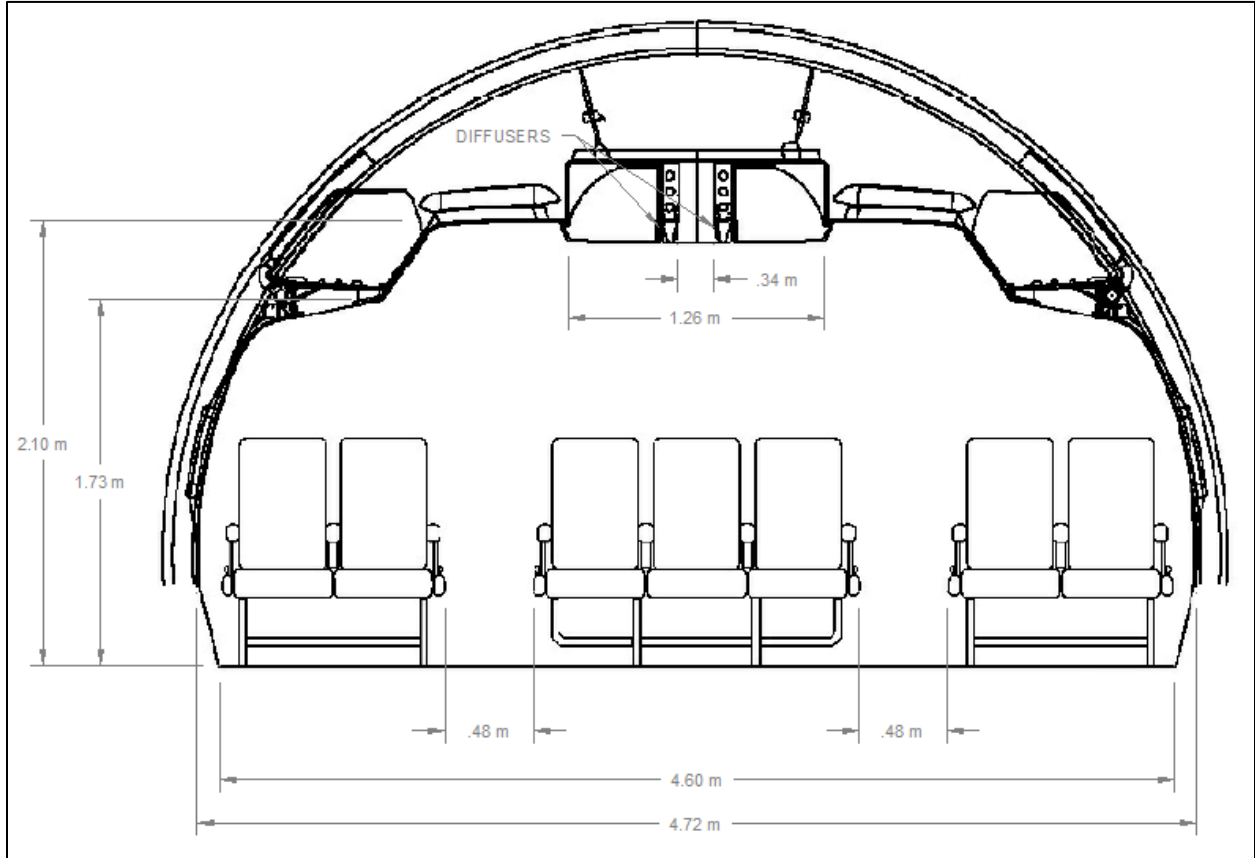
Figure 3.5 Cabin Cross Section

3.1.2 Seat Dimensions

The seats used in the mockup cabin are actual seats form a Boeing 767 aircraft. The seats are mounted in the commercial economy class 2-3-2 arrangement. Figure 3.6 and Figure 3.7 show the dimensions of double and triple seat configurations, respectively. Figure 3.8 shows dimensions of the profile view typical to both the double and triple seat configurations.
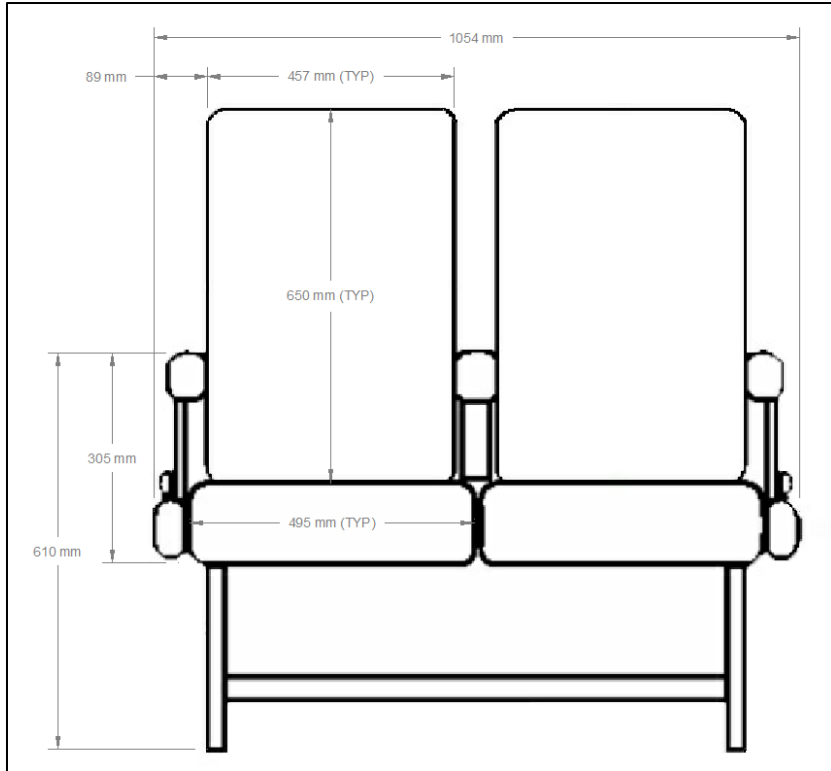
Figure 3.6 Double Seat Dimensions
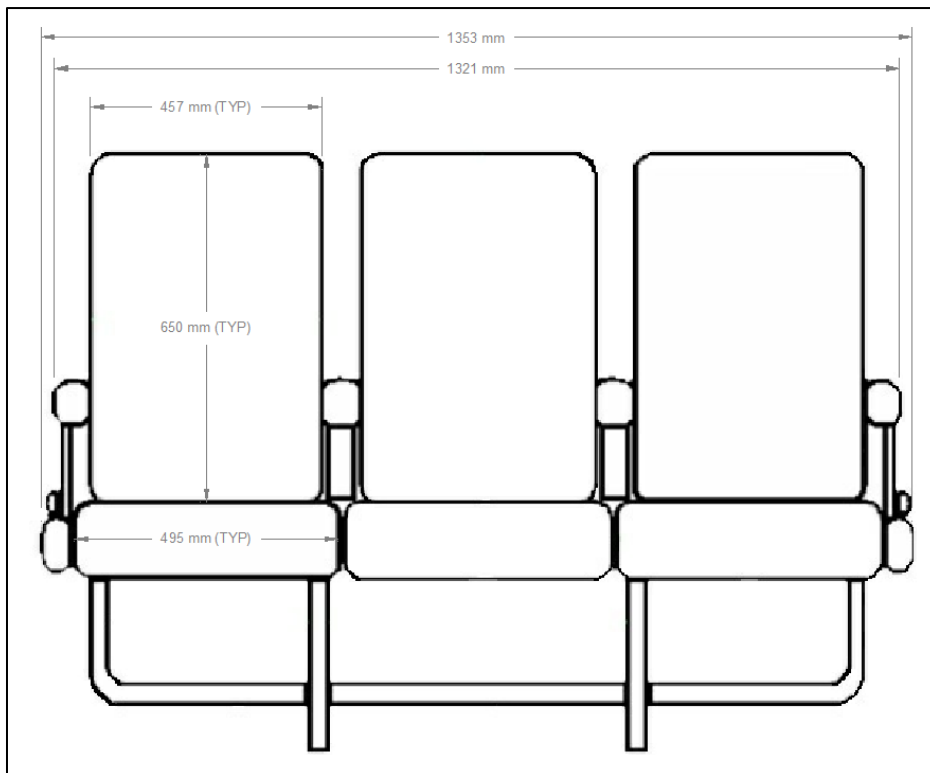
Figure 3.7 Triple Seat Dimensions
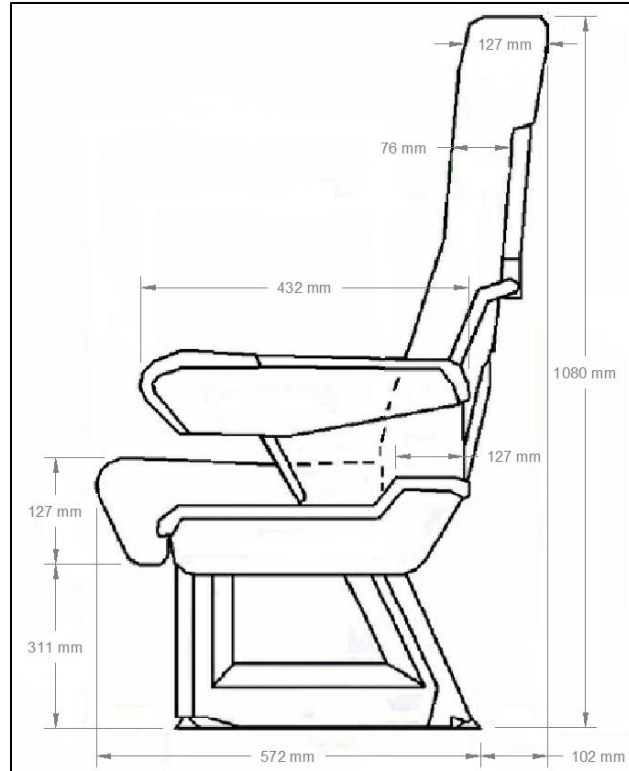
Figure 3.8 Seat Profile Dimensions

3.1.3 Beverage Cart

The west aisle of the cabin is equipped with a moving beverage cart and manikin. The manikin was attached to the south end of the cart during all experimental testing to simulate real world actions as well as maximize any "carry" of contaminated air the cart would induce. The cart is propelled by a Baldor 0.16 horsepower 3-phase motor. The use of an Altivar 31 variable frequency drive (VFD) allows the cart to operate in forward and reverse at variable speeds.

Figure 3.9 shows the beverage cart with attached manikin, highlighting notable dimensions (in mm). The plug protruding from under the cart toward the center of the side panel is connected to the 3-phase power cable. To alleviate interference issues with the wheels of the cart and the power cable, guards were added to the corners to keep the cable from going under the cart.

The cart is constructed with an aluminum angle frame and skinned with galvanized sheet metal. The bottom of the cart is enclosed with sheet vinyl and all seams were sealed with duct tape to prevent any air circulation from the motor fan affecting cabin airflow patterns.

13
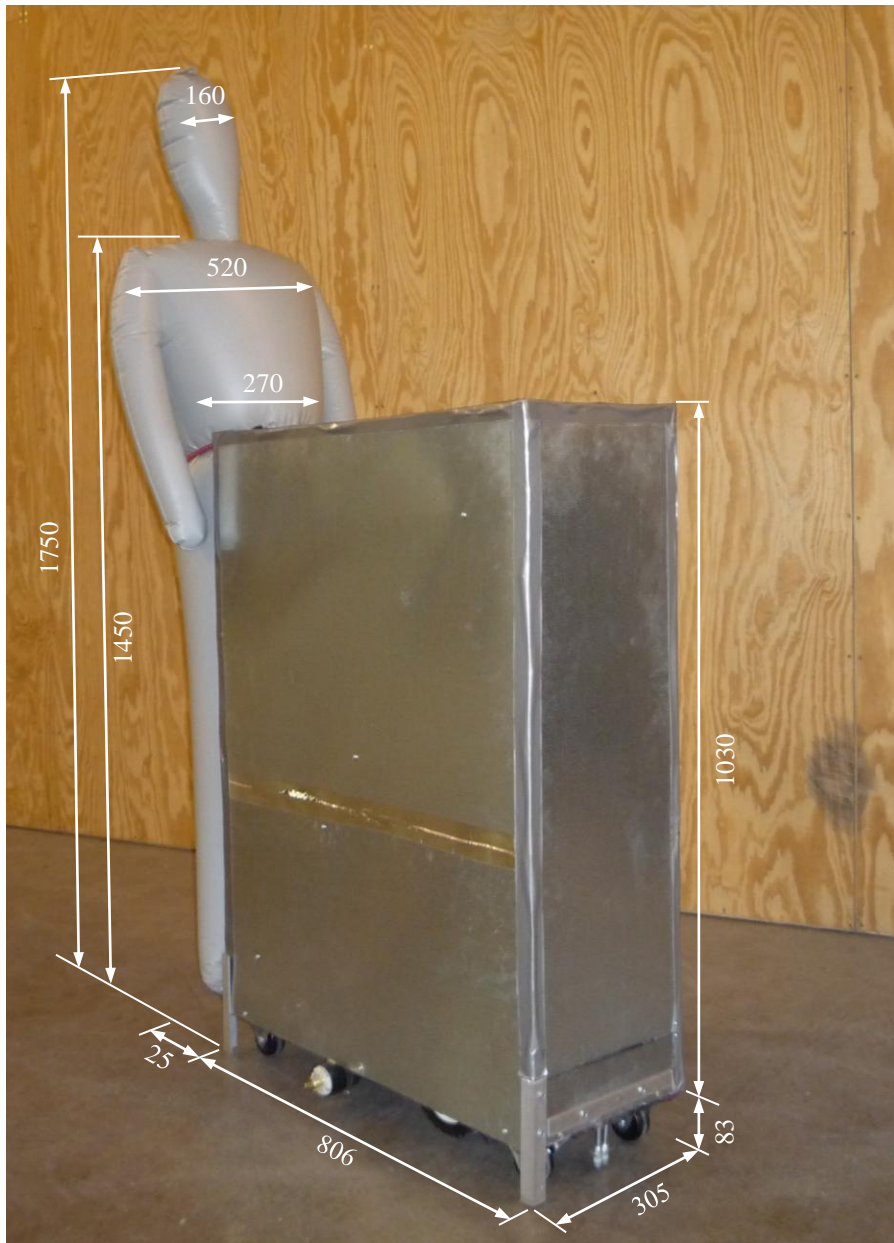
Figure 3.9 Beverage Cart

3.1.3.1 Movement Locations

The beverage cart is propelled down the center of west aisle of the cabin along an aluminum angle guiderail. Position sensors at either end of this guiderail sense the presence of the cart and

initiate a motor-braking procedure by the VFD. Figure 3.10 highlights the location of the guiderail and position sensors. The cart was always positioned with the manikin towards the front of the cabin. The traverse toward the front of the cabin was stopped short of the wall to minimize the effect of contamination being pushed perpendicular to the cart movement along the front wall of the cabin. The length of traverse toward the rear of the cabin was maximized so the cart could completely come up to speed by the time the injection location was reached.
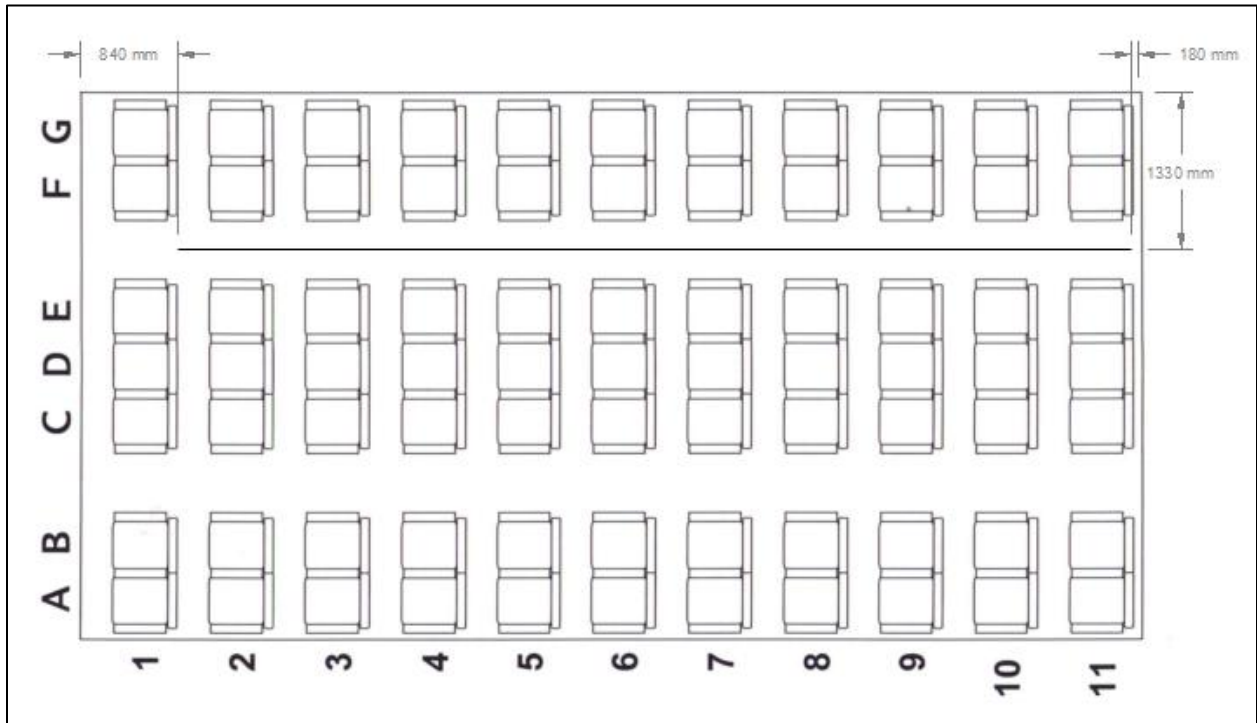
Figure 3.10 Cart Movement Locations

3.1.3.2 Control Program

The cart motor VFD is computer controlled through a secondary LabVIEW program which integrates with the main tracer gas injection control and data acquisition program. Since the cart control program is run on a separate computer than the main data acquisition program, Transmission Control Protocol (TCP) was used to synchronize the programs between computers. A message is sent from the main data acquisition program to the cart control program to initiate cart movement and a reply assuring the beverage cart reached its destination is returned.

15

Figure 3.11 shows a screenshot of the cart control LabVIEW program. The program has user inputs of cart speed, initial delay, and intermediate delay. The initial delay is the time (measured in seconds) before the cart moves from the rear of the cabin, past the injection location, to the front of the cabin. The intermediate delay is the time the cart spends at the front of the cabin waiting for tracer gas measurements to be taken. An additional steady state delay is calculated from information received from the main data acquisition program. This delay is only utilized on the initial cart movement per experimentation cycle and is associated with the time the cabin requires to reach a steady state concentration of tracer gas. This procedure is fully outlined in Chapter 4 - .
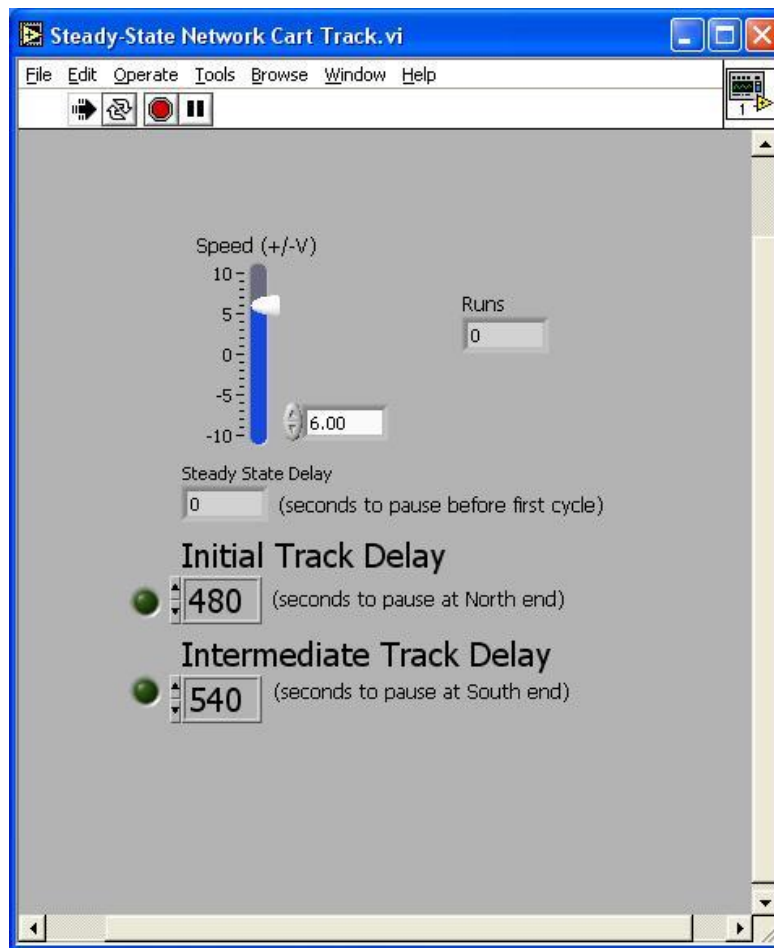
Figure 3.11 Cart Control Program

The speed of the cart is controlled by sending a signal of -10 to 10 V to the cart VFD. Negative voltage signifies operating the motor in reverse. The VFD multiplies the control signal by six to

calculate the drive frequency applied to the 3-phase motor. Hence, 0 to 60 Hz can be applied to the motor in forward or reverse orientation.

3.2 Air Supply System

The mockup cabin is supplied 661 L/s outdoor air at 15.6 ± 0.3 °C. The air is brought into the facility and conditioned before entering the cabin ductwork. The 406 mm supply duct containing conditioned air is mated to ductwork out of an actual Boeing 767 once inside the mockup enclosure. Figure 3.1 shows the supply ductwork entering the cabin enclosure just before it is mated to the Boeing ductwork. Figure 3.12 shows the Boeing ductwork, in the enclosure above the cabin mockup, supplying the linear diffusers in the cabin. Flexible hoses mate the supply duct to the diffusers as seen in Figure 3.13. The diffusers are also noted in an interior view of the mockup in Figure 3.2.

Figure 3.12 Boeing Supply Duct   **Figure 3.13 Diffuser Connection**

3.2.1 Conditioning System

The conditioning system consists of a supply fan, pre-heating subsystem, cooling subsystem, and electric heater. The pre-heating or cooling subsystems are used, depending on outdoor air conditions, to precondition the air before the electric heater fine tunes to the specified temperature. Figure 3.14 shows a schematic of these systems and accompanying Table 3.1

describes each element. The primary loop operates regardless of outdoor air conditions to transfer heat between either the heating or cooling loop and the supply air.
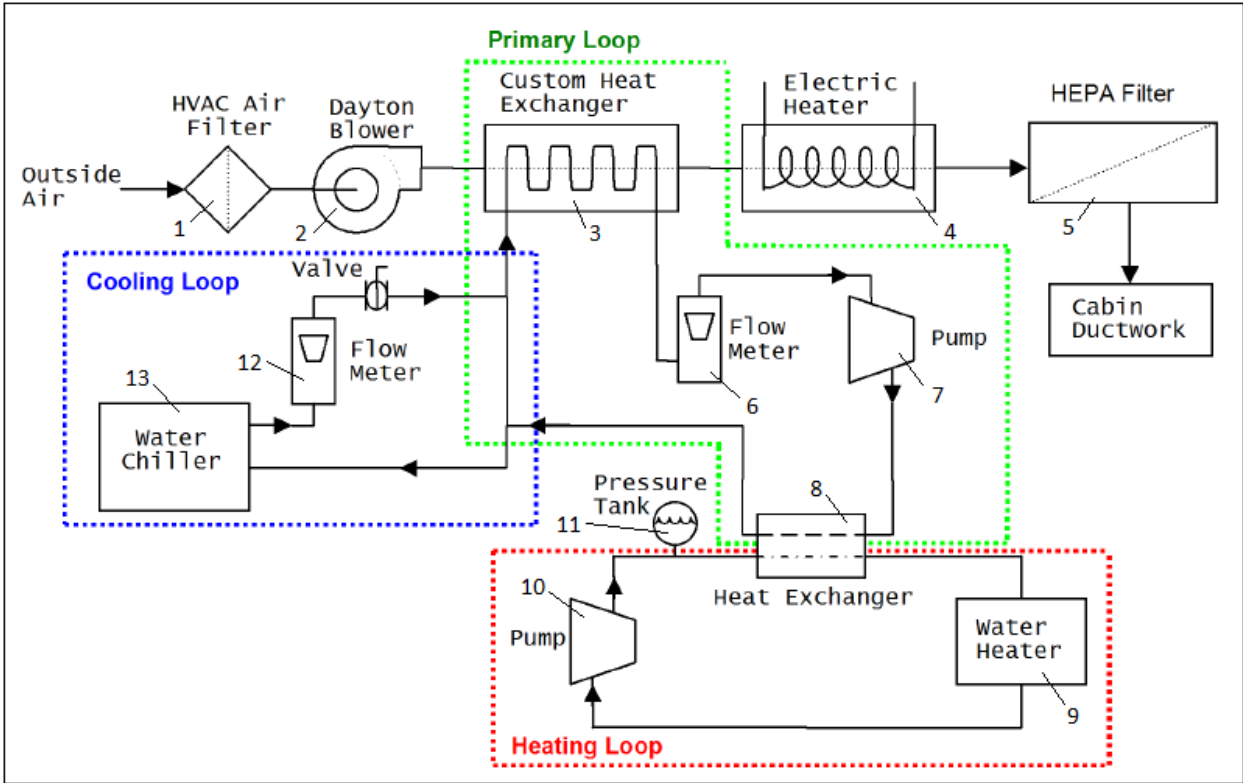
Figure 3.14 Conditioning System Schematic (Beneke, 2010)

Table 3.1 Conditioning System Components

No.	Item	Model	Notes
1	Air Filters	Ace 2025134	20"x25"(2 filters in parallel)
2	Fan	12 ¼" Dayton Blower	Yaskawa GPD315/V7 VFD
3	Heat Exchanger	Custom 0.6 x 0.6 m	
4	Electric Heater	AccuTherm DLG-9-3	240 V, 3 ph., 9 kW
5	HEPA Filter	Custom 1.1 m^2	99.97% to 0.3μm efficiency
6	Flow Meter	Omega FL7204	
7	Pump	Marathon CQM 56C34D212OF P	120 V, ¾ HP
8	Heat Exchanger	Alfa Laval CB27-18H T06	
9	Water Heater	Rheem GT-199PV-N-1	19,000 - 199,900 BTU
10	Pump	FHP C4T34DC35A	Yaskawa GPD205-1001 VFD
11	Pressure Tank	Dayton 4MY57	6.5 gal @ 30 psi
12	Flow Meter	King 7205023133W	
13	Water Chiller	AccuChiller LQ2R15	PV-B311 condensing coils

Figure 3.15 shows the major components of air supply system. The only major component which cannot be seen is the natural gas water heater located on the other side of the laboratory. The hot water is pumped through pipes running under the walkway and chiller from the water heater to a heat exchanger connecting to the primary loop as seen in the foreground of Figure 3.15.
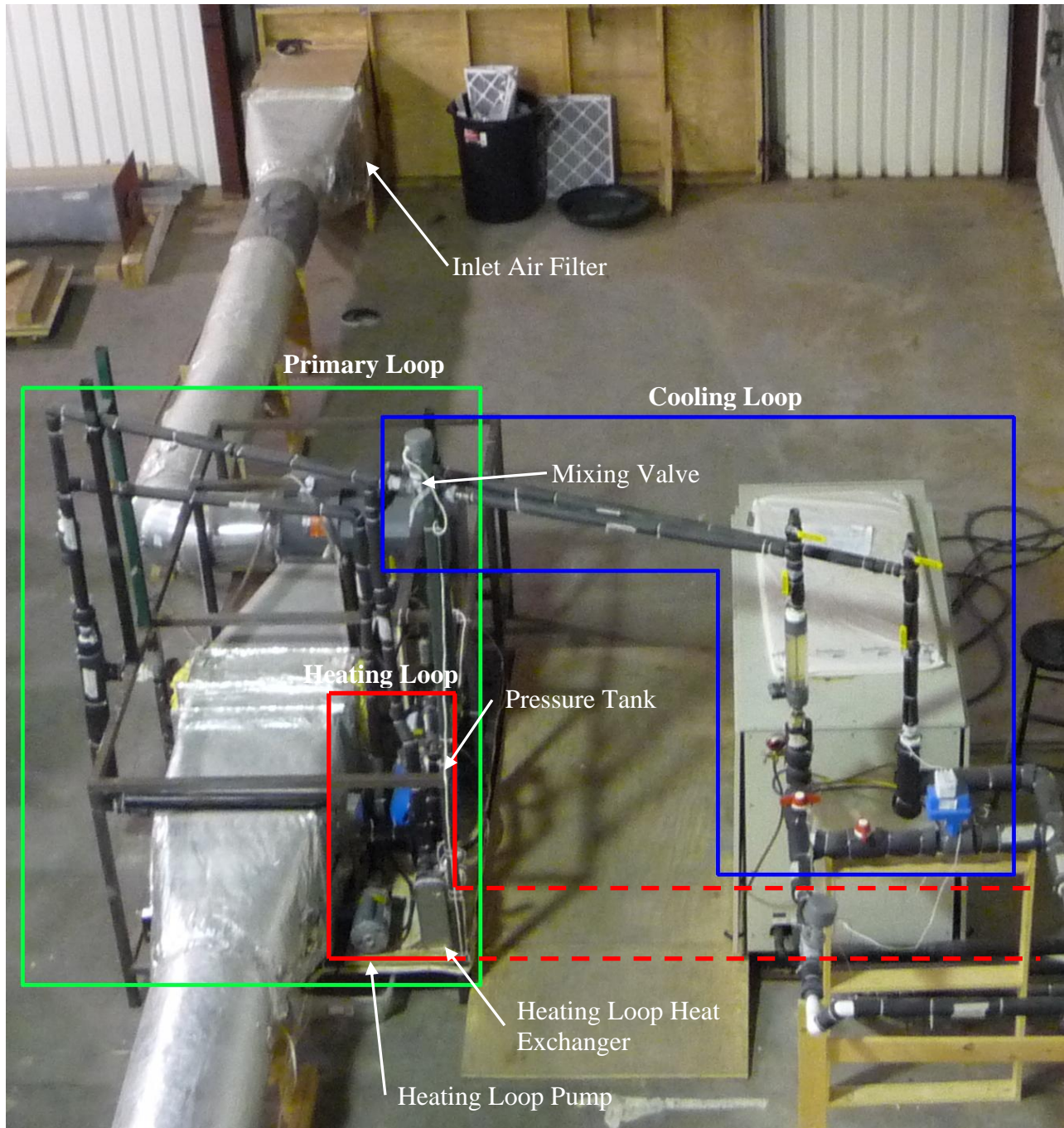
Figure 3.15 Conditioning System

The conditioning system operates under three typical scenarios laid out in Table 3.2. Since the air needs to be conditioned to exactly 15.6 °C, the objective of heating/cooling loop is to condition the air to about 12.8 °C, allowing the electric heater to fine tune the temperature. In particular scenarios, due to limitations of the heating system lower capacity, the heating and

cooling loops are used simultaneously to generate an acceptable supply temperature. When

neither the heating or cooling loop is necessary, the primary loop is still operated to cycle a mass

of water through the system. The mass of water in the primary loop, even if only marginally

altering the air temperature, acts as a buffer for outdoor air temperature fluctuations.

Table 3.2 Conditioning System Operation Modes

OA Temperature	Operating Mode
> 13 °C	Cooling loop is utilized to bring temperature down to 7 °C.
$7 \leq T \leq 13$ °C	Only electric heater is used.
< 7 °C	Heating loop is utilized to bring temperature up to 7 °C.

3.2.2 Control System

The control of the conditioning system is rather complex due to the intertwined systems, but is

easily handled through a computer interface running LabVIEW. The computer acquires data

through Agilent 34970A and National Instruments FP-1000 DAQ's and controls several output

variables via the National Instruments FP-1000 with add-on modules PWM-520 and AO-210 for

pulse width modulation and analog voltage output, respectively. The system senses temperature

at seven key locations as well as supply relative humidity and supply airflow rate. The primary

control points are the electric heater and supply fan speed controlled by VFD. Additionally, a

mixing valve and the pump for the heating loop can be controlled when necessary. Details

regarding all control and feedback parameters can be seen in Table 3.3.

Table 3.3 Conditioning Systems Control and Feedback Parameters

Feedback	Notes	Control	Notes
Inlet Air Temp.	Near inlet filter	Blower VFD	
Electric Heater Temp.	Fast acting thermistor	Heating Loop Pump VFD	
Hot Water Temp.		Mixing Valve	Primary/cooling loop mixing
Glycol Supply Temp.	To heat exchanger	Duct Heater	Pulse-width-modulation
Glycol Return Temp.	From heat exchanger		
Heating Loop Heat Exchanger Temp			
Supply Relative Humidity			
Supply Flow Rate			
Supply Air Temp.	Primary feedback		

The only parameter of the system which cannot be controlled through the computer interface is the set point of the chiller. This needs to be done manually, but since the duct heater can accommodate up to an 8 °C temperature variation, the chiller set point can generally be selected for an operating cycle without needing to be altered. A screenshot of the user interface during system warm-up, hence supply temperature is not yet steady, can be seen in Figure 3.16.

The majority of control points are handled automatically by simple PID controllers designed in LabVIEW. The program also allows several user overrides as can be seen in the lower right corner of the user interface. Typically, the user only needs to select the supply temperature, flow rate, and ambient barometric pressure. The overrides are useful when operating on the edge of requiring either the heating or cooling loops. The program also keeps a log of temperatures and supply flow rate for each operational cycle.
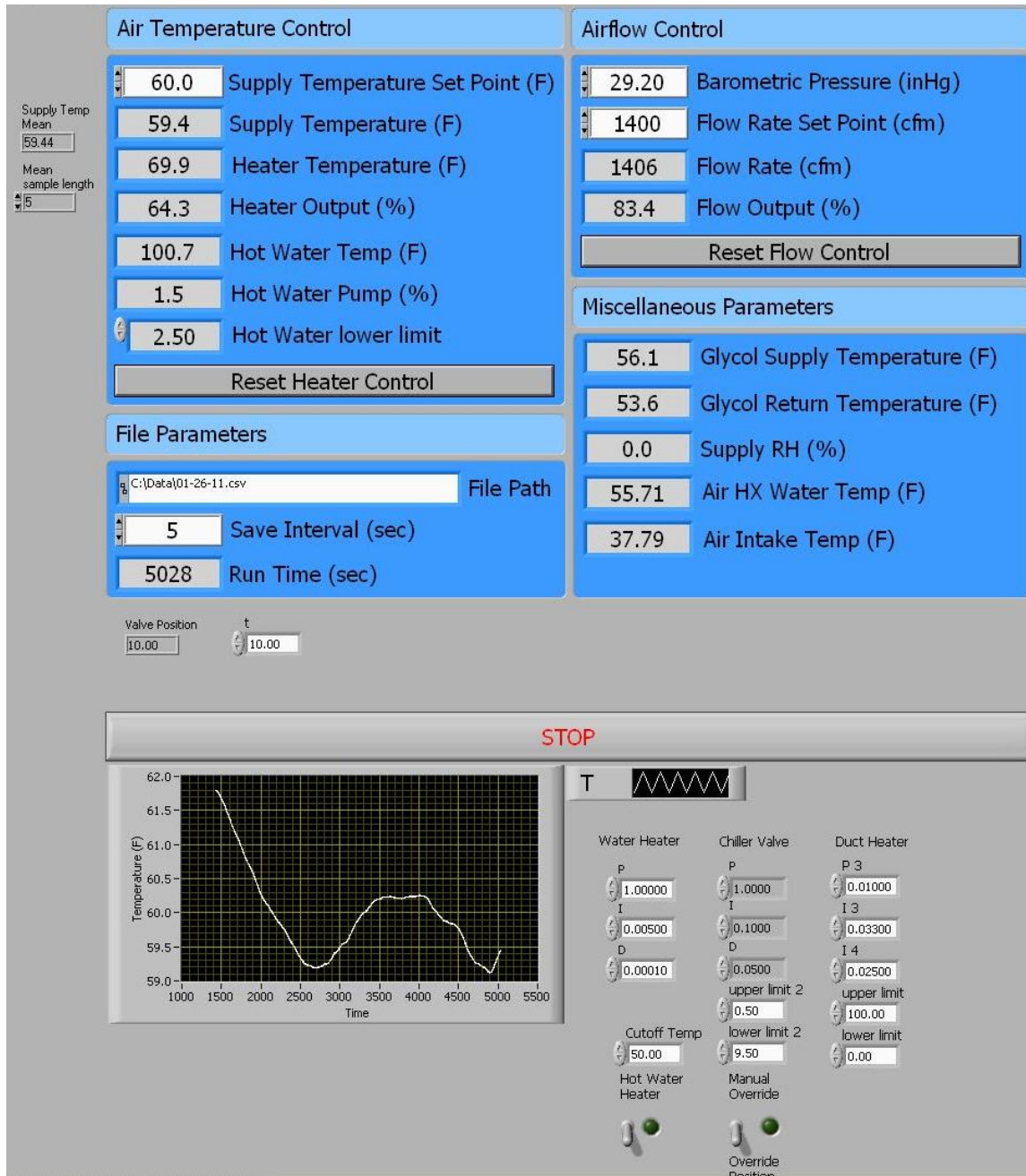
Figure 3.16 Air Supply Control System

3.3 CO$_2$ Injection and Sampling

To track air and contaminate movement throughout the cabin, carbon dioxide is injected and

concentrations are sampled in test locations throughout the cabin. Because CO$_2$ weighs more

23

than air, Helium (He) is blended with the CO_2 prior to injection to achieve neutral buoyancy in ambient cabin air. The ratio of CO_2 and He was calculated using ideal gas principles based on molecular weights.

3.3.1 Injection System

The industrial grade CO_2 and high purity He arrive at the facility in 50 lb and type T cylinders, respectively. The compressed gases are then regulated to about 200 kPa. To allow computerized control of the injection system, mass flow controllers were installed to regulate the flow rate of each gas. These flow controllers are operated by the main tracer gas injection control and data acquisition program to sync injections, cart movements and sampling procedures.

3.3.1.1 Mass Flow Controllers

For CO_2 injection, an electric MKS 1559A-200Ll-SV-S controller was used. Similarly, a pneumatic MKS 2179A00114CS controller was used for He. Both mass flow controllers, shown in Figure 3.17, are operated by an MKS PR4000 power supply and RS-232 interface unit. The black brackets seen above the mass flow controllers house flow meters, used to verify the CO_2 and He flow rates. The power supply can be seen in Figure 3.18 along with an Agilent 34970A DAQ, used in several locations throughout the laboratory.

Figure 3.17 Mass Flow Controllers   Figure 3.18 Power Supply/Controller

3.3.1.2 Injection Apparatus

Once the CO_2 and He leave the mass flow controllers they are mixed in a simple brass tee fitting. Vinyl tubing 12 mm in diameter connects to the injection apparatus shown in Figure 3.19. To slow the velocity of the tracer gas, the 500 mm long injection tube expands to 25.4 mm inside diameter. The centerline of the copper injection tube is mounted 180 mm above the armrest of the injection seat location. The tracer gas exits the face of the injection tube at 0.37 m/s at the standard injection rate. The face of the injection tube reaches 55 mm into the aisle and injects the tracer gas directly toward the centerline of the cabin. The apparatus can be quickly moved between seat locations to examine effects of an altered injection location.

Figure 3.19 Tracer Gas Injection Apparatus

3.3.2 Measurement System

The tracer gas measurement system consists of a sampling tree with a CO_2 analyzer in the mockup cabin in addition to inlet and exit sensors. The inlet and exit sensors are used to factor out environmental CO_2 concentrations and perform a mass balance of tracer gas on the entire experimental mockup.

3.3.2.1 Sampling Tree

The sampling tree allows four seat locations in a single column of seats to be sampled during an experimental procedure. As can be seen in the foreground of Figure 3.20, the sampling tree houses a manifold block with SMC Pneumatics NVKF334V-3G two-way solenoid valves connecting each of the four sampling lines to a common outlet port. Each sampling line is made

of 304 stainless steel welded tubing with an inside diameter of 5 mm. The valves are normally closed to the common rail. In addition to a solenoid valve for each sampling line, an additional valve is mounted to the manifold in reverse orientation so it is normally open. The fifth valve is connected to a barb open to atmosphere, rather than connected to a sampling line. This allows the vinyl tube connected to the common rail of the manifold, as seen on the near end of the manifold block, to constantly be pulling a sample through to the CO_2 analyzer.

Figure 3.20 CO_2 Sampling Tree

When a particular port is to be sampled, the corresponding valve is opened and the reversed valve is closed. This ensures the only air which is leaving the manifold originates from the intended sample location. These valves are controlled by an Agilent 34970A, which can function as a switching unit as well as a DAQ when equipped with a 34903A SPDT module. The switching module is supplied with 115V AC power which is then distributed to the poppet solenoid valves to control their state.

The sampling tree itself is 3.1 m long and is positioned along the centerline of the column of seats being sampled. The sampling ports are spaced 840 mm apart, corresponding to the spacing between rows in the cabin. The sampling point for each seat location is 140 mm above and 240 mm in front of the top edge of the seatback. This location is directly fore the nostril location of the manikin in the respective seat.

27

3.3.2.2 Sensors

To enable the ability to normalize tracer gas readings for different injection rates as well as CO_2 variations in environmental air, three analyzers are used. An inlet sensor samples air entering the cabin mockup just before the insulated duct passes into the chamber enclosure as seen in Figure 3.1. The exit sensor has sampling ports attached to both exhaust fans also seen in the figure.

The inlet and exit sensors were custom made using Edinburgh Instrument gas sampling cards and 24V power supplies with 60 Hz noise filters. Both analyzers are locatated on top of the cabin enclosure to limit the length of the sampling line. The interior of one of these analyzers can be seen in Figure 3.21. Several specifications of each sensor as well as the in-cabin unit are outlined in Table 3.4.

Figure 3.21 Inlet and Exit CO_2 Sensors

Table 3.4 CO$_2$ Analyzer Specifications

Sensor	Model	Range	Notes
Inlet	Edinburgh Gascard NG	0 to 3000 ppm	
Outlet	Edinburgh Gascard II	0 to 3000 ppm	
Cabin Measurement	NOVA Analytical 420	0 to 5000 ppm	Gascard II with additional filtering circuitry

The sensor connected to the sampling tree in the interior of the mockup cabin is a NOVA Analytical Model 420, as shown in Figure 3.22, under one of the cabin seats. It uses the same Edinburgh Instruments Gascard II (with a different sampling range), but adds several filtering elements to clean noise from the signal. Much of this extra filtering was deemed unnecessary and actually masked the transient behavior of the tracer gas concenteration. Therefore, the filters were bypassed. Since all analyzers are calibrated using a software linear regression rather than manually using span and zero calibration gas, the LCD display concentration is not accurate. A line measuring voltage difference produced by each of the analyzers is connected directly from each CO$_2$ analyzer to an Agilent 34970A DAQ.

Figure 3.22 NOVA CO$_2$ Analyzer

Originally, each of the CO$_2$ analyzers was equipped with its own diaphragm pump, which pulled a continuous sample through the instrument. It was found through earlier experimentation that the diaphragm in the pump could develop a leak, fouling the sample with additional ambient air.

To alleviate this scenario, a single vacuum pump was installed downstream of all three analyzers. This configuration ensures that the quantity of any air leakage is consistent throughout calibration and experimentation, and therefore negated. Since the lengths of sampling line, and therefore pressure drop, from the sampling location to the analyzers and from the analyzers to the pump are varied, a balancing system was installed to ensure each analyzer received a sample at 1 liter per minute (lpm). This balancing system, pictured in Figure 3.23, incorporates an Omega FL-2012 flow meter for each sample and merges the three lines into one before being plumbed to the vacuum pump.

Figure 3.23 Sample Flow Balancing System

3.3.3 Control Program

To measure tracer gas movement throughout the cabin, a measurement from each of the CO_2 analyzers was recorded every five seconds during experimentation. All measurements were

30

conducted by an Agilent 34970A DAQ controlled by the main data acquisition LabVIEW program. At each sampling interval, temperatures were also recorded for each CO_2 analyzer, cabin supply air inlet (separate from supply control system temperature), twelve locations on each of the east and west cabin walls, and fourteen locations on a temperature tree in the center of the cabin.

The data acquisition program, as seen in Figure 3.24, also controls the tracer gas injection rate, duration, and timing. The program can also control the sampling interval and selects which ports to sample on the sampling tree. This enables all four ports of the sampling tree to be utilized in four separate seat locations during a single experiment as discussed in Chapter 4 - .

Figure 3.24 DAQ Program Screenshot

31

Chapter 4 - Test Procedure

The testing procedure consists of injecting tracer gas into the cabin mockup until the tracer gas concentration reaches a steady state. Then, the beverage cart is traversed past the tracer gas injection point and fluctuations in tracer gas concentration are measured throughout the cabin. For initial testing, it was necessary to determine the time constant, or time for the cabin to reach a steady state level of tracer gas as well as the time for CO_2 levels to decay to ambient concentration once injection is ceased.

Figure 4.1 shows the CO_2 concentration recorded at a location relatively far from the injection point, near the centerline of the cabin, during a tracer gas injection event at 7.00 lpm. The injection began at minute 1 and continued until minute 21. As can be seen by the highlighted portion, a steady state concentration was reached at minute ten, or after nine minutes of injection. It also took a little less than ten minutes after the injection ceased for tracer gas to completely leave the cabin. These times were used as baseline measures for further steady state testing procedures.
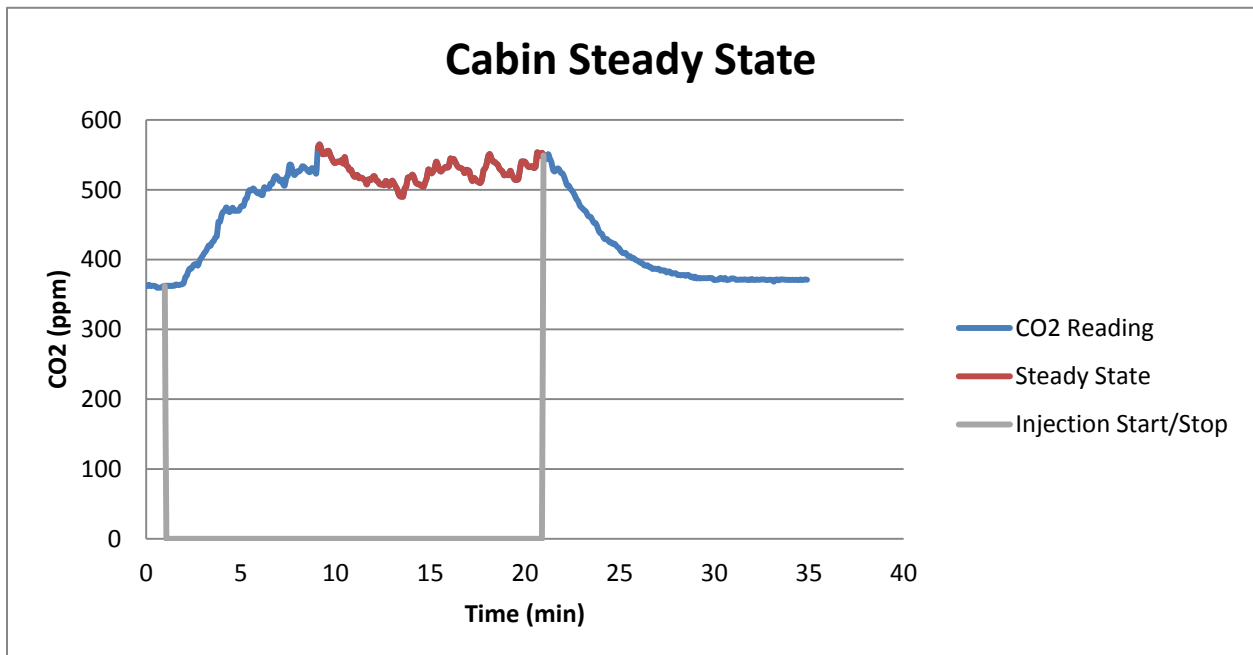
Figure 4.1 Cabin Steady State Time

Studies were conducted to determine optimal injection locations, injection rate and cart movement speeds. To determine the optimal injection rate, the sampling tree was placed at varying distances from the injection point and the steady state CO_2 level was obtained. This level needed to be large enough to suppress noise in the signal, but not breech operating ranges of the sampling equipment.

The primary piece of equipment limiting the injection rate was the flow meter used to visually verify the injection rate of CO_2. The maximum flow rate of the Omega FL-113 flow meter used to verify CO_2 flow is 14 lpm, but sudden influxes of gas by the mass flow controller can pin the float to the top of the glass tube, impeding flow. To alleviate this issue, the maximum reliable flow rate was found to be less than 8 lpm. The largest possible CO_2 injection rate was chosen to lessen the effect of uncertainty in cabin locations where the tracer gas was only a very small portion of the absolute CO_2 concentration.

The optimal injection rate for the CO_2 was found to be 7.00 lpm. Because pure CO_2 at atmospheric conditions is roughly 1.5 times as dense as atmospheric air, Helium was blended with the CO_2 to achieve neutral buoyancy. Using ideal gas principles and molecular weights of CO_2, He, and air it was calculated that the injection needed to consist of 62.4% CO_2 and 37.6% He. Therefore, the He injection rate for all experimental tests was 4.22 lpm.

The main cart traverse speed was chosen by measuring the pace of a slow walk, which would be symbolic of a flight attendant moving the cart the length of the aisle to begin or end beverage service. Additional studies were to be conducted examining the effect of a quicker cart speed. The secondary speed was chosen as the fastest reasonable speed sustainable by the laboratory equipment, namely the 3-phase motor braking and cart position sensors, to provide a worst case contaminate transport scenario.

4.1 Eight-Row Baseline Test

To be able to track any effects of cart movement on cabin airflow patterns, similar tests needed to be completed without any cart movement. A baseline test was run three times for each seat in rows one through eight. The results of the three experiments were then averaged for statistical

presentation purposes. The procedure, controlled by the main data acquisition program, for the
baseline testing is outlined in Table 4.1.

Table 4.1 Baseline Testing Procedure

Seq.	Name	Time (min)	Gas	Notes
1	Pre-Test Scans	1	Off	This period is used to get an atmospheric CO_2 reading from each analyzer. This time was extended to 12 minutes in later testing when it was discovered that offsets needed to be calculated from these values for instrument synchronization. This is further discussed in Appendix A.3.
2	Steady State Delay	12	On	Brings chamber to steady tracer gas level.
3	Test Scans	10	On	Sampling Port 1
4	Test Scans	10	On	Sampling Port 2
5	Test Scans	10	On	Sampling Port 3
6	Test Scans	10	On	Sampling Port 4
7	Post-Test Scans	12	Off	Brings chamber back to environmental CO_2 level.

It should be noted the program was written so tracer gas sampling could be conducted in a steady
state or injection-decay mode. Since all testing in this phase of experimentation was run using
steady state injections, not all available program sequences were used. The sampling tree allows
four seats in a single column in either rows one through four or five through eight to be tested
during a single steady state tracer gas event.

4.2 Eight-Row Cart Test

The first phase of testing for the forward eight rows of the cabin was very similar to the baseline
testing with the addition of a cart movement fore and aft during the "test scans" sequence for
each port location being sampled. After the cart returns to the original location in the rear of the
cabin, there is a delay for any cart wake to clear. Then, the sampling tree switches to the next
port and the cart traverse process beings again. After all four locations on the tree have been
sampled and the cart has returned for the final time, the injection is ceased and the tracer gas
concentration decays to environmental levels. Table 4.2 shows the sequences involved in a
typical experimental run with cart movement.

Table 4.2 Testing Procedure with Cart Movement

Seq.	Name		Time (min)	Gas	Notes
1	Pre-Test Scans		1	Off	This period is used to get an atmospheric CO_2 reading from each analyzer. This time was extended to 12 minutes in later testing when it was discovered that offsets needed to be calculated from these values for instrument synchronization. This is further discussed in Appendix A.3.
2	Steady State Delay		12	On	Brings chamber to steady tracer gas level
3	3.1	Cart Pause	8	On	Sampling port 1 with cabin at steady state
	3.2	Cart Movement	~ ½	On	Cart traverses from rear of cabin to front past injection point.
	3.3	Cart Pause	9	On	Pause at front of cabin while wake settles
	3.4	Cart Movement	~ ½	On	Cart traverses from front of cabin to rear past injection point.
	3.5	Cart Pause	2	On	Pause at rear of cabin while wake settles
4	Sampling Port 2		20	On	Repeats sequences 3.1- 3.5 for sampling port 2
5	Sampling Port 3		20	On	Repeats sequences 3.1- 3.5 for sampling port 3
6	Sampling Port 4		20	On	Repeats sequences 3.1- 3.5 for sampling port 4
7	Post-Test Scans		12	Off	Brings chamber back to environmental CO_2 level

Chapter 5 - Results and Analysis

The results of many tests are presented in the following chapter. Due to scope and length constraints of this thesis, generally only average results from several runs are shown. However, data used to form these averages as well as data from every individual experimental test is available in spreadsheet format in the electronic appendix. Refer to Appendix B for guidance using the electronic appendix.

5.1 Data Manipulation

To be able to make meaningful comparisons between data of separate test runs, results needed to be put in a presentable form. Data manipulation began by taking the comma separated value files created by the data acquisition program and importing them into a spreadsheet utility. Because the CO_2 analyzers were calibrated biweekly throughout experimentation, the related calibration data was not incorporated in the data acquisition program. The files created by the program simply contain voltage readings from the analyzers, which when paired with corresponding calibration data for the testing time period, form tracer gas concentration counts. Keeping the calibration data paired with the data files is an easier proposition over months of testing than manipulating program parameters throughout the experimentation process. If the program were modified with each calibration data set, no history of which calibration data was used with particular experimental runs would be created for later troubleshooting and analysis.

Once data have been converted to spreadsheet format, unnecessary data was trimmed so relevant data from identical time periods of different runs could be compared. The data from periods while bringing the cabin to steady state concentration as well as decay after injection was ceased is trimmed. For comparison purposes, data from four seats of a single column are plotted together. Plotting all eight seats from a column of seats on a single chart would allow the concentration measurements of seats nearer the injection location to overpower seats further away.

To enable data to be compared when different tracer gas injection rates were used and to account for environmental CO_2 variations, the data was all normalized using Equation (5.1), where N is

the normalized count and C is the measured CO_2 concentration in ppm. In later phases of testing, it was discovered the CO_2 analyzer measuring outlet air was producing unreliable readings. As a check for this, the flow rates of tracer gas and ventilation air were used to calculate an alternate version of the equation as seen in Equation (5.2), where V is the volumetric flow rate. Equation (5.2) proved to be more reliable in calculating the normalized concentration and was used when analyzing all data for consistency. Equation (5.1) was then used as a secondary mass balance check to ensure all CO_2 analyzers were operating correctly during a particular test.

$$N = \frac{C_{measured} - C_{inlet}}{C_{outlet} - C_{inlet}} \tag{5.1}$$

$$N = \frac{C_{measured} - C_{inlet}}{V_{tracer\,gas} \Big/ V_{vent.\,air}} \tag{5.2}$$

5.2 Averaged and Transient Inlet Reading

Originally, the mean value of the inlet reading for all data taken at a particular seat location (around 20 minutes) was calculated and substituted in the normalization equation. It was noticed, however, that some transient environmental variations in CO_2 were too quick for this process to accurately represent. In the suburban setting of Manhattan these variations can occur due to changing weather, winds, and traffic levels. Using the raw inlet reading for each sample taken introduced a great deal of noise to the normalized count. To alleviate the short-term transient noise introduced by the inlet concentration, it was decided to use a rolling average method to calculate a new value each time the normalizing function was evaluated.

In several instances, when the fluctuation of environmental CO_2 was significant during testing at a particular seat location, the normalized reading was skewed by the inlet variation as seen in seat 4A of Figure 5.1. The spike in inlet variation causes the normalized value to rise and fall suddenly towards the end of the test run. To counteract this, a transient inlet value was implemented which uses a 31 count moving average. At five seconds per scan, the inlet CO_2 value used for each normalization calculation is an average of the previous 2.5 minutes in inlet

data. The 31 counts were chosen for a balance between maintaining transient inlet concentration properties while minimizing noise in the raw signal as can be seen in Figure 5.2.
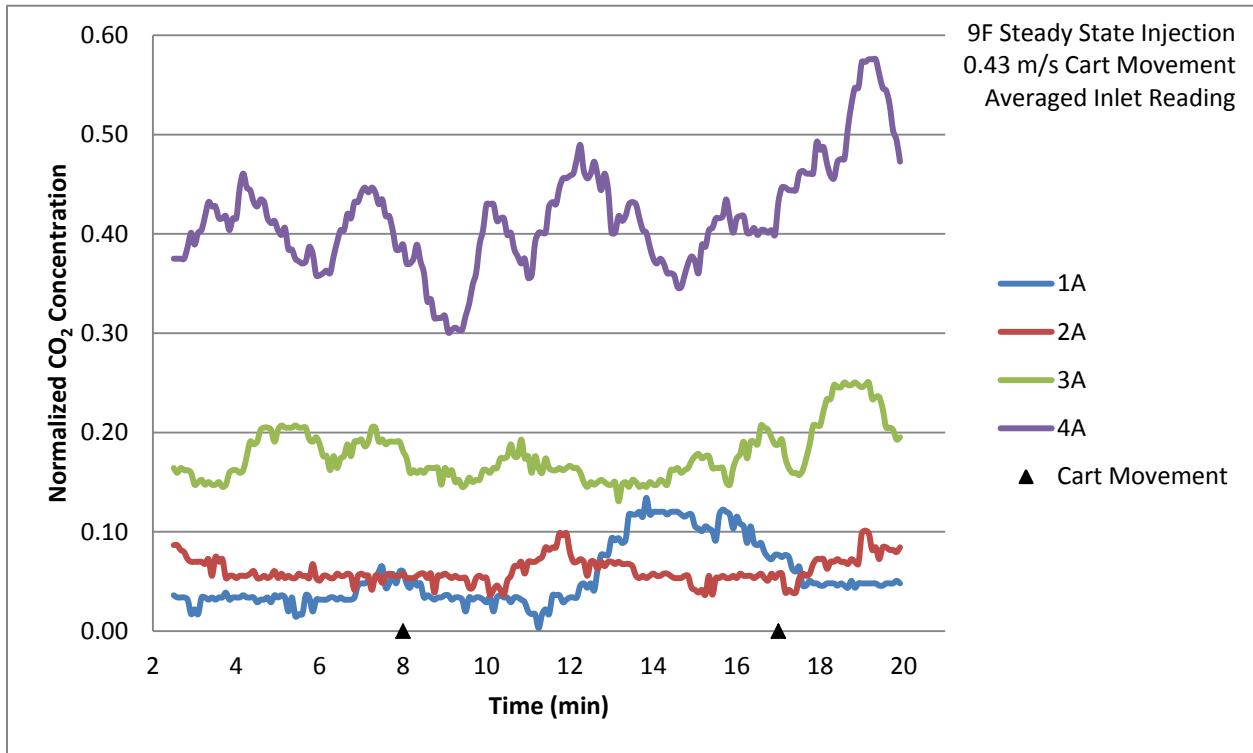
Figure 5.1 Seats 1-4A Cart Run 1 *Averaged Inlet Reading*
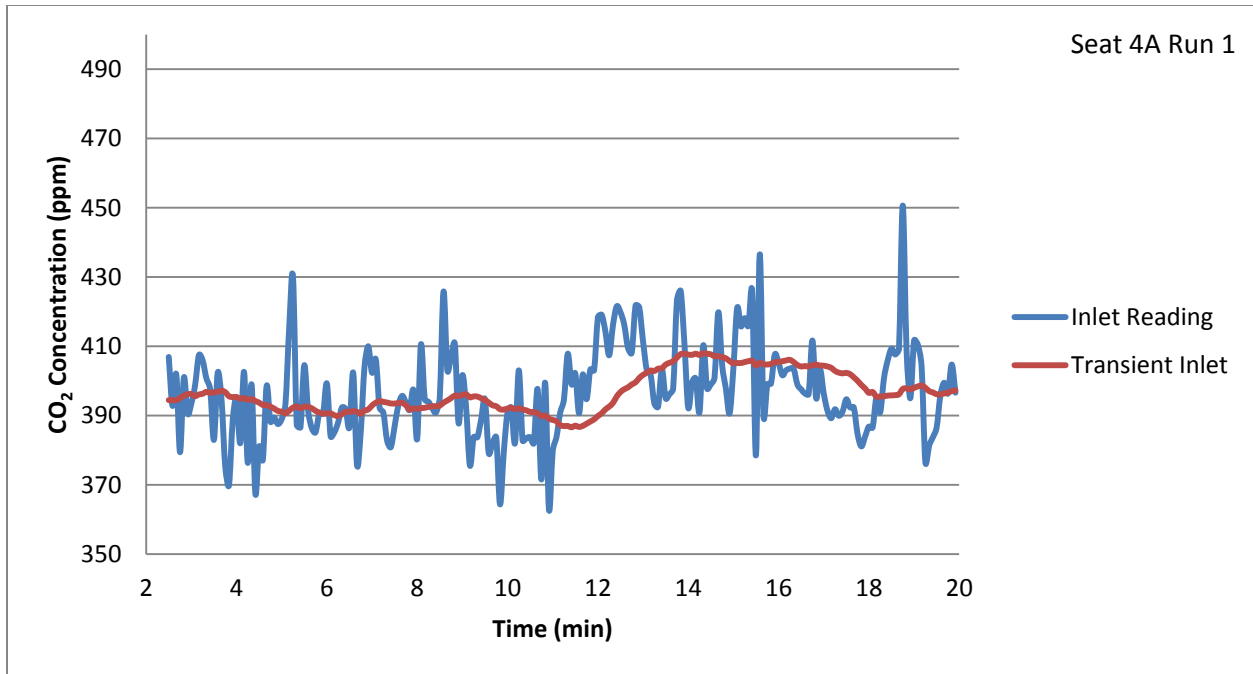
Figure 5.2 Inlet Concentration Comparison

Utilizing the calculated transient inlet value clearly smoothes the raw reading while still allowing actual variation in the signal to be reflected. Figure 5.3 presents the same results as Figure 5.1 but uses the transient inlet value to normalize the data. Using the transient inlet value appears to have leveled the reading for each of the seat locations to a certain extent. A shift toward the end of the 3A measurement rises slightly rather than falling when comparing the average to the transient inlet version. It was concluded the transient inlet reading helped eliminate variation due to inlet fluctuation in general for nearly all tests in the study. Thus, all data presented uses the transient inlet normalization method.

Figure 5.3 Seats 1-4A Cart Run 1 *Transient Inlet Reading*

It was also noticed in a few rare instances a very sudden shift in inlet CO_2 concentration could not be accommodated by the transient inlet algorithm. Figure 5.4 presents an experimental run where the averaged inlet reading appears to serve the normalization calculation sufficiently. There is a gradual growth towards the end of samp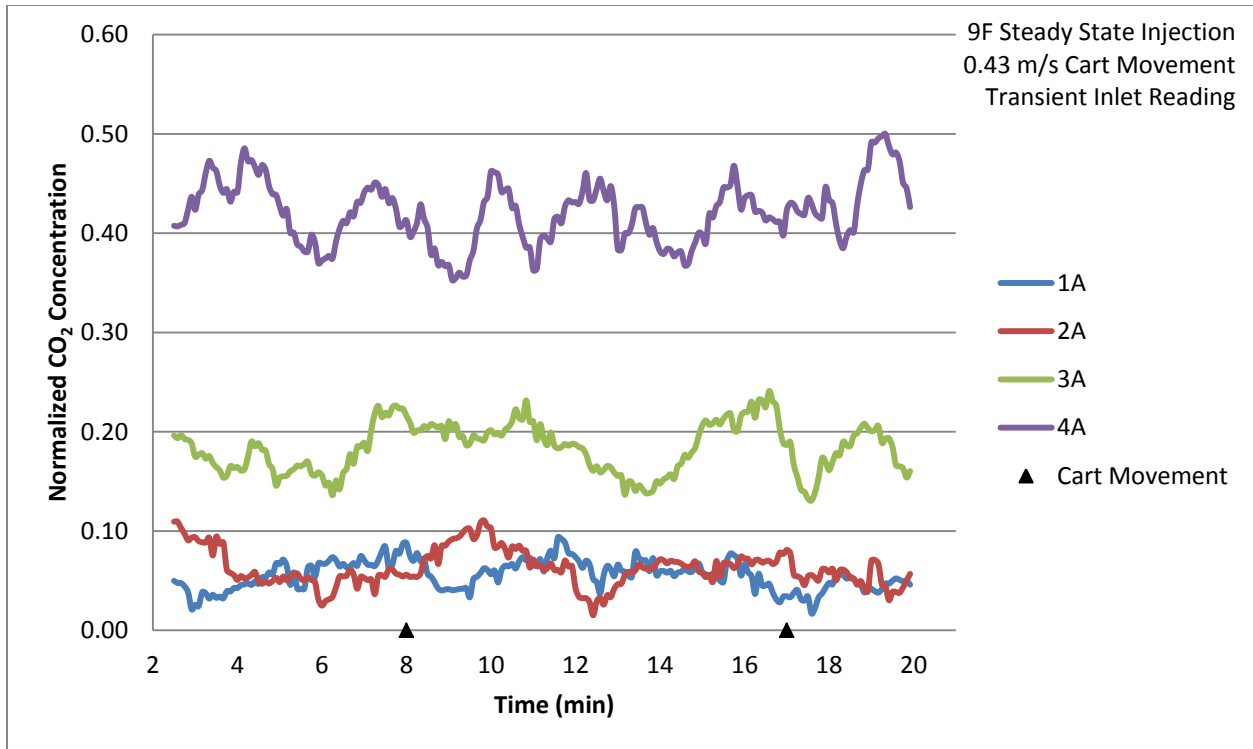ling at seat 4D. This growth would likely not be alarming or even be noticed unless the inlet value for the time period was also examined.

Due to the arrangement of the sampling tree, seat location 4D is actually sampled immediately prior to seat 3D. As can be seen in Figure 5.5 and Figure 5.6, the inlet air had a large spike of environmental CO_2 toward the end of sampling at seat 4D and beginning of sampling at seat 3D. The gap between the two inlet readings is due to 2.5 minutes of data being trimmed from the chart which was used to achieve the initial 31 samples needed for calculation of the transient inlet moving average. Figure 5.7 presents the same results as Figure 5.4, but calculated using the moving average inlet value. In this particular case, the averaging algorithm cannot keep pace with such a large CO_2 variation in a short timeframe.
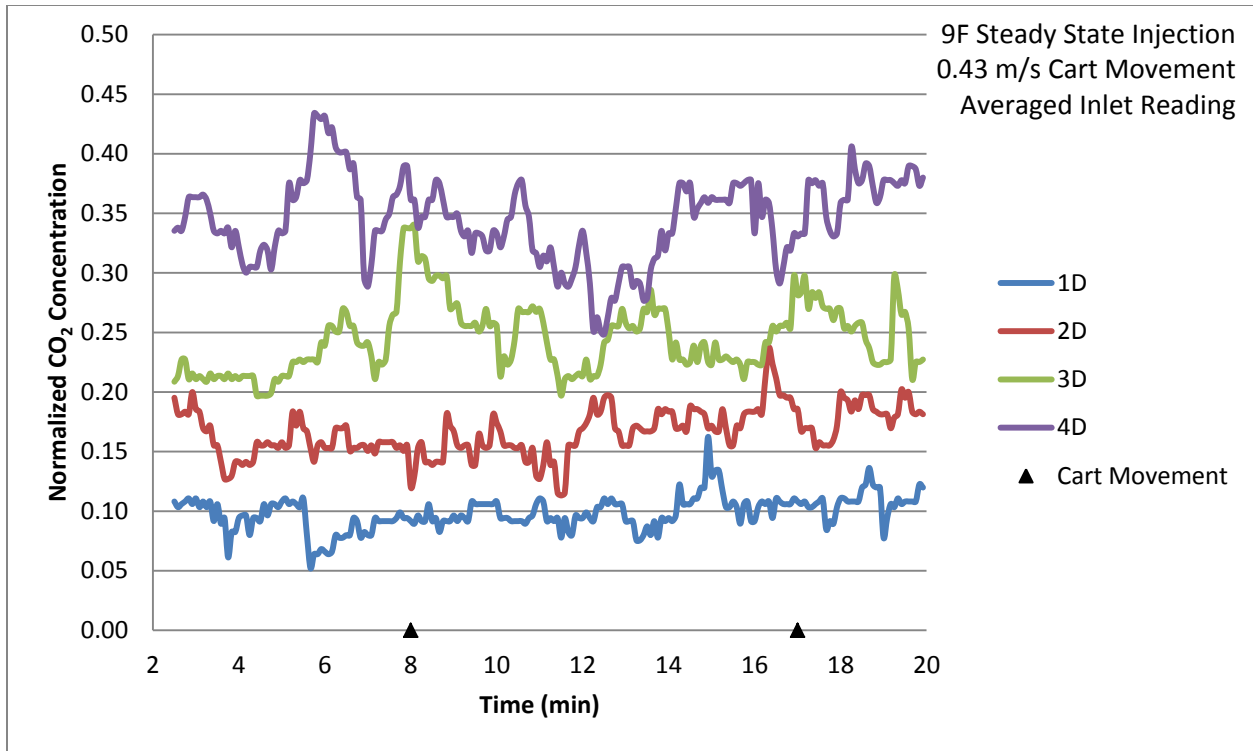
Figure 5.4 Seats 1-4D Cart Run 2 *Averaged Inlet Reading*
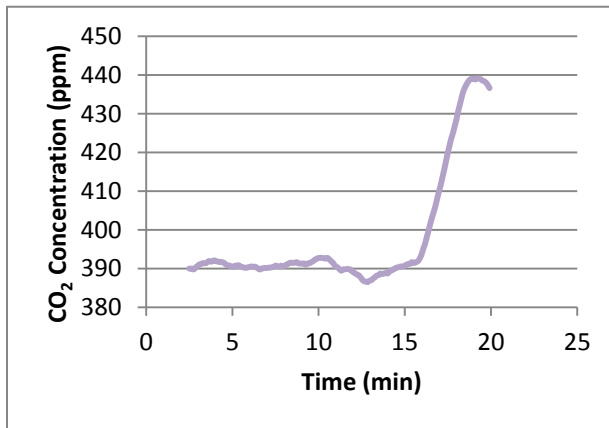
Figure 5.5 Seat 4D Inlet CO$_2$ Concentration
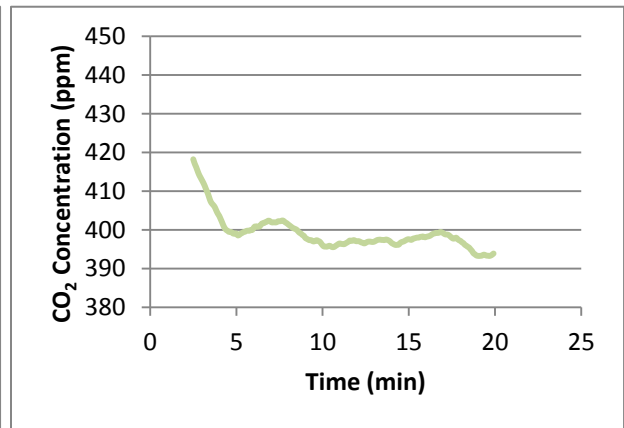
Figure 5.6 Seat 3D Inlet CO$_2$ Concentration
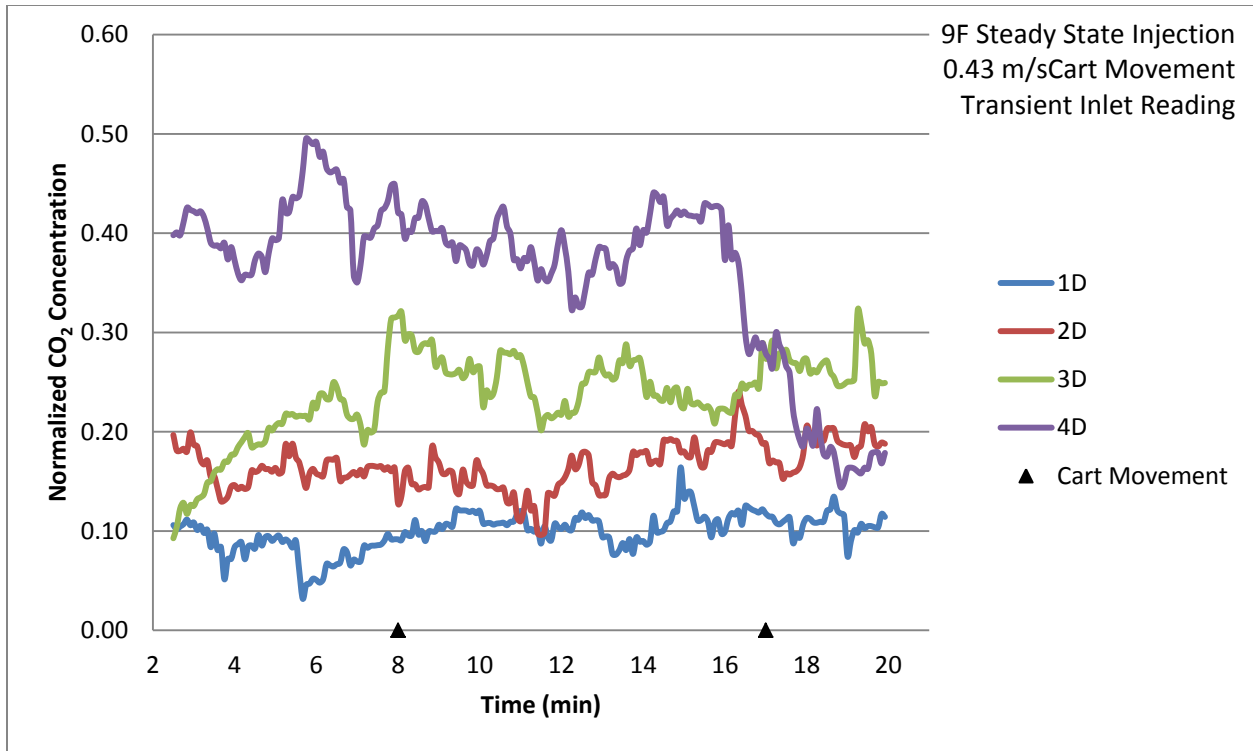
Figure 5.7 Seats 1-4D Cart Run 2 *Transient Inlet Reading*

The averaged inlet reading would be a better normalization process in this case. For consistency, all data in this paper is presented using the transient inlet calculation method, but identical analysis using an averaged inlet reading is available for all tests in the electronic appendix. When data from all three tests in these locations are averaged, the shift in normalized value due to inlet concentration spike nearly disappears even though the transient inlet reading is used.

5.3 Eight-Row Baseline Test

Experimental tests for each seat in rows one through eight were conducted three times without any cart movement using the procedure outlined in Table 4.1. The following figures compare the average of the three readings for each location and group them in either the forward or rear four seats of the sample area in each column. Each column of results is split into high and low concentration subgroups to prevent fluctuations in tracer gas concentration toward the front of the cabin from being overpowered by larger fluctuations in rows near the injection location. Expanded results including a similar style chart for each of the three separate runs is available in

42

the electronic appendix. Figure 5.8 through Figure 5.14 present the normalized experimental data for the front four rows of the test cabin with no cart movement.

Figure 5.8 Seats 1-4A No Cart Average (3 Runs)

Figure 5.9 Seats 1-4B No Cart Average (3 Runs)

Figure 5.10 Seats 1-4C No Cart Average (3 Runs)

44

Figure 5.11 Seats 1-4D No Cart Average (3 Runs)

Figure 5.12 Seats 1-4E No Cart Average (3 Runs)

45

Figure 5.13 Seats 1-4F No Cart Average (3 Runs)

Figure 5.14 Seats 1-4G No Cart Average (3 Runs)

The results are as would be expected; the normalized tracer gas concentration is a function primarily of longitudinal distance from the injection location. The concentration also diminishes, to a lesser extent, as lateral distance from the injection location is increased. Some anomalies occur toward the east wall of the cabin in columns A and B. The concentration of tracer gas generally decreases as the sample location is moved across the cabin, away from the injection except in the far corner of the mockup. Tracer gas appears to become trapped in the stagnant air in the forward rows of columns A and B.

Figure 5.15 through Figure 5.21 present identical data sets for seats in rows five through eight. It can be seen in the results from the four rows nearer the injection location, the normalized tracer gas concentration is much higher than in the forward four rows. This is especially evident in seat locations within two rows of the injection location. Similar to the forward rows on the opposite side of the cabin from the injection, it appears as if contamination becomes isolated in stagnant air zone between the diffuser flow patterns in the center of the cabin (seat column D).

Figure 5.15 Seats 5-8A No Cart Average (3 Runs)

Figure 5.16 Seats 5-8B No Cart Average (3 Runs)

Figure 5.17 Seats 5-8C No Cart Average (3 Runs)

48
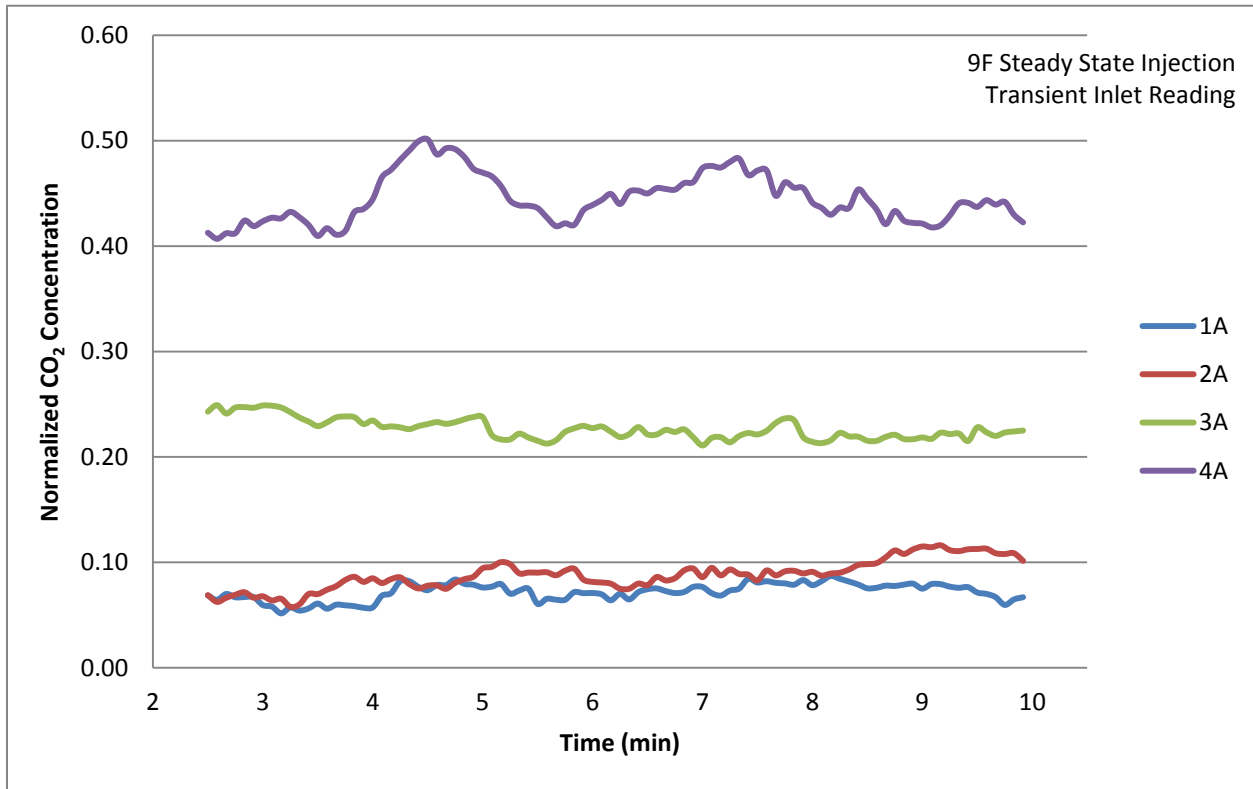
Figure 5.18 Seats 5-8D No Cart Average (3 Runs)

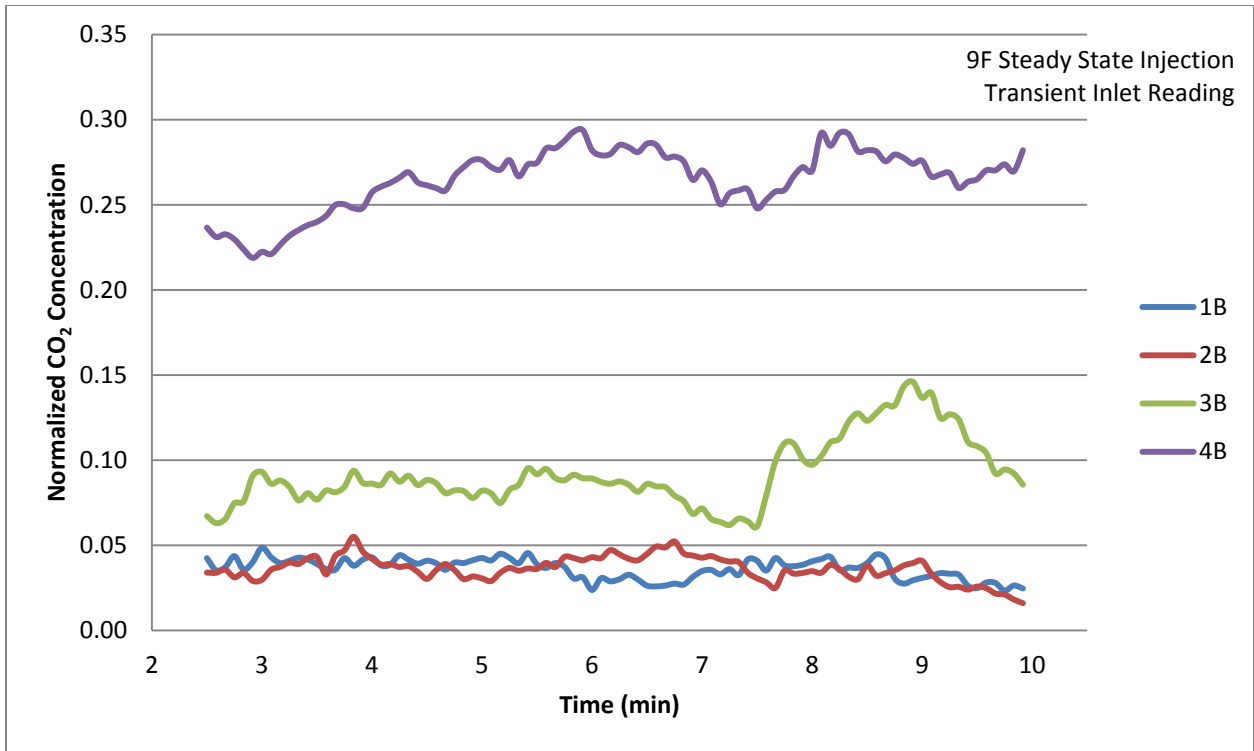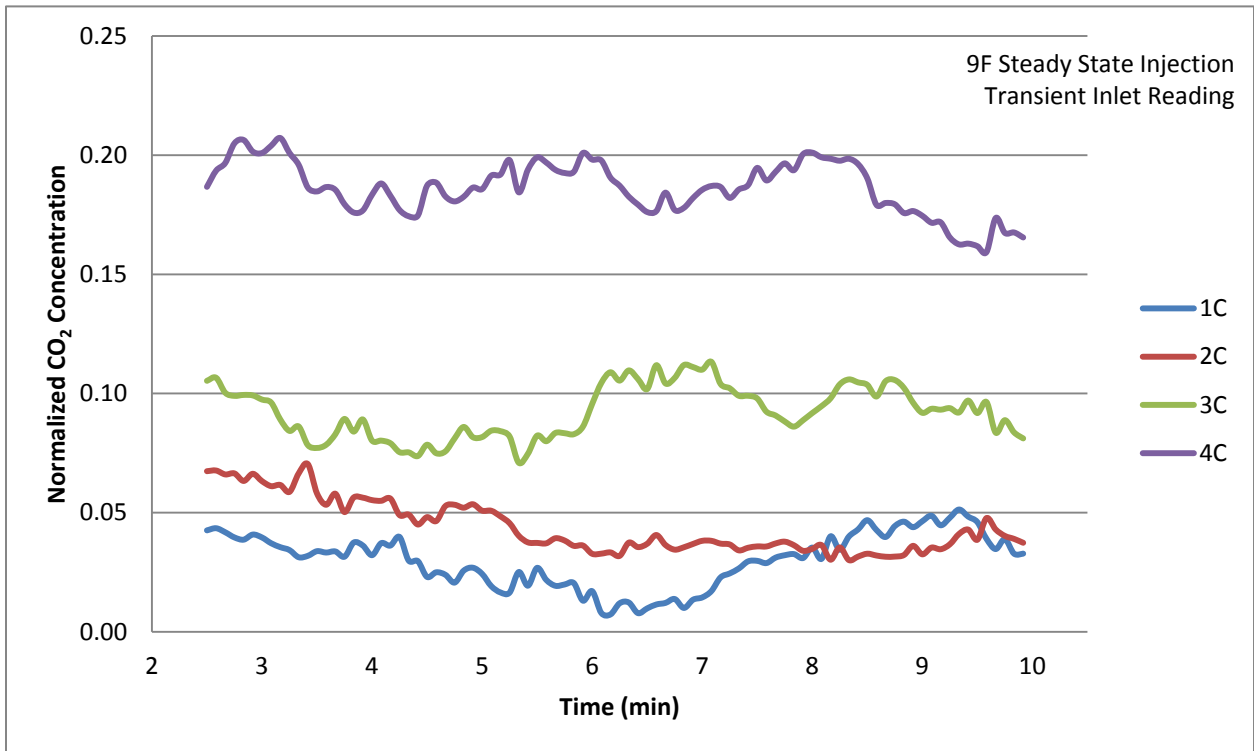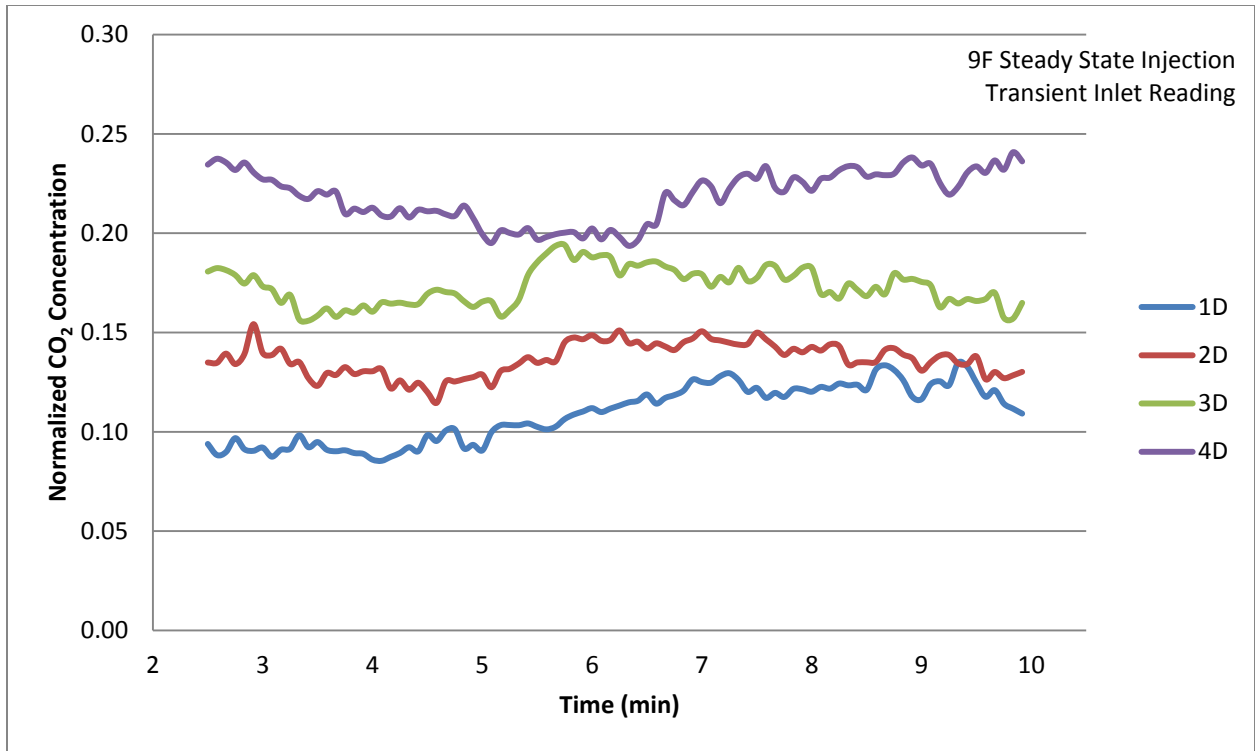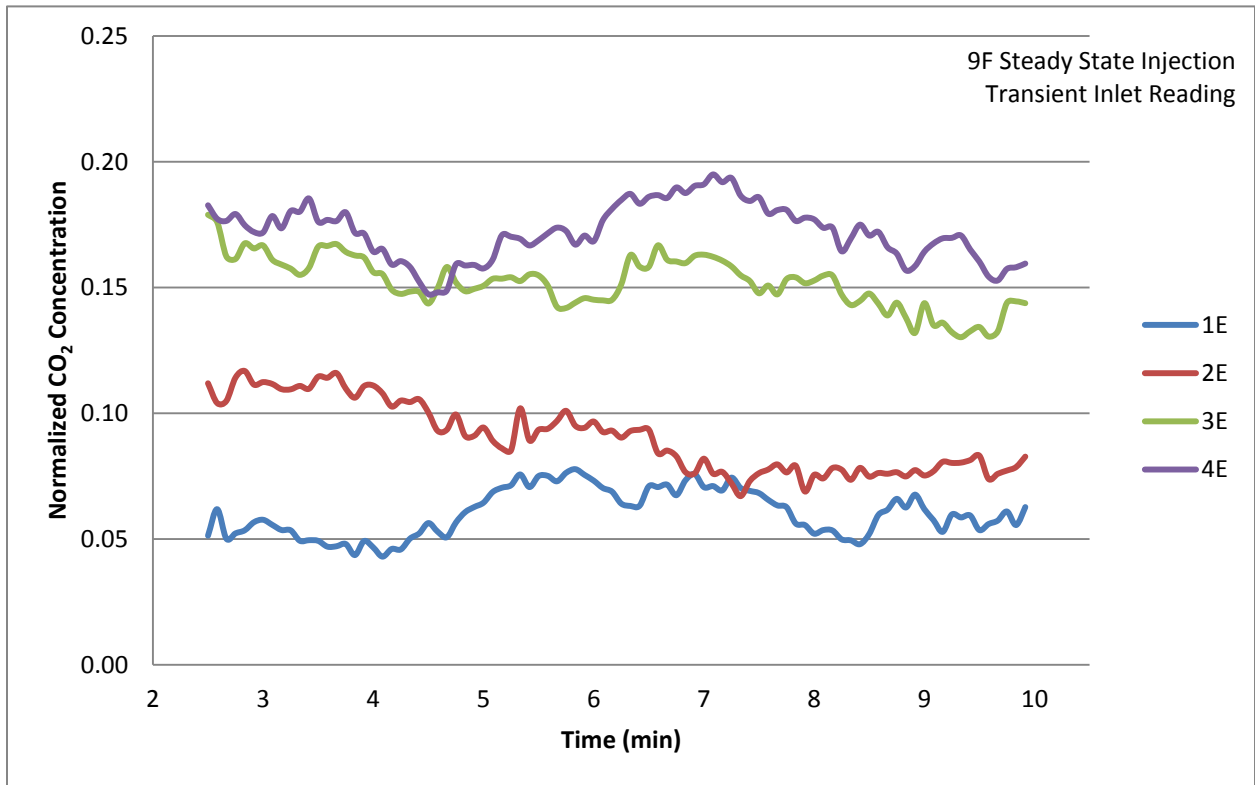**Figure 5.19 Seats 5-8E No Cart Average (3 Runs)**

Figure 5.20 Seats 5-8F No Cart Average (3 Runs)
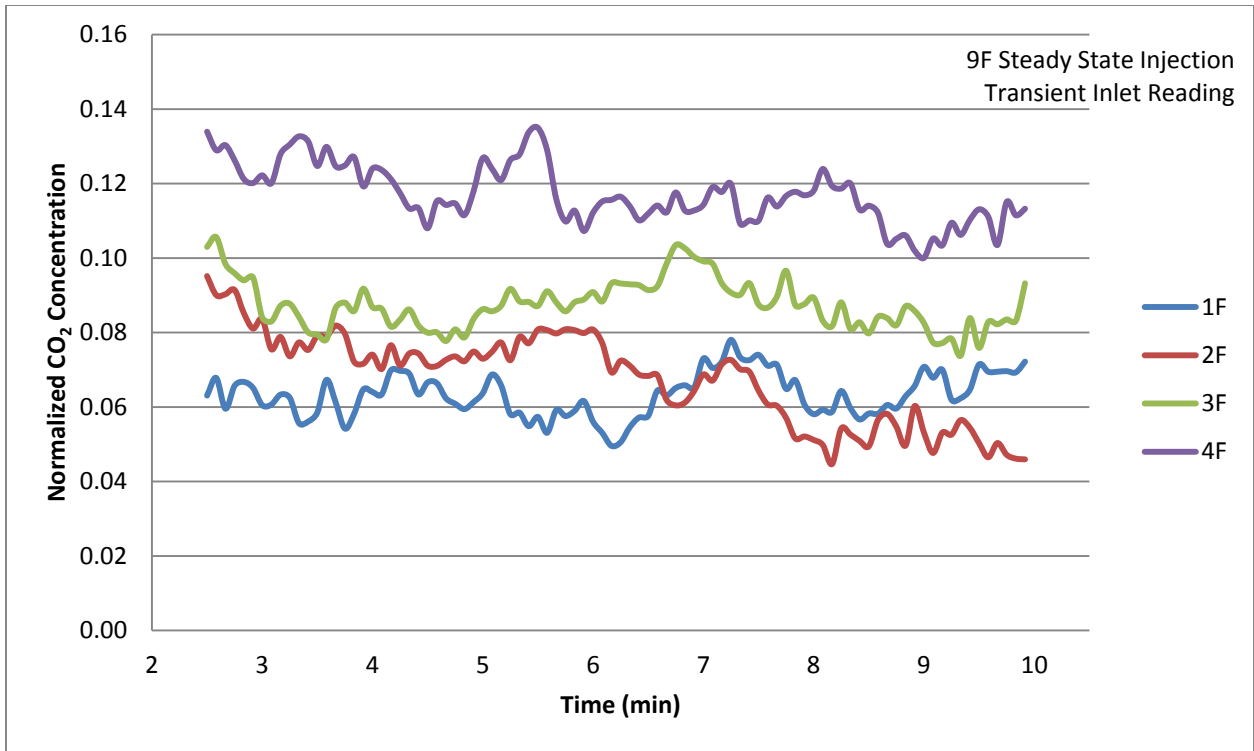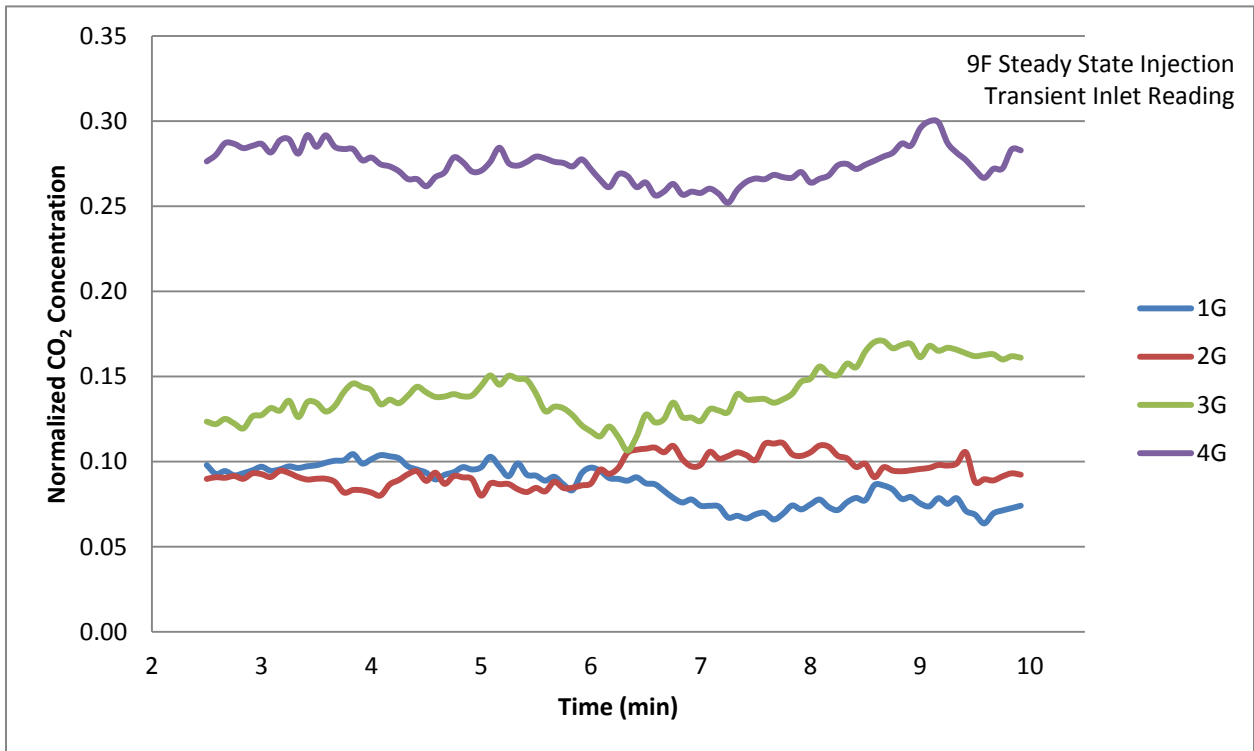

Figure 5.21 Seats 5-8G No Cart Average (3 Runs)

50

5.4 Eight-Row Cart Test

For this phase of testing, cart movements were at 0.43 m/s or the speed of a slow walk. All testing was conducted using the procedure outlined in Table 4.2. The injection apparatus injects the tracer gas directly in the path of the cart traverse. The face of the injection tube extends 55 mm into the aisle to within 32 mm of the sidewall of the passing cart.

Figure 5.22 to Figure 5.28 present the averaged data from the three experimental runs in each seat location in the front four rows of the cabin during the forward and reverse cart traverse. A well-formed peak in CO_2 concentration relating to forward cart movement can be seen for many of the locations near the aisle in the forward seats of the cabin. Locations laterally across the cabin and far from the injection location show little evidence of concentration variation due to cart movement.

One of the more interesting observations is in comparing 3E to 3F in Figure 5.26 and Figure 5.27. Seat 3E appears to not be affected by cart movement, while 3F is affected to a much greater extent than seat locations fore and aft. Upon further inspection, it was noted there is a feeder duct to diffuser connection at 2.6 m from the front wall of the cabin. This ductwork connection location is directly across the aisle from seat location 3F. Figure 3.13 shows these typical flexible hose connections. It appears there is a "jet" of air which consistently pushes ventilation air from the diffuser above 3E directly across the aisle toward 3F. This jet carried the modeled contamination across the F column of seats to seat 3G before it was exhausted in the cabin wall. The tracer gas concentration at seat 3E experienced no distinguishable effect due to cart movement in any of the six runs completed in that location. The forward seat locations of the E column of seats produced some of the most interesting results of the study so the number of experimental runs was doubled from three to six for statistical purposes.
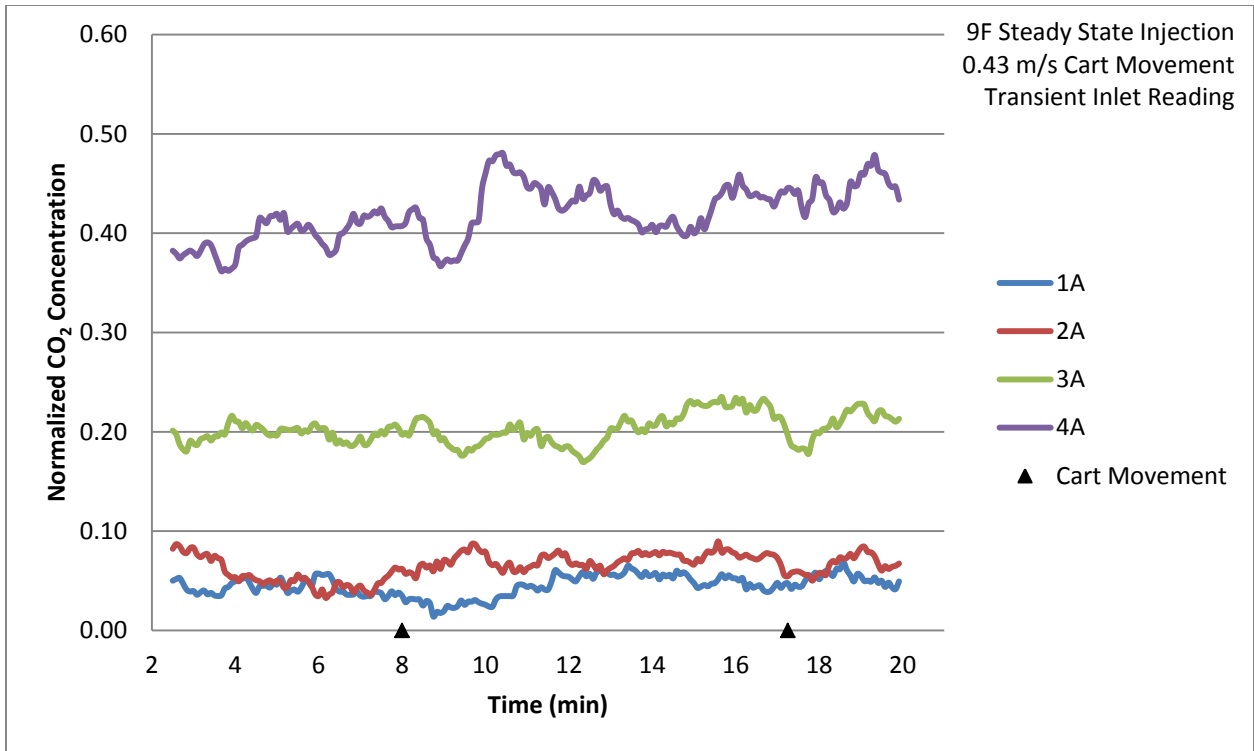
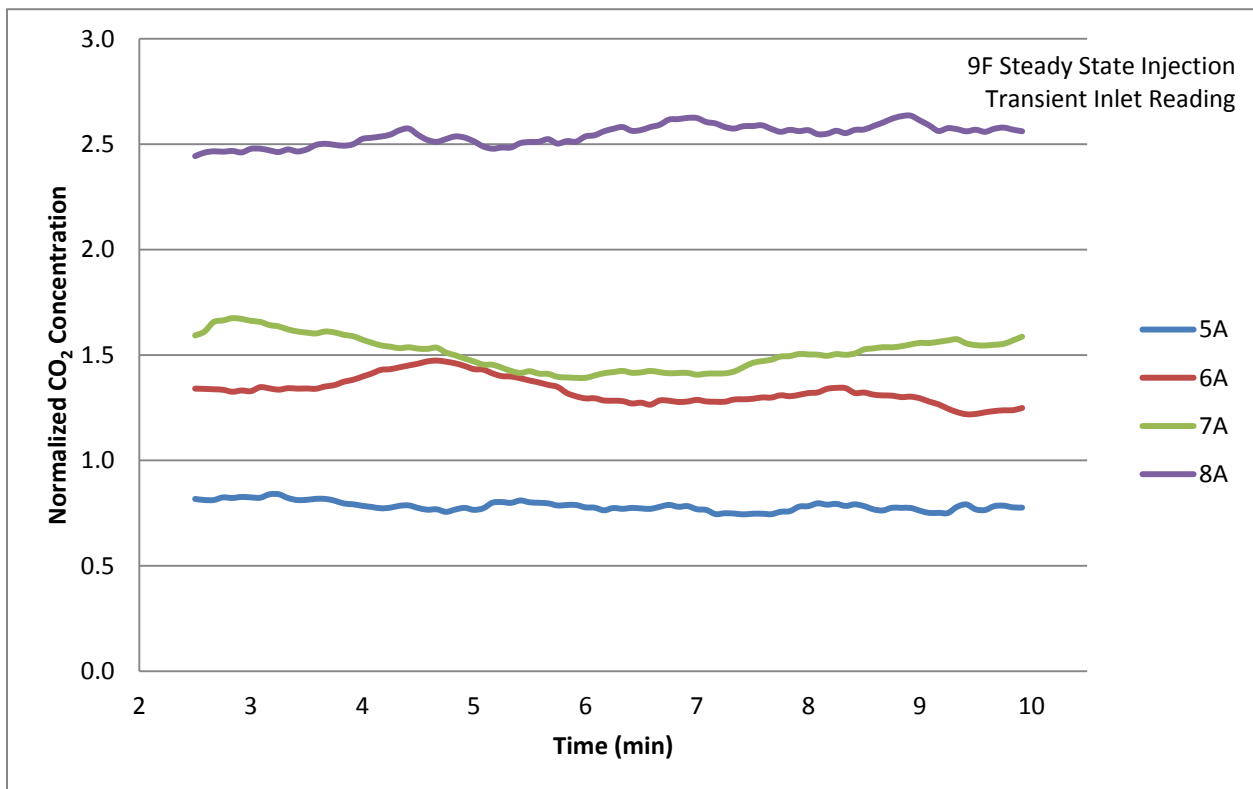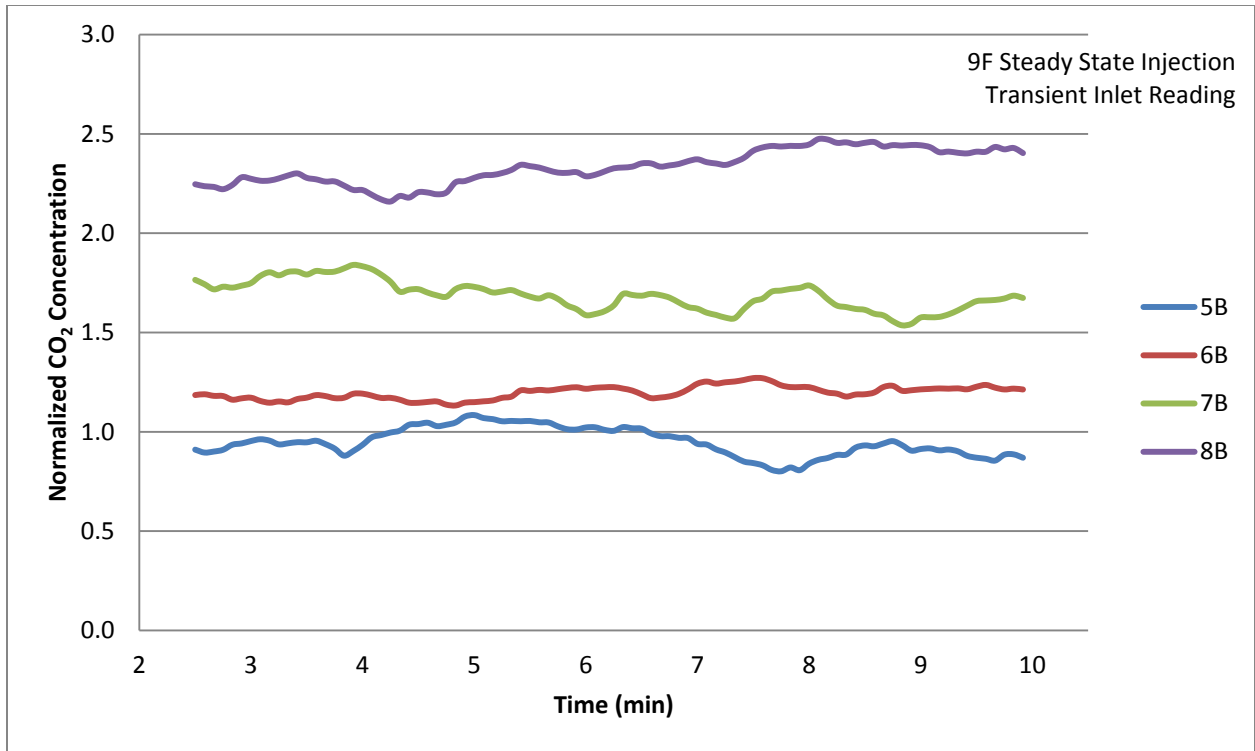**Figure 5.22 Seats 1-4A Cart Average (3 Runs)**
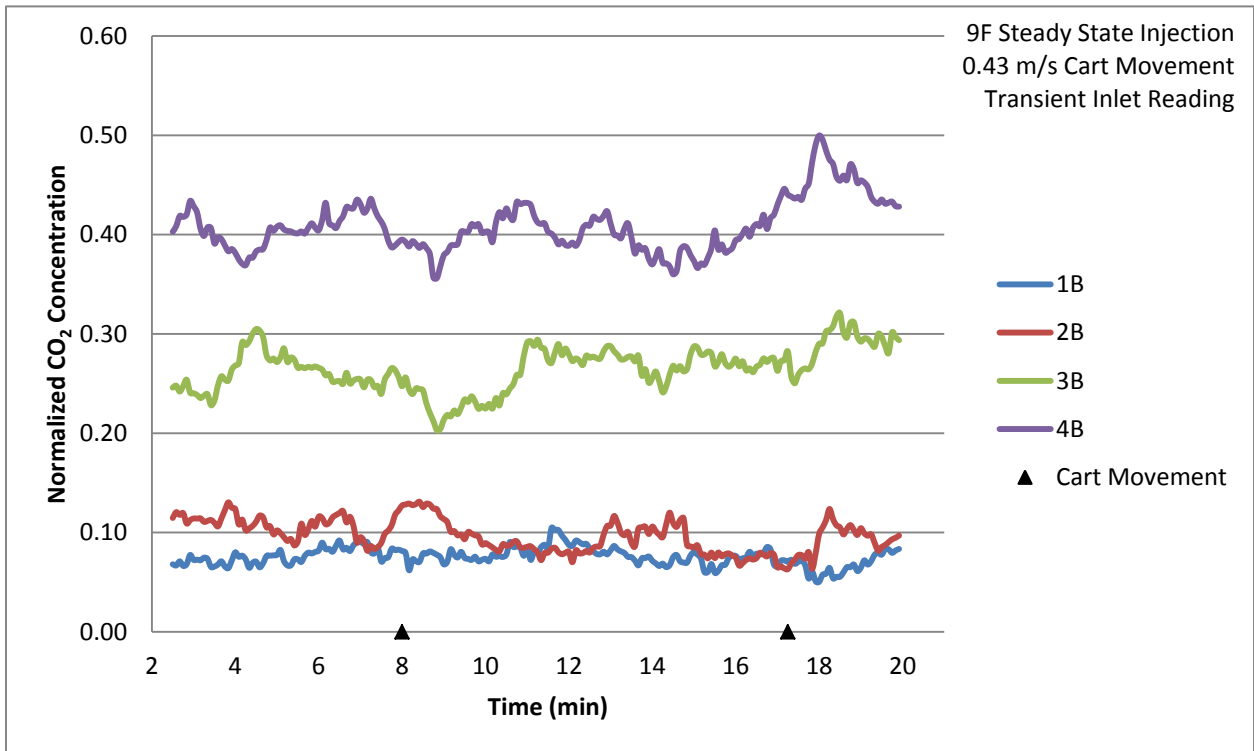
Figure 5.23 Seats 1-4B Cart Average (3 Runs)
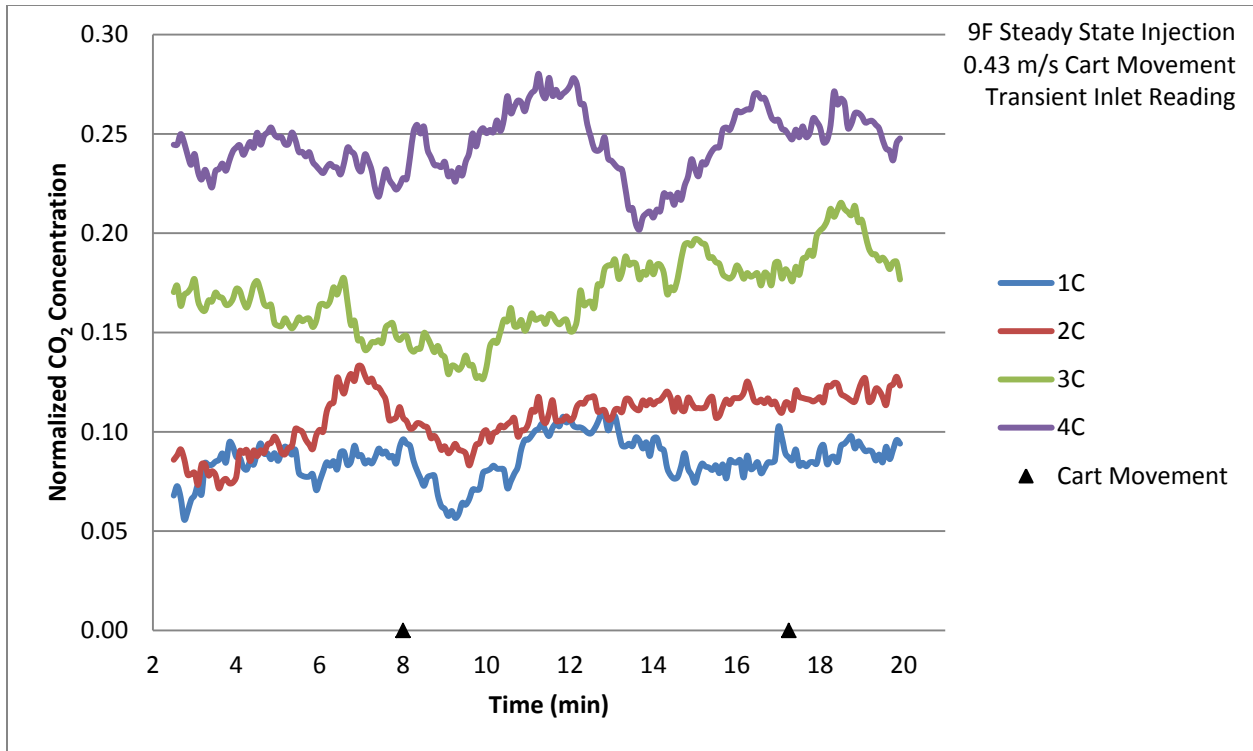
Figure 5.24 Seats 1-4C Cart Average (3 Runs)
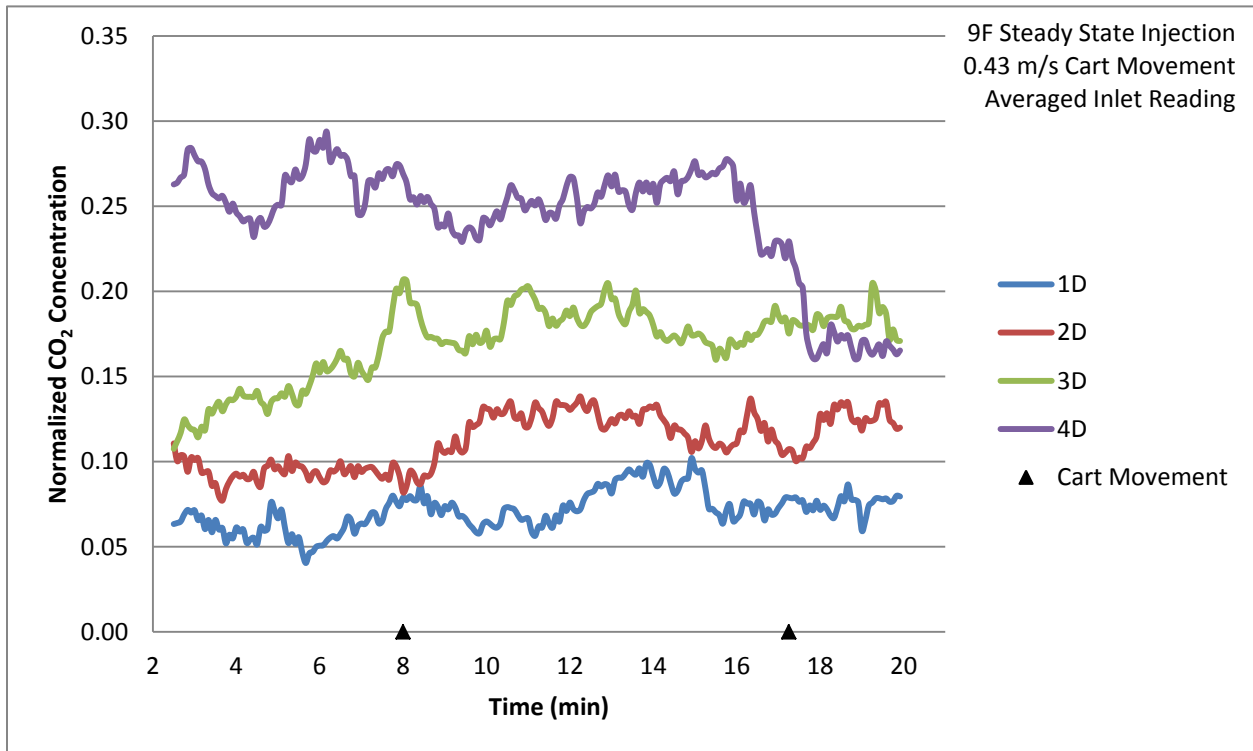
Figure 5.25 Seats 1-4D Cart Average (3 Runs)
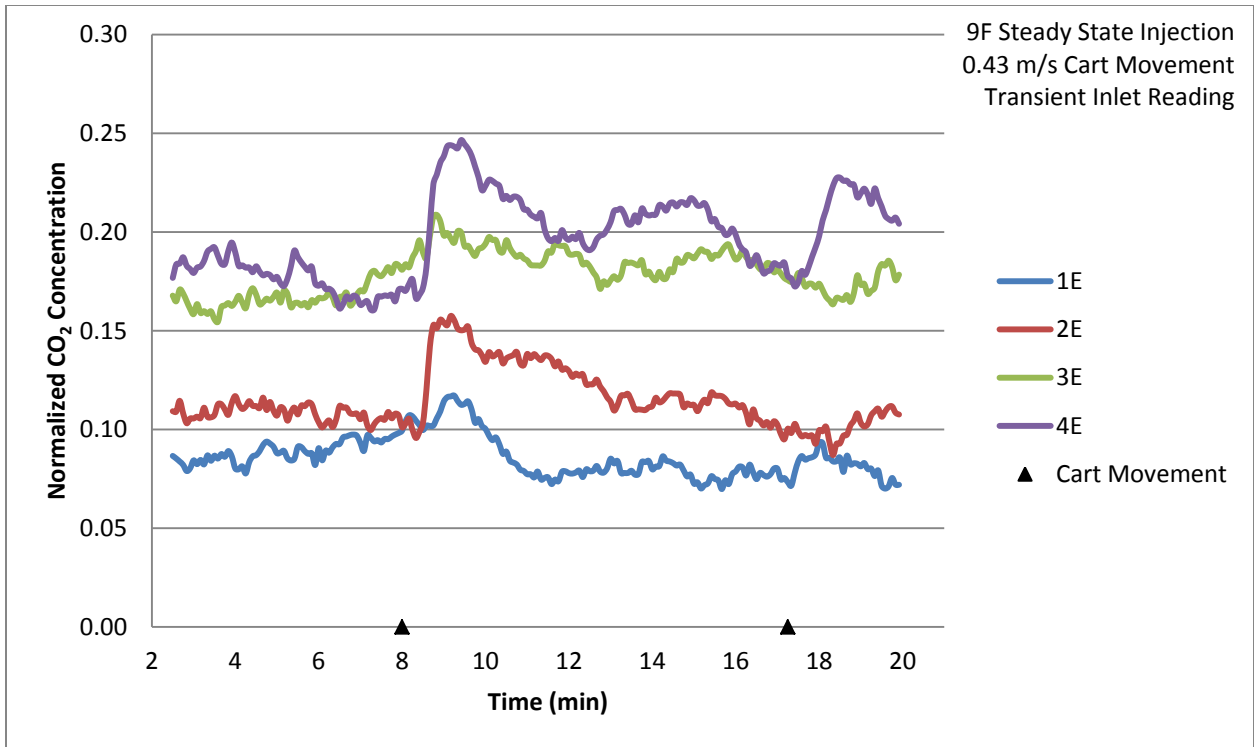
Figure 5.26 Seats 1-4E Cart Average (6 Runs)
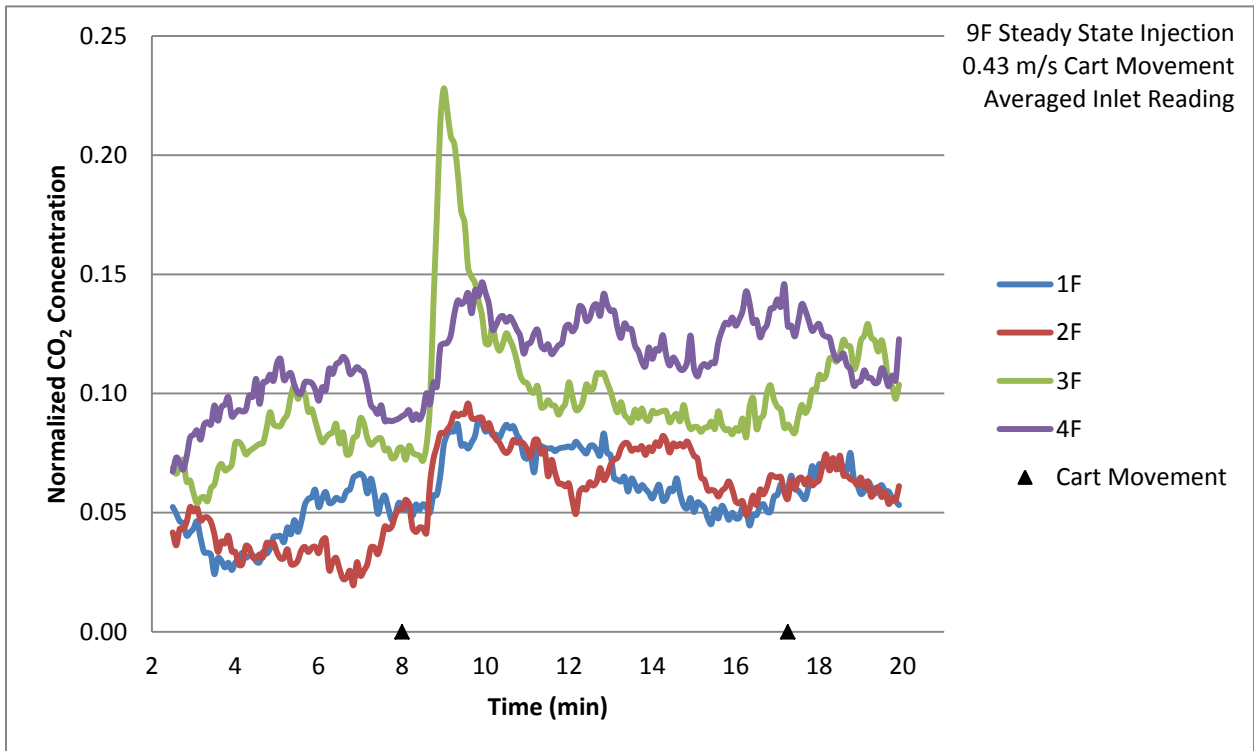
Figure 5.27 Seats 1-4F Cart Average (3 Runs)

54
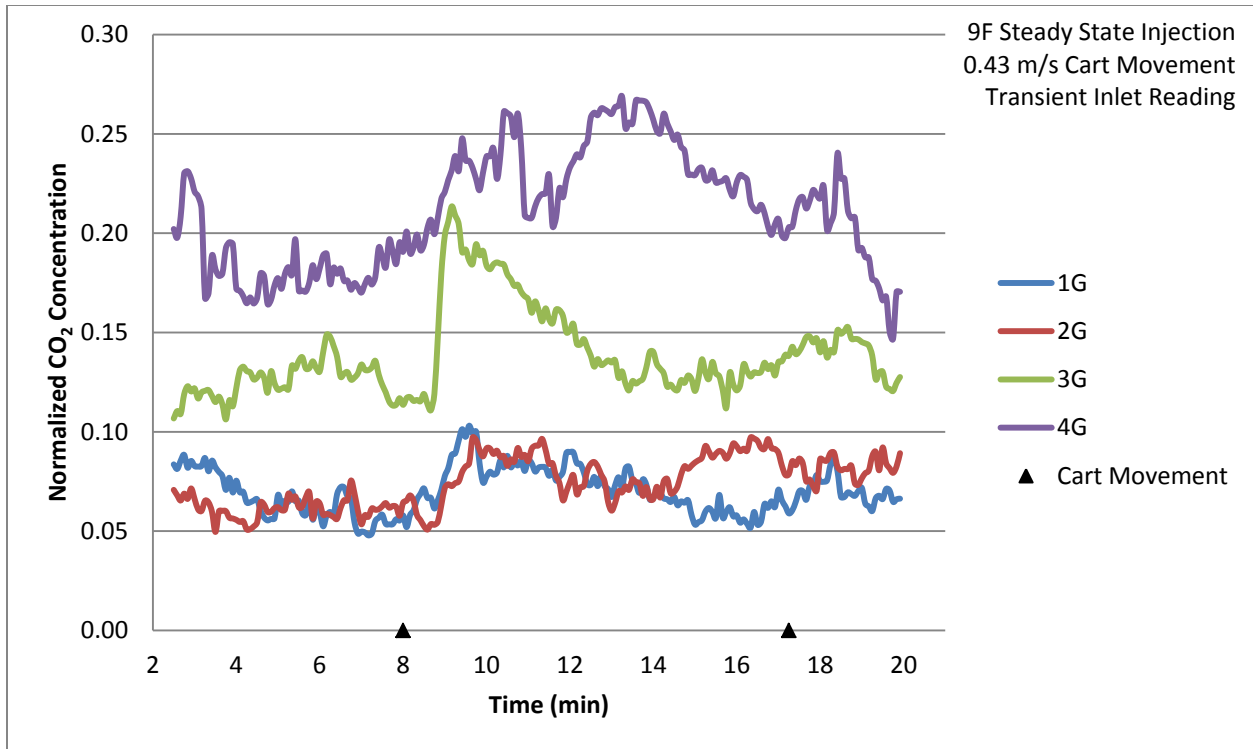
Figure 5.28 Seats 1-4G Cart Average (3 Runs)

Similar charts for the rear four rows of the test sample are shown in Figure 5.29 through Figure 5.35. The measurements from rows five through eight show less "peak" fluctuation due to cart movement, but still offer insight into the significance of cart movement wake in relation to other cabin variables. The majority of tracer gas concentration fluctuations in this area of the cabin are thought to be due, in large part, to the erratic behavior of the cabin ventilation airflow. The cabin experiences quasi-steady state flow where flow patterns change in periodic randomness. This effect accounts for the vastly larger random concentration variations in the rear two rows of the study sample. These rows are within two rows of the injection location and, therefore, the design airflow pattern mixes air amongst these rows consistently with no additional body movement in the cabin.

55
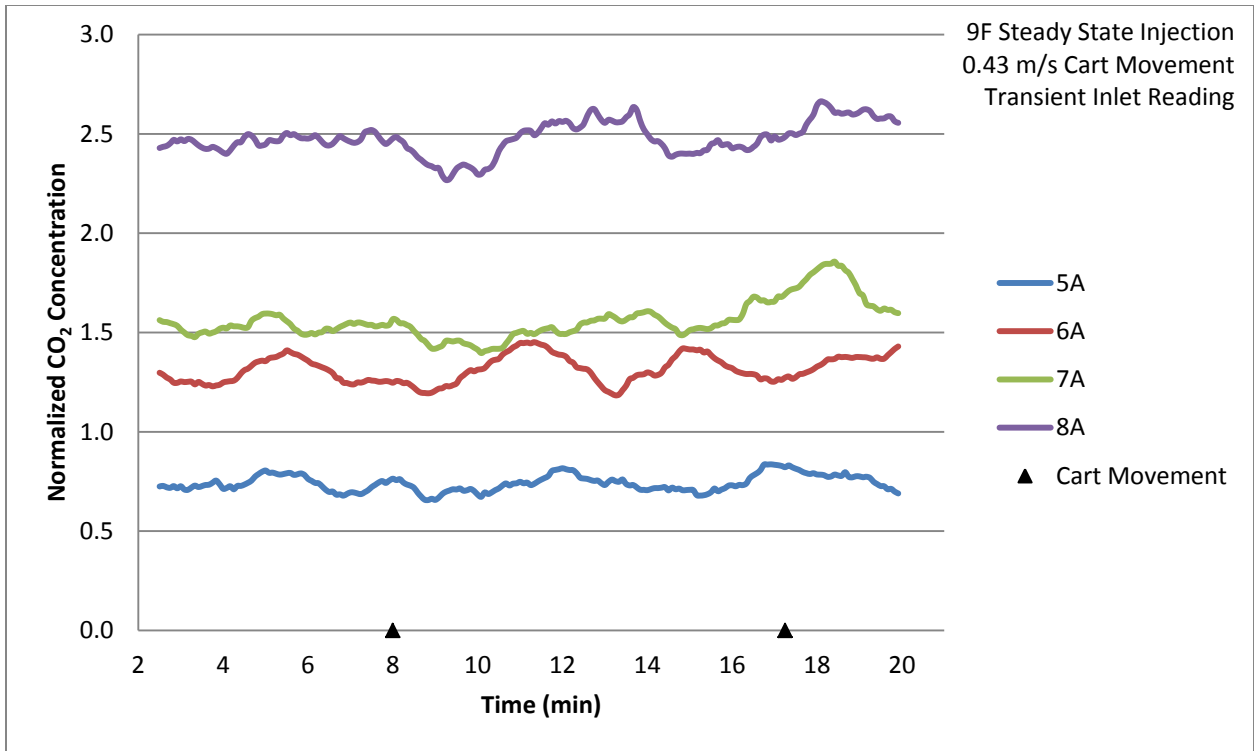
Figure 5.29 Seats 5-8A Cart Average (3 Runs)
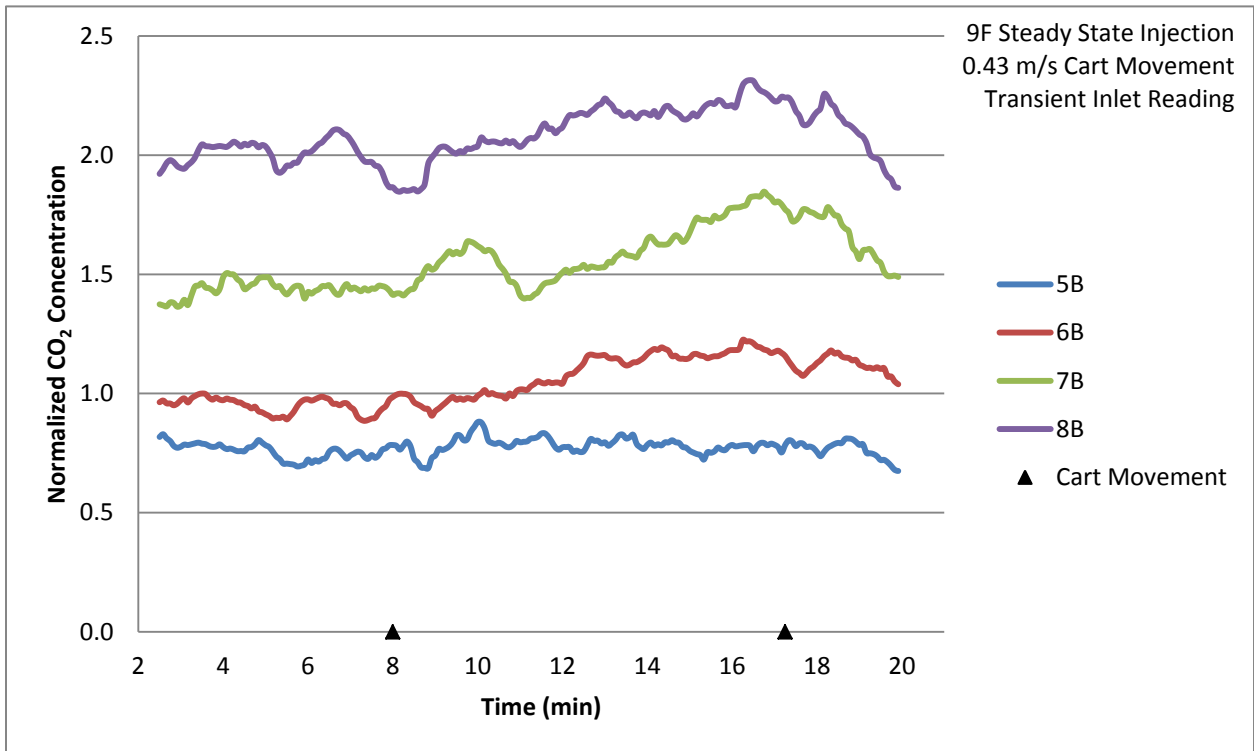
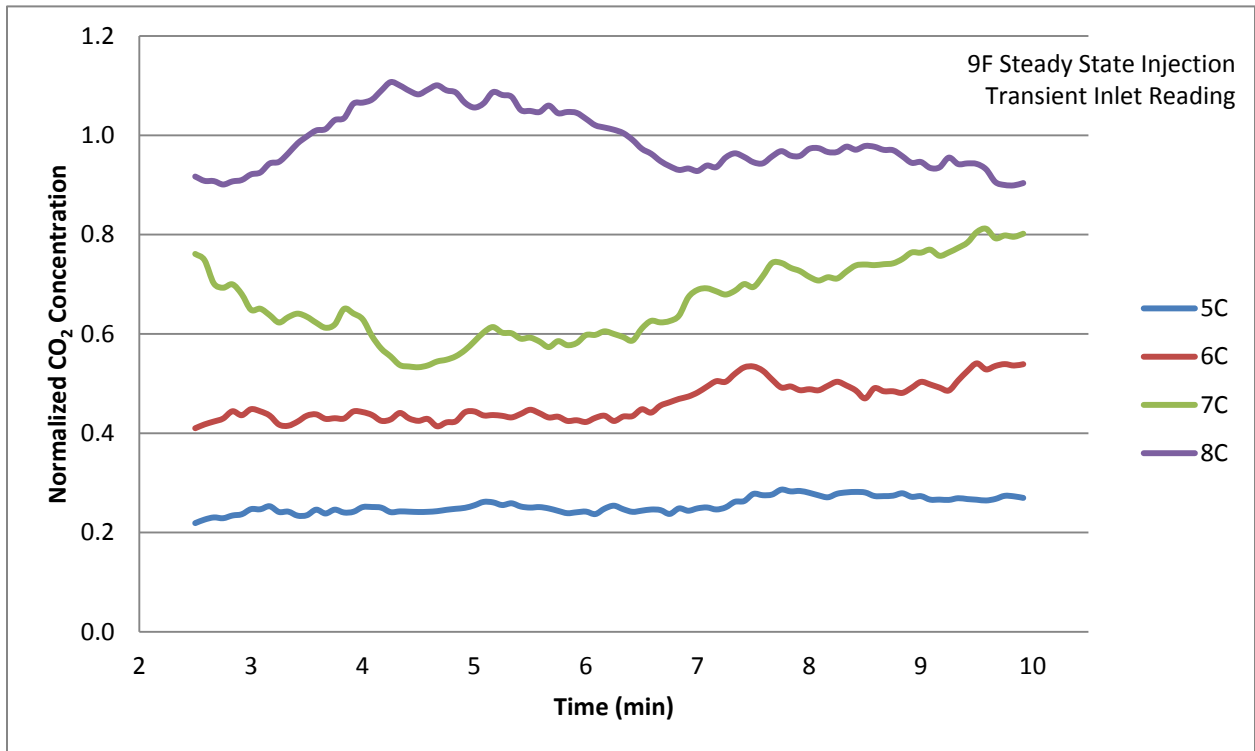**Figure 5.30 Seats 5-8B Cart Average (3 Runs)**

56
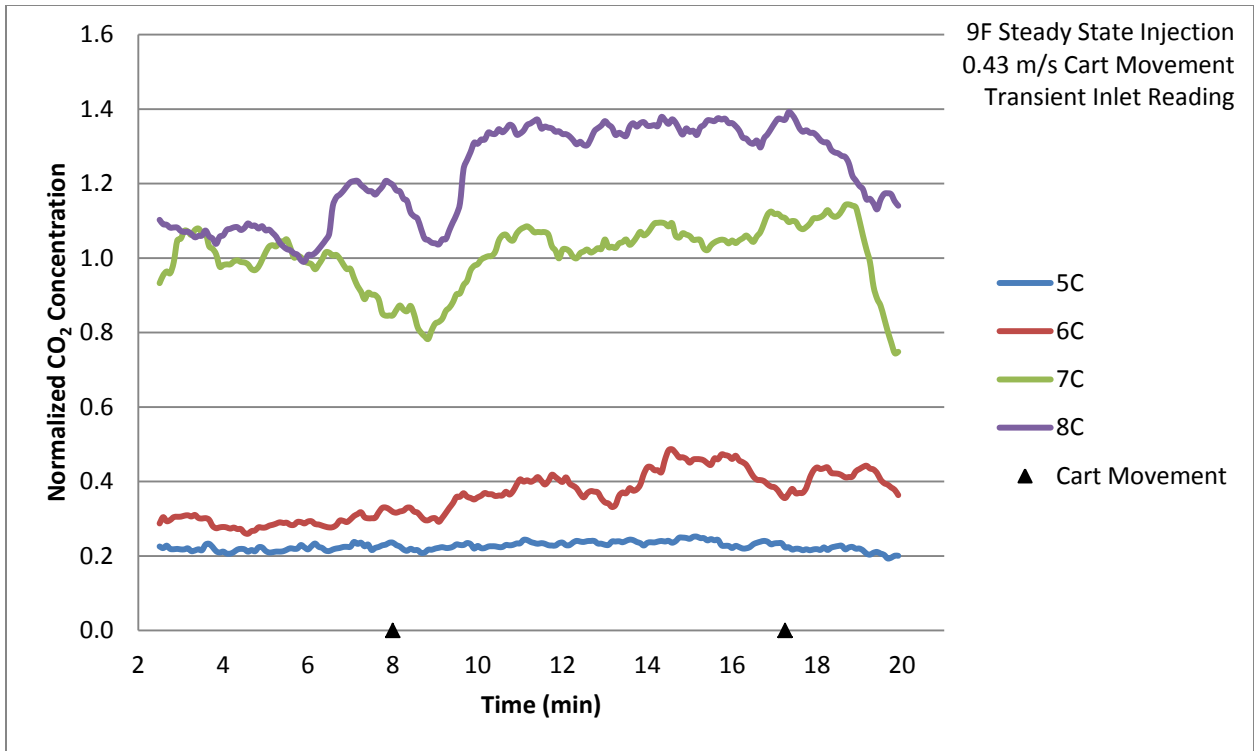
Figure 5.31 Seats 5-8C Cart Average (3 Runs)
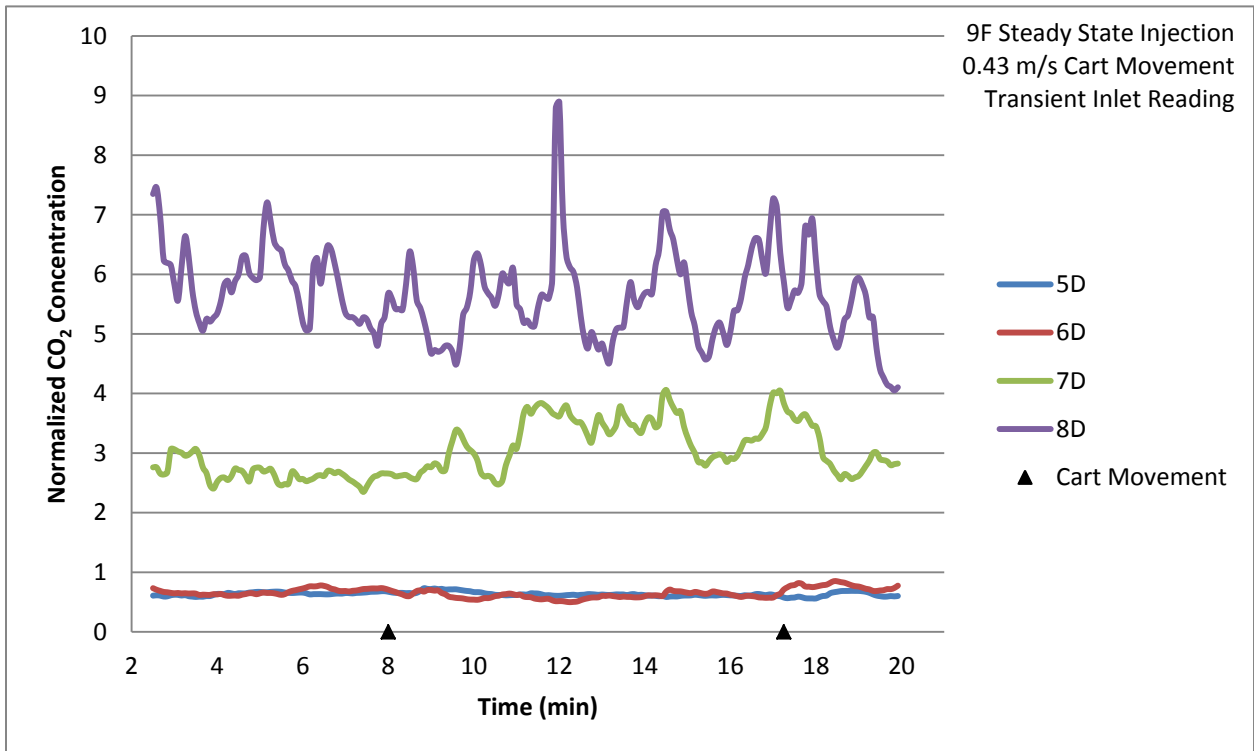
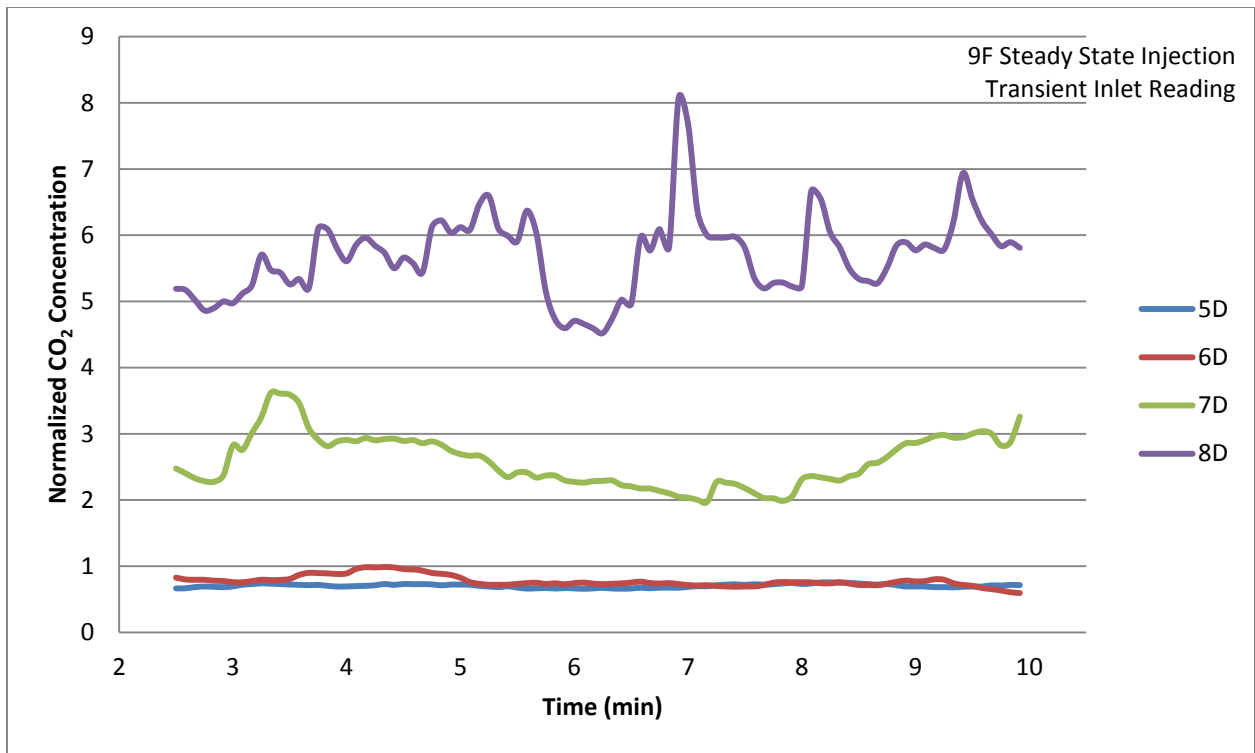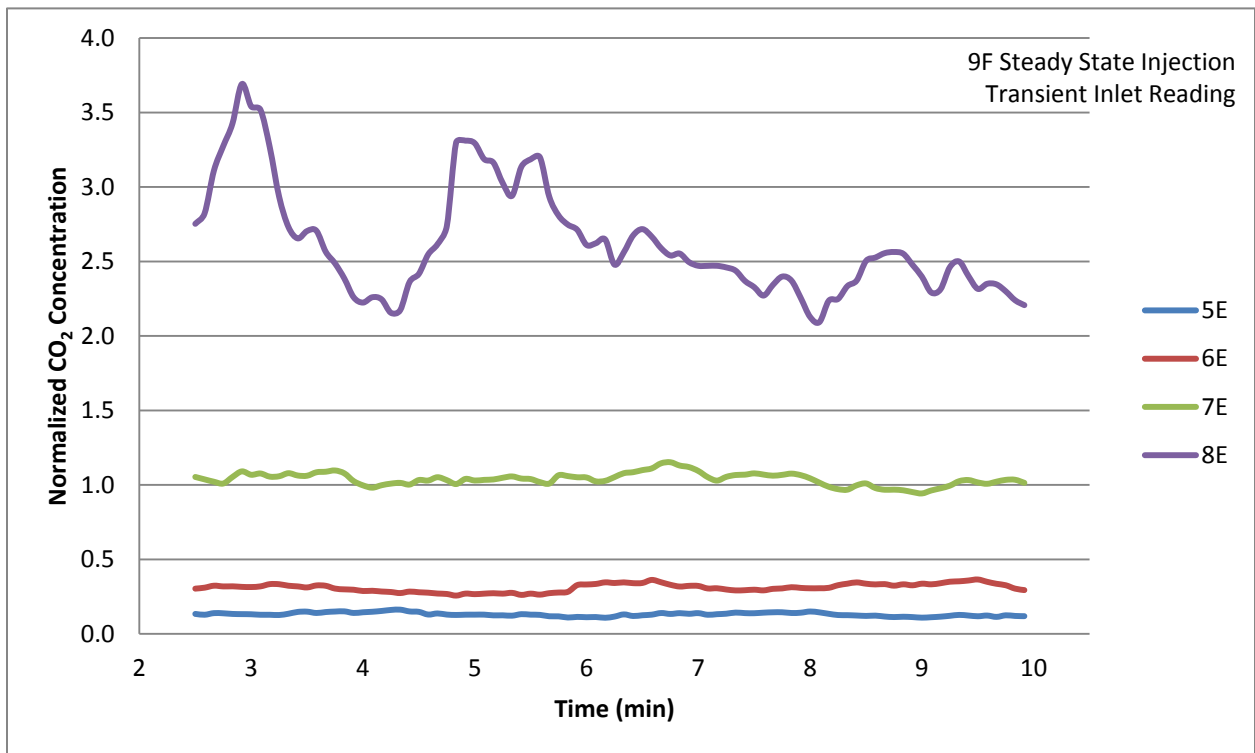**Figure 5.32 Seats 5-8D Cart Average (3 Runs)**
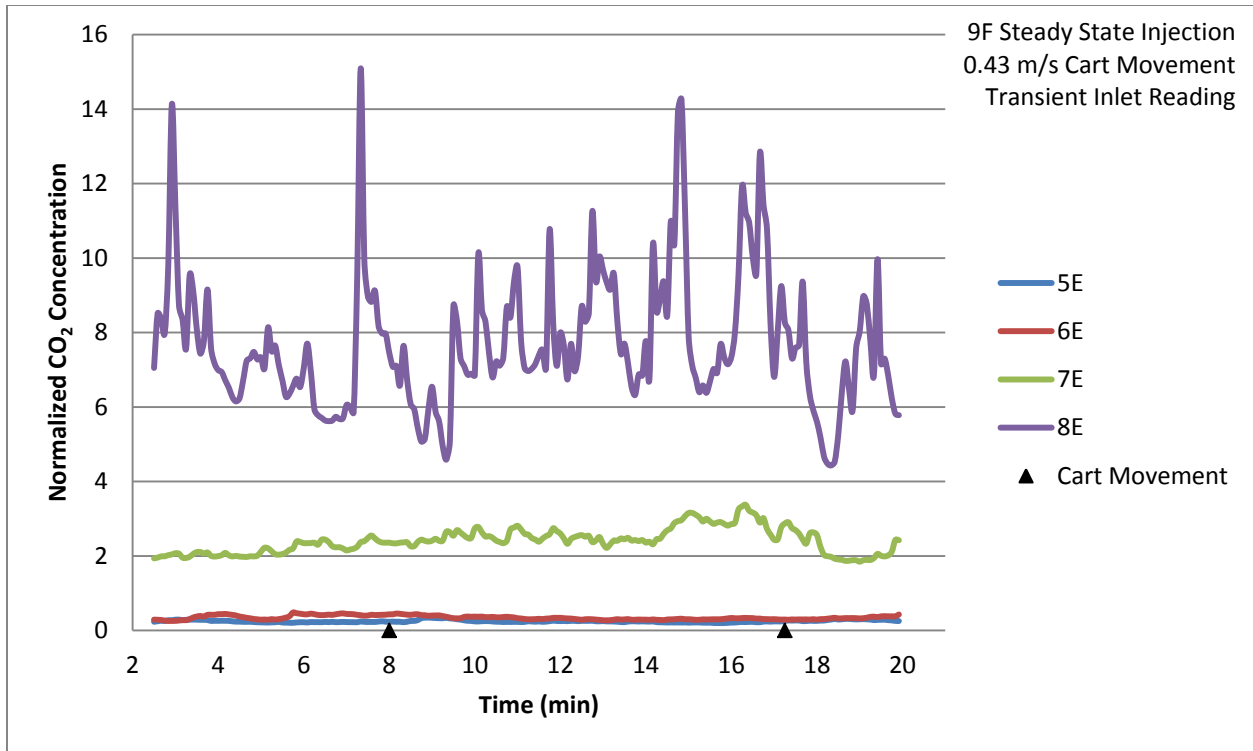
Figure 5.33 Seats 5-8E Cart Average (3 Runs)

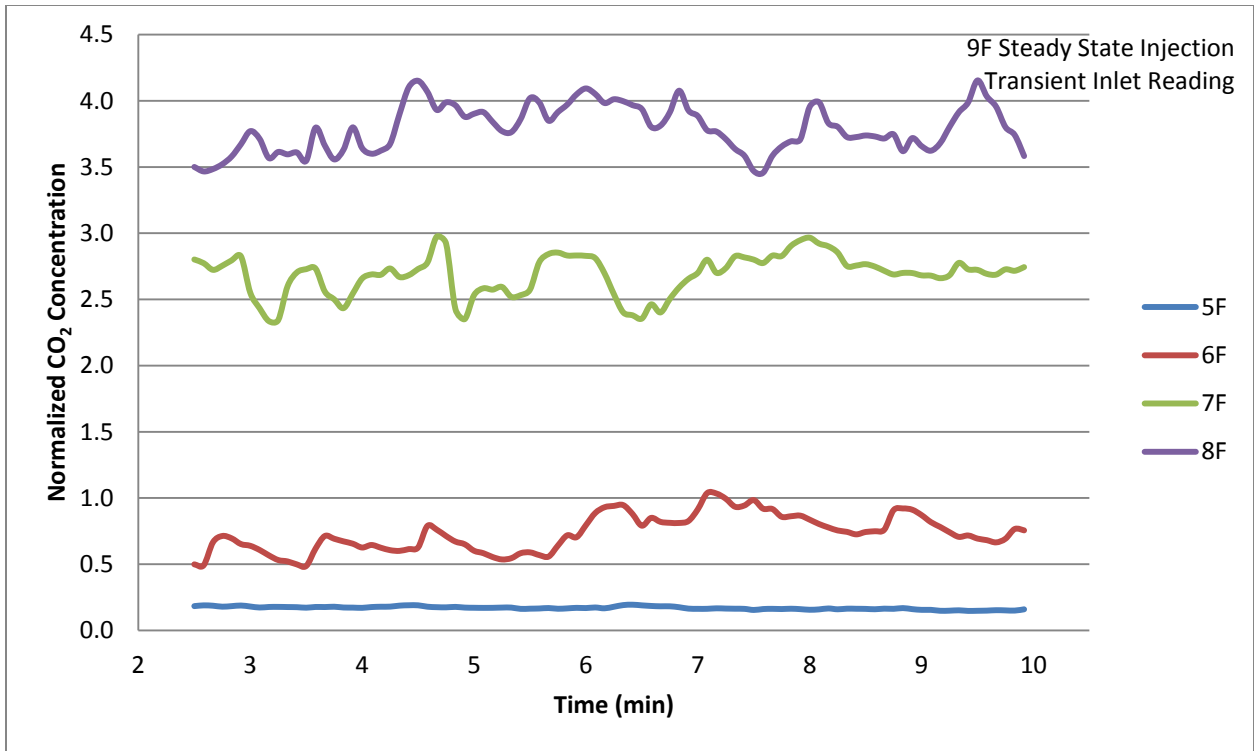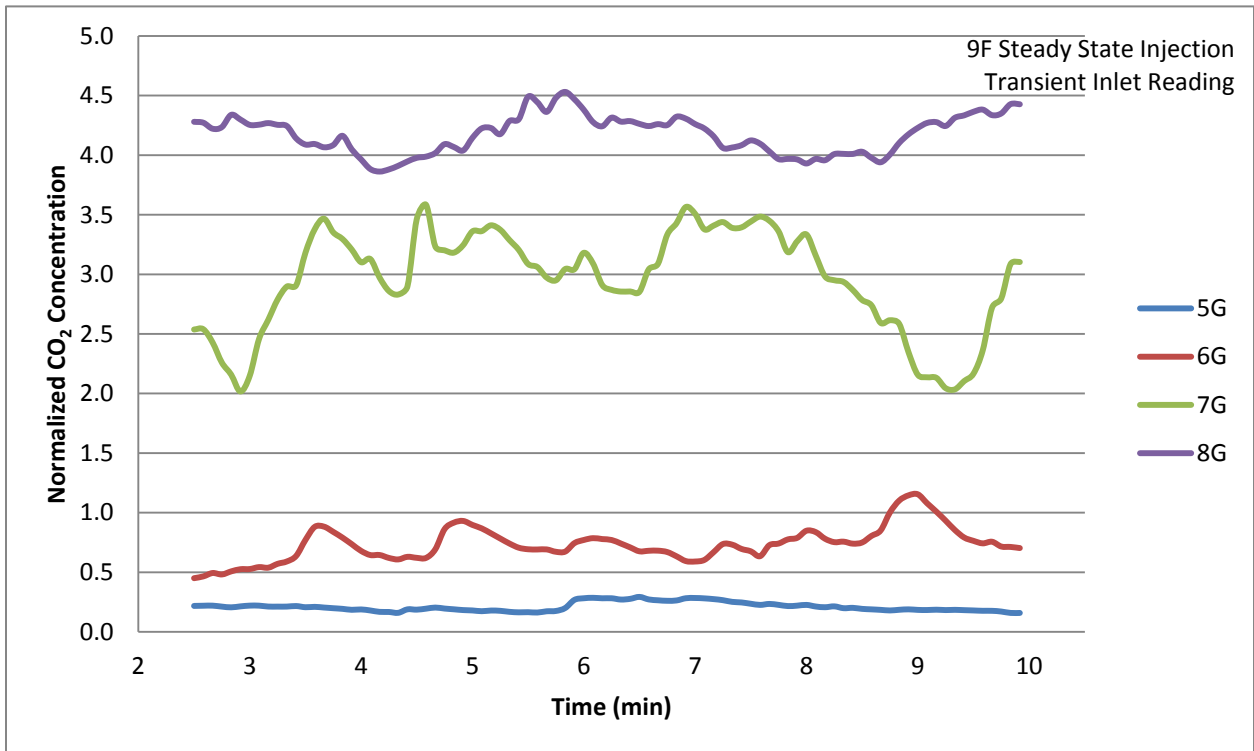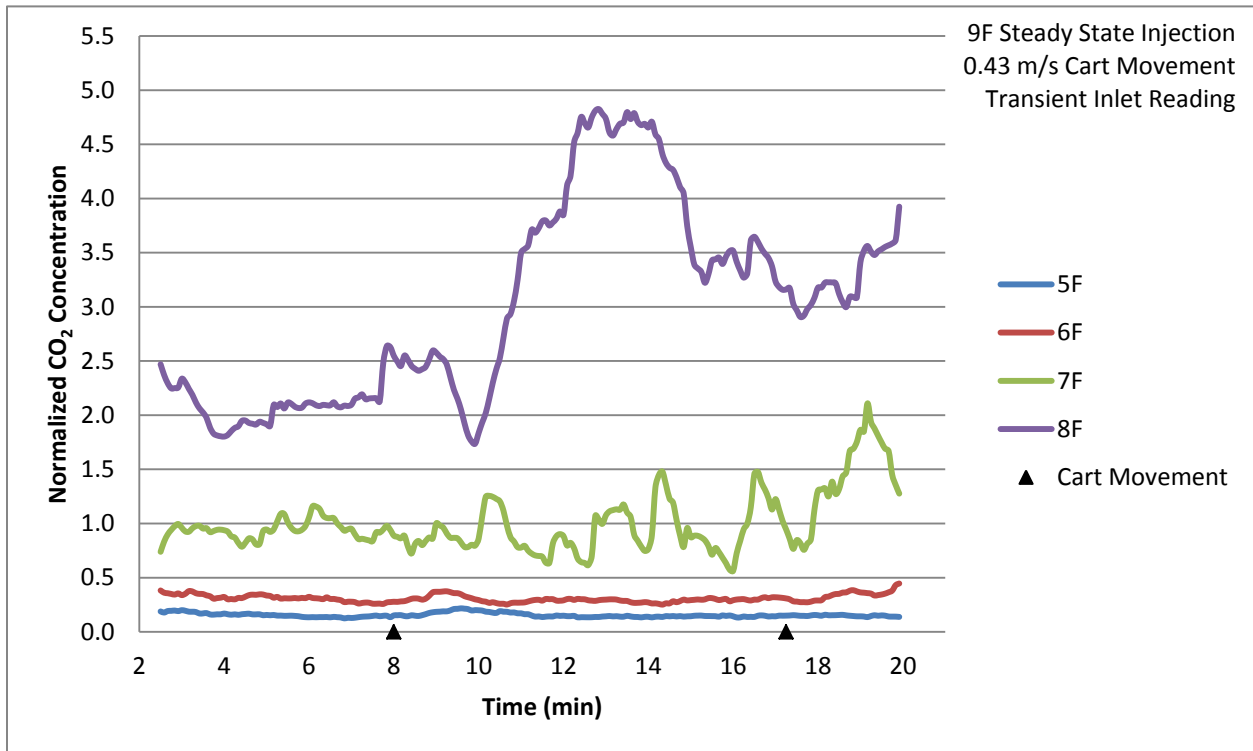
Figure 5.34 Seats 5-8F Cart Average (3 Runs)

58
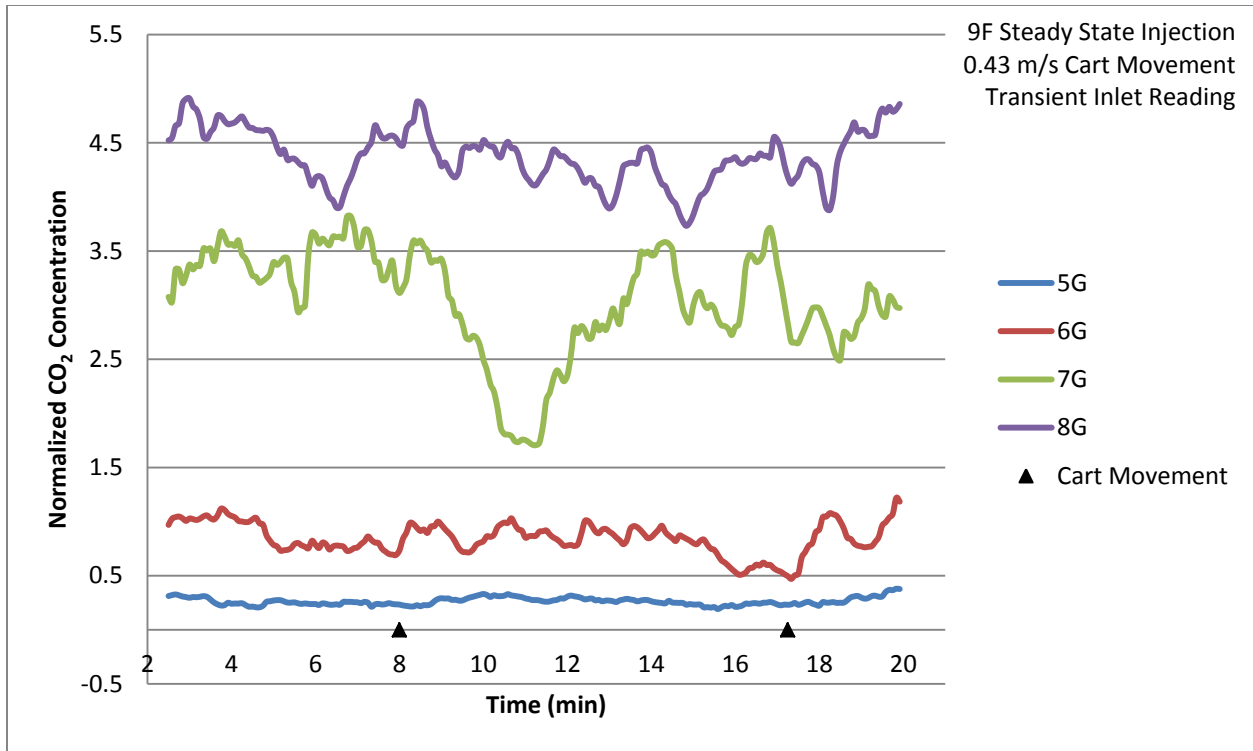
Figure 5.35 Seats 5-8G Cart Average (3 Runs)

When viewing averages for test runs with the cart, misinterpretations of the cart affecting tracer gas concentration can be made. Because the reader knows the cart movement timing, it can be easy to attribute randomness in tracer gas levels to a peak in concentration related to cart movement. It is important to put these variations into perspective by comparing seat location average readings with and without cart movement. To do this an algorithm was used to compare concentration level differences between runs with and without the cart movement.

5.5 Area under Curve Exposure Comparisons

While it was expected and reassuring to see cart movements affect the tracer gas concentration at particular locations, the effects need to be taken within context. For experimental findings to be relative to real-world situations, exposure duration needs to be accounted for as well as peak exposure levels. To enable comparisons between runs with and without the cart and relate these to term exposure rates, the average reading value for an entire run with and without the cart was calculated. The difference between the run with the cart and without was then tabulated and is presented conveniently in Figure 5.36.
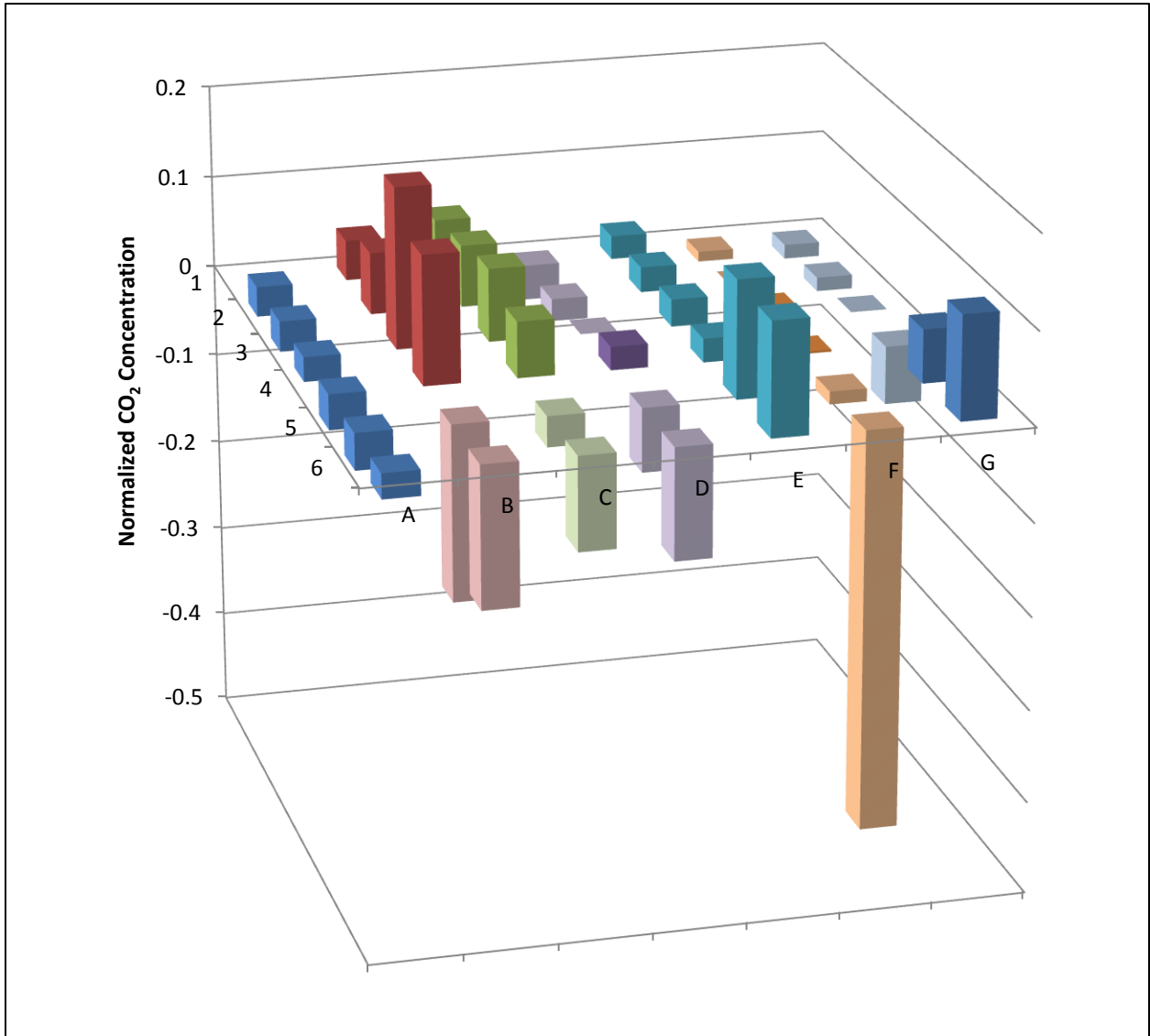
Figure 5.36 Area under Curve Exposure Cart/No Cart Comparison

It is possible for this calculated value to be negative, demonstrated by slightly faded coloring, due to random air movement fluctuations as well as negative concentration effects due to cart movement. This simply illustrates that cart movement had no positive effect on tracer gas concentration in these locations, and in fact, the noise of the signal and experimental variation were larger in magnitude than any increased concentration or the cart actually had a negative impact on concentration. This is especially true in rows six through eight because they are so near the injection location. Consequently, rows seven and eight were omitted due to the tracer

gas level being so high that variations in these readings would prevent any visible results from being realized in the forward rows.

It could be deduced from Figure 5.36 that the cart movement had a nearly random influence on tracer gas concentration throughout the cabin with the exception of the E column of seats. This seems odd when comparing this data to the data seen in Section 5.4, which show definite peaks in the tracer gas concentration corresponding to the cart movement for many seat locations. However, experimental randomness and airflow variations between tests run with and without the cart are so large this peak is lost in this data presentation. This result further solidifies the fact that ventilation airflow and experimental randomness are very significant factors in varying tracer gas concentration compared to the beverage cart movement.

To help bridge the gap between these indications of data, it was chosen to use an integration method which calculates the exposure area (exposure level multiplied by exposure duration) each cart movement triggered during the testing sequence. To extract this information from the experimental data during test runs with cart movement, the tracer gas level for the time period from 8 minutes (beginning of cart movement) to 13 minutes (after forward cart wake had fully settled) was averaged to a single value and then had the average for the remaining time period removed. This, in effect, calculates any exposure consequence seen by a passenger in a particular seat location due to a beverage cart passing by a contamination source at a location removed from the passenger while negating any steady state exposure to the contamination. Figure 5.37 illustrates these calculated exposure levels.
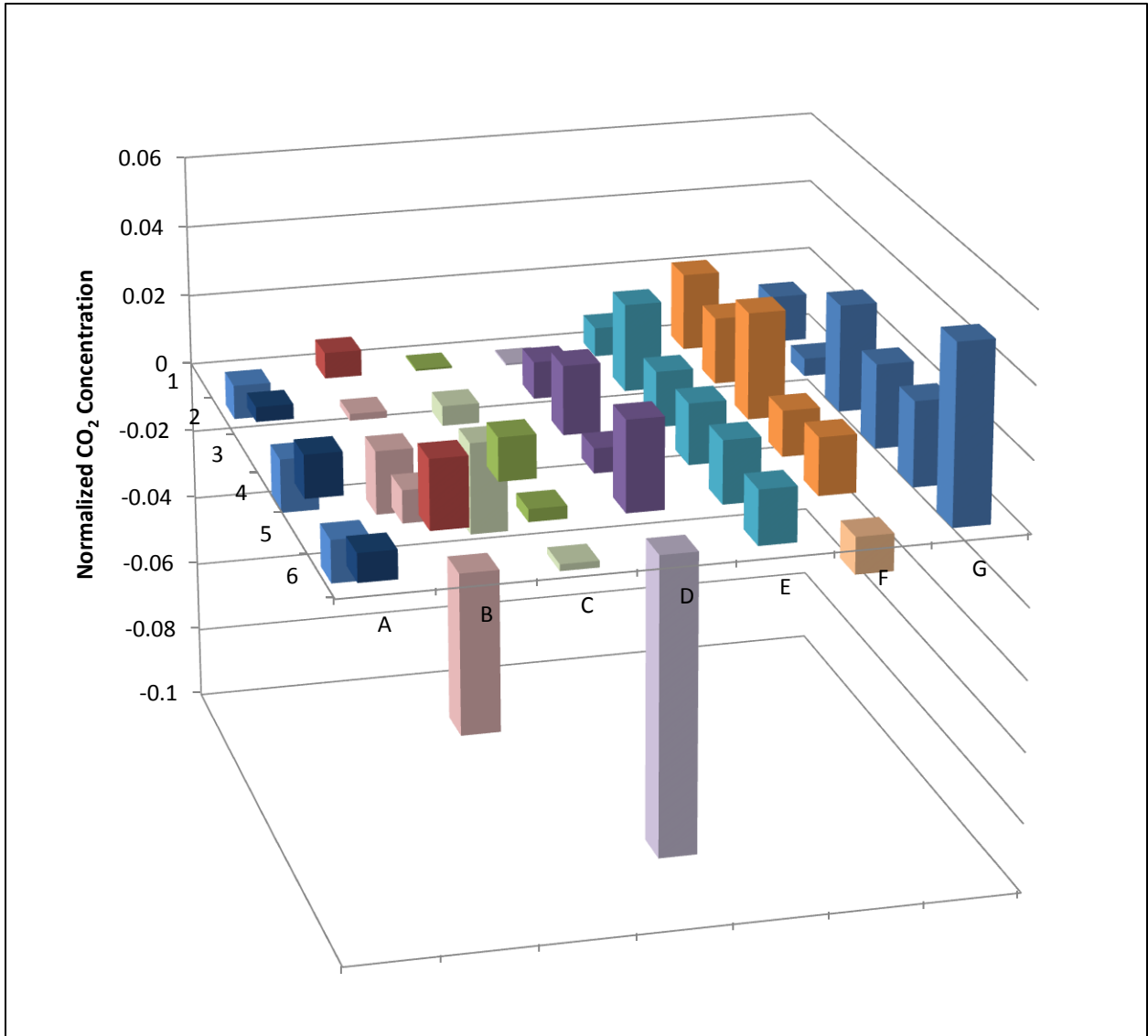
Figure 5.37 Area under Curve Cart Exposure

The phenomenon discussed earlier pertaining to a jet of ventilation air pushing across the aisle from 3E to 3F can be seen in these results as well. Seat locations beyond the centerline of the cabin from the injection location received marginal levels of additional tracer gas due to cart movement. Again, it is important to put these concentration variations in perspective. To aide in doing this, Figure 5.38 represents a single value average normalized concentration level for all three cart runs for a particular seat location. Notice the perspective of this chart is in the opposite corner of the sample area than previous three dimensional charts since the largest magnitude readings occur in the opposite corner.
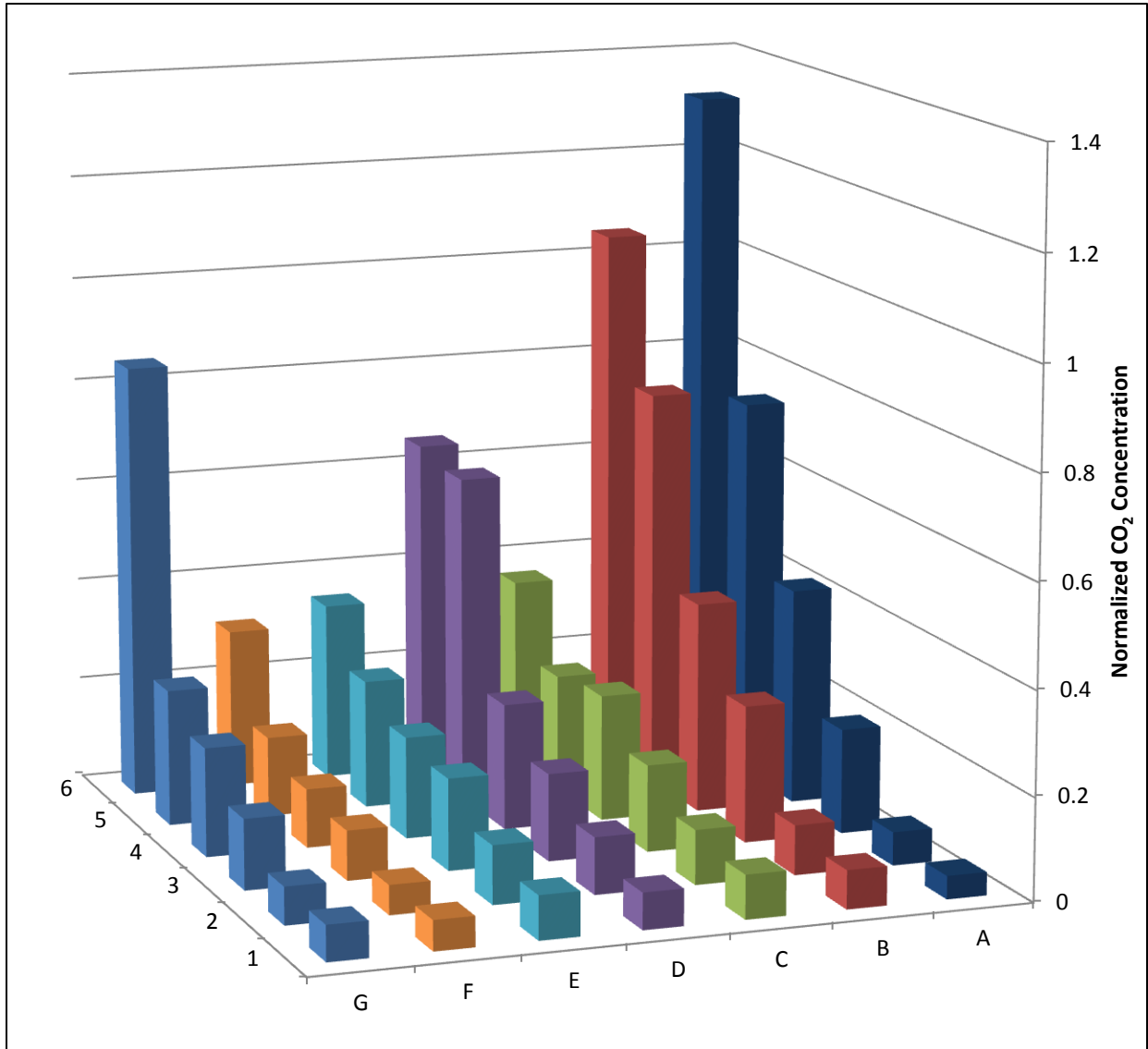
Figure 5.38 Single Value Cart Run Total Exposure Averages

A comparison between Figure 5.37 and Figure 5.38 shows the magnitude of variation due to the cart movement (including negative variations) to be generally less than 6% (average) of the single value average for the entire test. The relative variation is calculated by taking the difference between the normalized concentration during cart movement peak (five minutes) and the steady state concentration and dividing it by the steady state concentration to form a relative increase per seat location. The 6% variation does need to be weighted by a standard deviation of nearly 12% to account for the spread of positive and negative values. The largest concentration increases due to cart movement in the sample were seats 1F through 3F with increases in

normalized concentration of 37, 32, and 31%, respectively. This result is largely due to the low steady state concentration in this area of the cabin. Table 5.1 tabulates the relative concentration variation due to beverage cart movement for each seat location in the sample.

Table 5.1 Relative Concentration Variation Due to Cart Movement

	A	B	C	D	E	F	G
1	-21.4%	9.8%	0.6%	-0.7%	9.6%	37.0%	19.0%
2	6.4%	-2.0%	-5.3%	9.4%	21.6%	32.3%	6.7%
3	-7.4%	-6.8%	-15.4%	11.5%	8.8%	30.9%	21.8%
4	2.9%	-2.3%	5.0%	2.8%	8.7%	11.3%	11.2%
5	-1.6%	2.5%	1.6%	4.0%	7.1%	10.4%	9.0%
6	0.6%	-4.2%	-0.5%	-12.8%	4.4%	-3.3%	5.9%
7	-6.8%	-4.1%	-5.6%	4.1%	5.6%	-19.6%	-19.9%
8	-2.0%	-2.6%	3.2%	-2.0%	-5.1%	3.7%	-0.2%

While inspecting these relative variations it is important to note that, with the quick air change rates in an aircraft cabin, the effect of increased concentration level due to cart movement is only sustained for, at most, five minutes. As can be seen in the figures in Section 5.4, any elevated concentration level decays quickly after reaching a peak. When considering the beverage cart may only pass a particular passenger location once or twice during a flight of several hours, a five minute elevated exposure of 20% is not particularly startling given the steady state exposure duration. This is assuming a biological exposure-infection relationship which is linearly proportional to exposure rate-duration.

5.6 Fast Cart Movement

In the standard eight row testing, some of the more interesting results occurred in the forward seats of column E. To determine the effect of a faster cart movement, it was decided to conduct analogous testing for these seats. For this phase of testing all cart movement was at 0.61 m/s, or the speed of a brisk walk, with identical timing events as the 0.43 m/s cart movement tests, as described in Table 4.2. Figure 5.39 depicts the average of six runs for each the slow and fast cart speeds for the forward seats of column E. The standard speed results are included in a coordinated, lighter color to allow for direct comparison.

Many trends extend between cart speeds including general concentration peak behavior relating to the cart movement, but with additional magnitude for the faster cart speed. Though the peaks of the concentrations are higher, there seems to be no tangible deviation in the decay rate of the heightened concentration. Similar to the standard speed test, seat 3E continues to show much less effect in normalized concentration due to cart movement than the seats fore and aft. A small peak looks to be beginning to form just after cart movement, but its magnitude does not reach the level of concentrations at other instances in throughout the averaged experimental run. Thus, any effect due to cart movement is less than the magnitude of experimental and instrument variation.
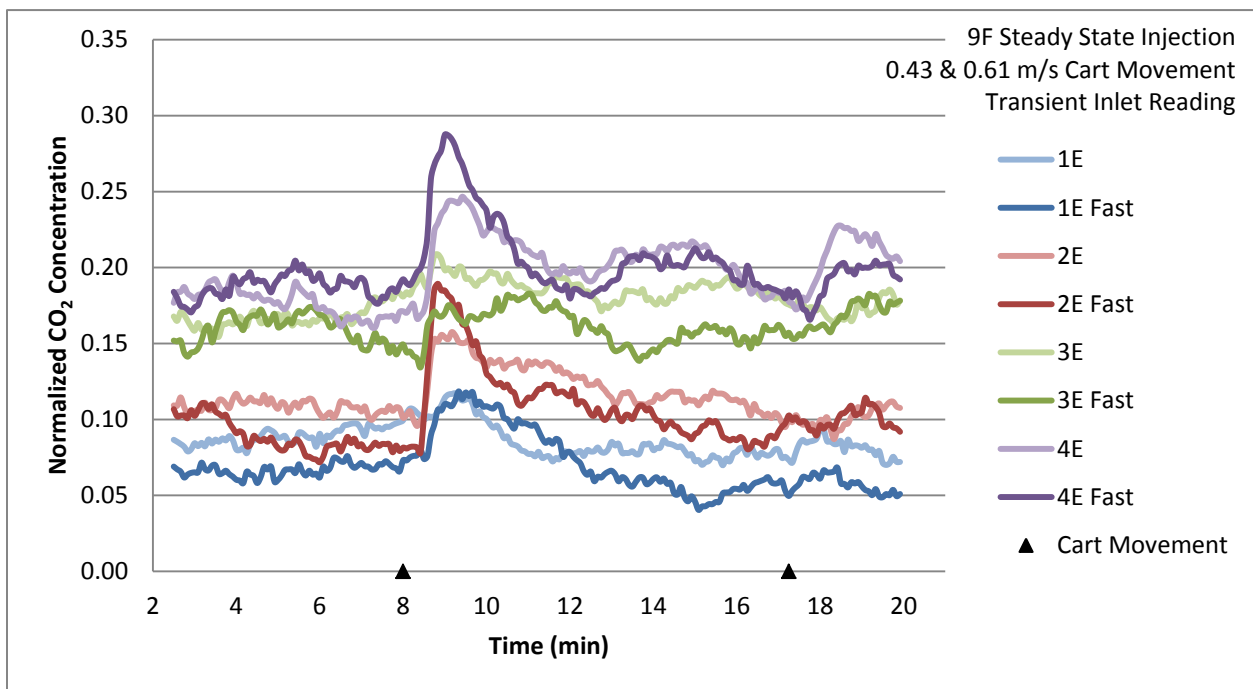
Figure 5.39 Seats 1-4E Fast & Standard Cart Average (6 Runs)

The area under the curve was also calculated for the fast cart tests for direct comparisons with the standard eight row test. For seats 1-4E, Figure 5.40 illustrates the calculated exposure for the concentration increase due to the cart movement for both cart speeds.

As would be expected from the results seen in Figure 5.39, the cart wake clearly becomes a larger portion of the total concentration level experienced at a particular location with the 0.61 m/s compared to the 0.43 m/s cart movement. For seats 1E through 4E, the relative concentration increase due to cart movement was 33.2, 26.0, 4.5, and 11.2%, respectively.

65

While larger than the relative exposure increase with the slower cart movement, a beverage cart wake at this speed is a worst case scenario. Actual aircraft cabin scenarios would rarely, if ever, reach aisle speeds this fast with such a large profile body.
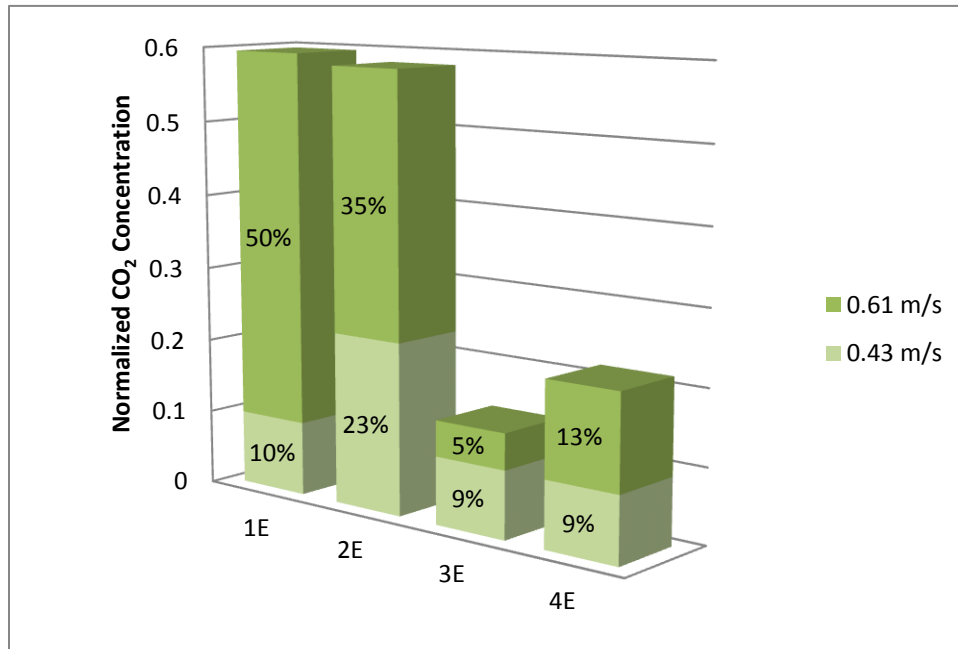
Figure 5.40 Fast and Slow Cart Area under Curve Exposure Levels

5.7 Moved Injection Location

To study the effect of moving the injection location, the injection apparatus was moved forward two rows to seat 7F. All other testing parameters outlined in Section 4.2 remain the same. It is important to note while comparing results, that analogous seat locations are now 1E to standard 3E, 2E to standard 4E and so on.

It can be seen in Figure 5.41, some phenomena experienced for the original injection location remain the same in relative seat locations, while others remain in absolute locations throughout the cabin. In general, the normalized concentration readings for an injection at 7F show a much cleaner (less noise) peak due to cart movement. This happened in all four seat locations, including 3E. With the relocated injection, seat 3E exhibited a large concentration peak corresponding to cart movement. This is in stark contrast to previous results with a 9F injection,

where no noticeable effect was seen other than a possible a hint with the faster cart speed. This is a very interesting point considering each individual experimental run with an injection at 7F produced a cart peak in seat 3E.
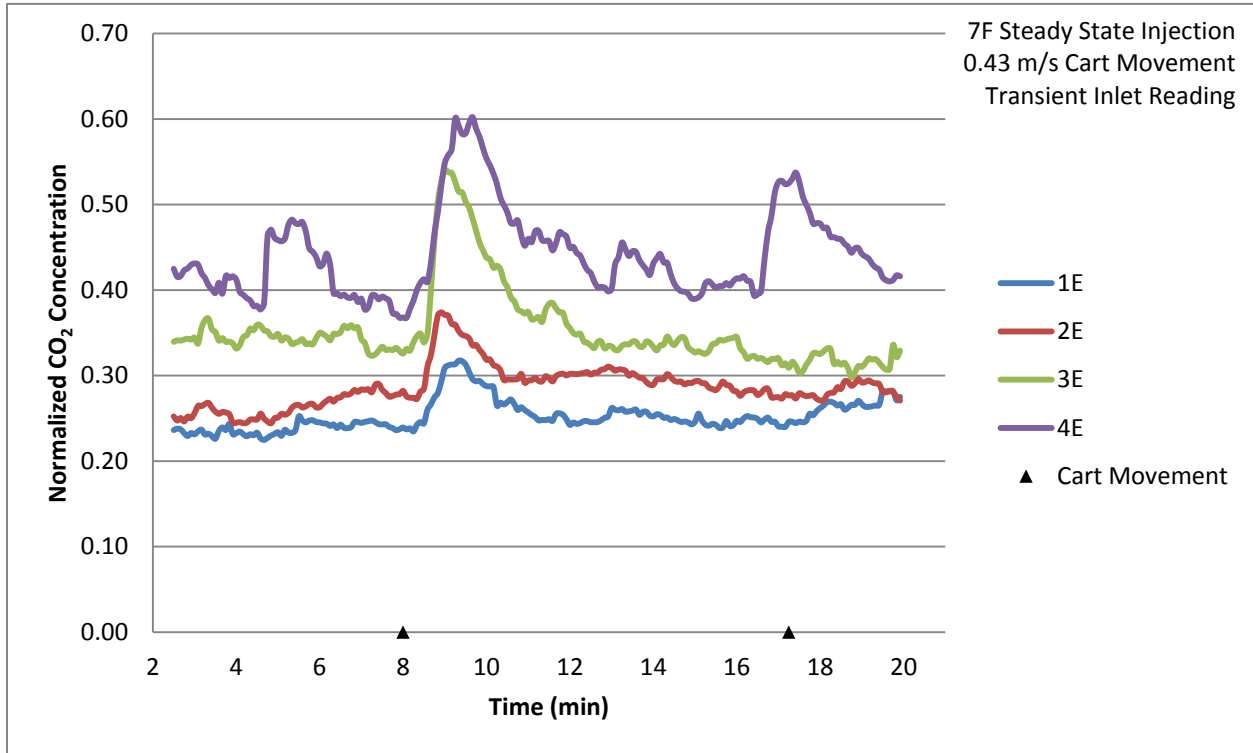
Figure 5.41 Seats 1-4E Cart Average with 7F Injection (3 Runs)

Figure 5.42 shows the same concentration readings with the corresponding relative seat location to the 9F injection plotted as well. Quick inspection reveals the concentrations for corresponding seat locations are larger across the board. It can also be seen the readings during the 7F injection generally have much less noise and appear cleaner throughout the experiment, not just around cart induced peaks.
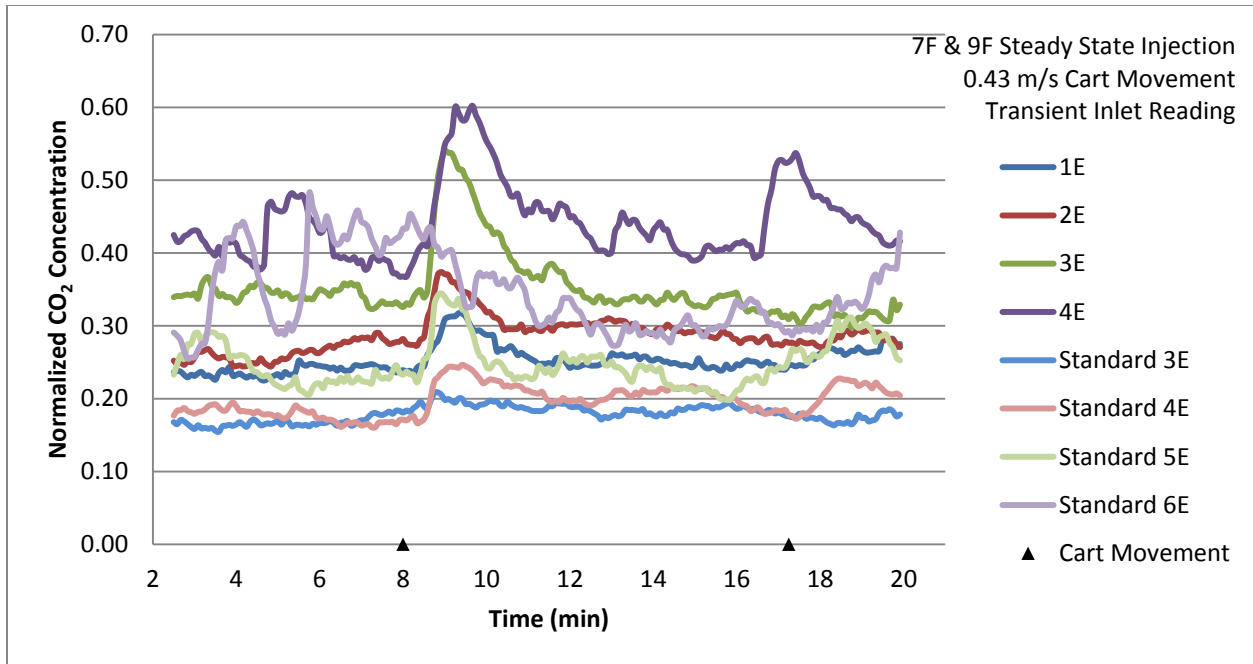
Figure 5.42 Seats 1-6E Cart Average with 7F & 9F Injection Comparison (3 Runs)

Combining these two observations would indicate the airflow pattern of the cabin is less erratic between the sampling locations and seat 7F than it is between the sampling locations and seat 9F. Beneke (2010) also documented a large clockwise eddy swirl which encompassed most of the cabin mockup. The north edge of this eddy, toward the rear of the cabin, could be a contributing factor to the much more random airflow patterns observed around seat location 9F than 7F.

During extensive diffuser velocity profile measurement, it was found the mean velocity in the west diffuser rises to a maximum of 1.8 m/s several times over the length as shown in Figure 5.43 (FAA, 2008). The peaks in velocity correspond to feeder duct connections as typically shown in Figure 3.12 and Figure 3.13. It was also noticed there is a sharp velocity transition near the supply "jet" located at seat locations 3E and 3F, 2 m from the front cabin wall. This is also the location of a union in the main supply duct as well as a feeder duct-to-diffuser connection. These variations in diffuser velocity as well as the boundary between the large cabin eddy and a smaller counter-rotating eddy across the front two or three rows of the cabin could contribute to the jet seen in these seat locations.
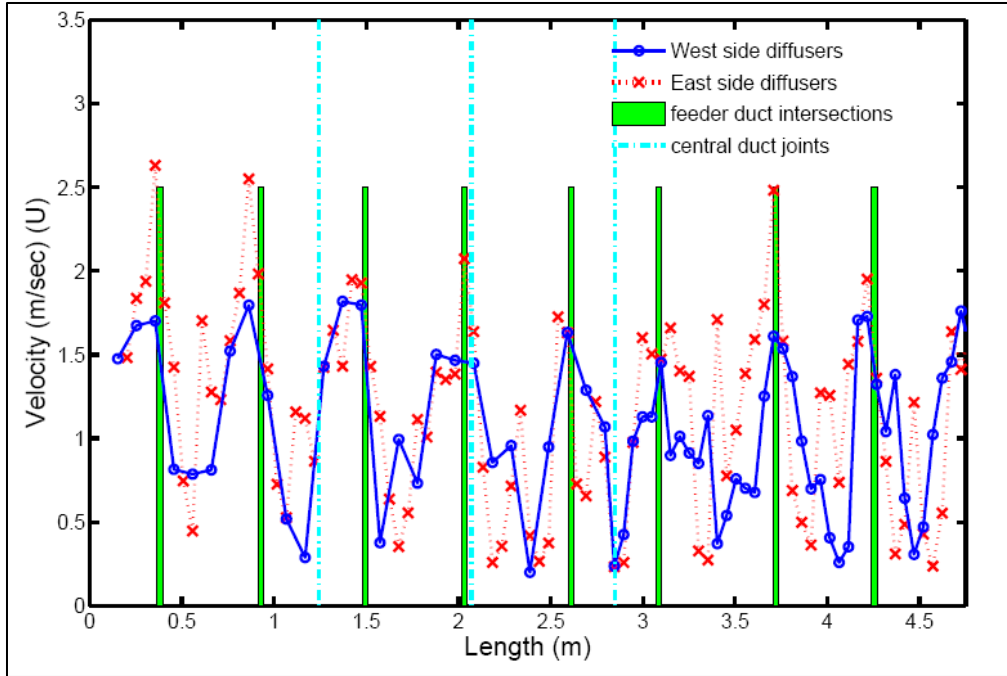
Figure 5.43 Diffuser Velocity Profiles

Chapter 6 - Confirmation

6.1 Visualization

As a supplement to numerical data presentation, the ability to visualize activities in the cabin mockup during tracer gas injection and cart traverse is oftentimes helpful.

6.1.1 Eddies & Erratic Flow

While the data sample collected certainly indicates there is a moderately predictable result when the beverage cart traverses past a contamination source, the measured effect becomes less clear with run-to-run variations. In many cases, the experimental variation between identical tests trumps the variation in tracer gas concentration linked to cart movement. It became obvious when using a tracer gas infused with smoke, the airflow pattern in the cabin can be quite erratic. The smoke can also visualize the eddy behavior in the cabin. A large eddy encompasses nearly 80% of the cabin in plan view while counter rotating eddies fore and aft fill the remainder.

6.1.2 Smoke Visualization

Videos were taken of tracer gas injection behavior during different beverage cart events. This video shows an injection at seat 9F during a 0.43 m/s cart traverse with smoke added in-line to the standard injection flow rate. Notice the injection flow pattern only remains steady for short periods of time due to cabin air movement even when no cart movement is present.

6.2 Uncertainty Analysis

Using large numbers of instruments simultaneously to conduct tests and collect experimental data, it is expected that experimental uncertainties propagate error throughout measurements and into calculated results. To estimate the overall uncertainty in experimental results, each subsystem of the experimental setup will be examined individually. Equipment controlling tracer gas injection, air conditioning and supply, and carbon dioxide sampling will be analyzed separately and then combined to estimate an uncertainty for overall experimental readings.

6.2.1 Calibration Methods

The NDIR CO_2 analyzers used allow for calibration using a zero concentration and concentration span gas. Using this method the analyzers have an accuracy of $\pm 2\%$ of full range, but tend to drift an additional $\pm 2\%$ over 12 months. To alleviate concerns with drifting and to enable a calibration data trail it was decided to forgo the onboard calibration in favor of software linear regression via calibration gases spanning the used sampling range. Additionally, the uncertainty is reduced because the repeatability of the analyzers is $\pm 0.3\%$ at zero and $\pm 1.5\%$ at span. This allows for an uncertainty value of around 0.6% when a sampling range of 500 ppm CO_2 is used. To eliminate issues with instrument drift, the analyzers are calibrated biweekly.

For calibration, the analyzers were left in original configuration, but the normal sampling line was plumbed to calibration gas of known concentration. Calibration gas of 490, 1000, and 2000 ppm CO_2 concentration was used for each analyzer. The data acquisition program used for tracer gas experimentation was modified to read output voltage of each analyzer while sampling calibration gas once every two seconds, for a total of twenty readings per calibration gas concentration. These readings were averaged and the three resultant data points for each analyzer were stored in a calibration data file for later linear regression by software during the data analysis procedure.

A custom made water manometer, as shown in Figure 6.1, was built to finely regulate the pressure of the calibration gas. The pressure supplied to the monometer was controlled via a pressure regulator on the gas cylinder to as little positive pressure which was steadily achievable.

This ensures no air is pulled in the sampling line by the vacuum pump but any excess pressure would alter the calibration reading due to density and ideal gas principles.

Figure 6.1 Custom Manometer for CO2 Analyzer Calibration

6.2.2 Measurement Uncertainty Analysis

The uncertainty associated with each instrument used to control ventilation flow or tracer gas injection, as well as sampling instruments, is calculated separately in the following sections.

6.2.2.1 Gas Uncertainty

The various gases used throughout experimentation each carry uncertainty values which affect the uncertainty of the overall tracer gas measurement. The carbon dioxide used was labeled "Industrial Grade" and, therefore, noted as 99.5% pure CO_2. To avoid injecting a quantity of gas with unknown constituent makeup, "High Purity" helium, with a stated purity of 99.997%, was used.

Calibration gases were not used directly in tracer gas sampling, but their accuracy is paramount to the accuracy of the tracer gas concentration readings during experimental runs. Table 6.1 lists the uncertainties for the three calibration gases as well as the CO_2 and He used for tracer gas injections. Using the root means squared error method, the uncertainties of the calibration gases are summed in Equation (6.1) to create a total calibration uncertainty value. This value is later incorporated in the overall tracer gas measurement uncertainty.

Table 6.1 Tracer Gas Uncertainty

Gas	Uncertainty
CO_2	99.5% pure
He	99.997% pure
490 ppm CO_2 Calibration	2%
1000 ppm CO_2 Calibration	1%
2000 ppm CO_2 Calibration	1%

$$U_{calib} = \sqrt{U_{490}^2 + U_{1000}^2 + U_{2000}^2} = 2.45\% \tag{6.1}$$

6.2.2.2 Injection Uncertainty

It is important to note that, similar to the CO_2 analyzers, the mass flow controllers have an accuracy of 1.0% full scale, but the repeatability is 0.2%. Since the experimental measurements are solely used to compare to one another once normalized, the repeatability rating was used rather than accuracy. Table 6.2 lists several uncertainty specifications for each of the mass flow controllers used as well as the corresponding interface unit.

73

Table 6.2 Tracer Gas Injection Uncertainty

Equipment	Uncertainty	Rated Flow
CO₂ Controller	1.0% F.S. (accuracy)	100 SLM
	0.2% F.S. (repeatability)	
	0.1% F.S. (resolution)	
	15 to 40 °C (operation)	
He Controller	1.0% F.S. (accuracy)	10,000 SCCM
	0.2% F.S. (repeatability)	
	0.1% F.S. (resolution)	
	0 to 50 °C (operation)	
PR4000 (Controller/Indicator)	16-Bit	-

Values from Table 6.2 are incorporated with values from Table 6.1 to from the uncertainty values for the injections of CO_2 and He in Equation (6.2) and Equation (6.3), respectively. To calculate the relative uncertainty due to repeatability the injection rates of 7.00 and 4.22 lpm are used for the CO_2 and He, respectively. The uncertainty due to the 16-Bit analog/digital converter is so small in comparison to the flow controller uncertainty, it is negated.

$$U_{CO_2} = \sqrt{U_{acc}^2 + U_{pure}^2} = \sqrt{2.86\%^2 + 0.5\%^2} = 2.90\% \tag{6.2}$$

$$U_{He} = \sqrt{U_{acc}^2 + U_{purity}^2} = \sqrt{0.474\%^2 + 0.003\%^2} = 0.474\% \tag{6.3}$$

6.2.2.3 Air Supply Uncertainty

Calculating and controlling the supply airflow is handled by several instruments including two DAQ's, two pressure transducers, a flow meter and temperature sensors. Table 6.3 lists the uncertainty values for all of these components as well as the operating range used. The system was originally configured to use modules in the National Instruments Field Point system to interface and control all equipment. It was found VFD's controlling the blower and cart motor caused signal noise which could not be filtered to significantly affect temperature readings. To

alleviate this problem, an Agilent 34970a DAQ was installed in tandem to handle all RTD temperature measurement.

Table 6.3 Air Supply Instrument Uncertainty

Equipment	Uncertainty	Range
Agilent 34970a DAQ	0.06 °C (RTD)	49 Ω to 2.1 kΩ
	0.003 °C Temperature Coefficient	0-18 °C, 28‑55 °C (environment)
NI Filed Point AI-110	0.07% of reading + 0.007% of range	0 to 5V
PCI FE-1500 Flow Meter	2%	100 to 10,000 fpm
Omega PX653	0.25% F.S.	1" WC
	0.05% F.S. repeatability	0 to 5V
Temperature RTD	0.42 °C	0 to 100 °C

Because ideal gas law is used to form the correlation between air temperature and density, the uncertainty in the temperature is important for calculating ventilation flow rate. Equation (6.4) shows the calculation of the temperature uncertainty at the standard supply temperature of 15.6 °C (288.75 K). The absolute temperature in Kelvin is used to calculate the relative uncertainty. The DAQ units for the air supply are located out of the cabin enclosure and can be exposed to temperatures as low as 10 °C. Therefore a temperature correction of 8 °C outside the standard operating range is needed.

$$U_{temp} = \sqrt{U_{RTD}^2 + U_{DAQ}^2} = \sqrt{0.145\%^2 + 0.0291\%^2} = 0.148\% \qquad \textbf{(6.4)}$$

To sample the supply airflow velocity a Paragon Controls Incorporated FE-1500 FX duct mounted airflow measurement station is used in conjunction with Omega FX635 pressure transducers connected to the National Instruments Field Point AI-110 (Analog In) module. The observed velocity (~5 m/s) by the airflow measurement station generates a differential pressure translated to an excitation voltage reading of around 3.5V by the pressure transducer. The uncertainty value for the voltage reading by the National Instruments unit is found to be 0.0800%.

The repeatability value for the pressure transducer is used over the accuracy value because the unit was fully calibrated in an ASME flow chamber prior to being installed. Utilizing the

Engineering Reference Table by Paragon Controls, the measurement station should produce 1.58 mm water column at a supply velocity of 5 m/s. This yields a relative uncertainty of 0.803% for the pressure transducer in the range used during experimentation.

A stated uncertainty value of 2% for the duct mounted flow station is also incorporated the pressure uncertainty value calculated in Equations (6.5) and (6.6). This uncertainty value is to account for inaccuracies due to velocity profile averaging across the pressure sensing elements in the duct.

$$U_{press} = \sqrt{U_{PCI}^2 + U_{NI}^2 + U_{Omega}^2} \qquad (6.5)$$

$$U_{press} = \sqrt{2\%^2 + 0.08\%^2 + 0.803\%^2} = 2.16\% \qquad (6.6)$$

Using the root means squared method the uncertainty of the ventilation airflow rate is calculated in Equation (6.7). Using the Bernoulli Equation, pressure is related to the square of velocity. The ideal gas law is solved for density and substituted into the Bernoulli Equation for calculation of velocity. Since pressure and temperature are the measured entities, but the airflow rate, and therefore velocity in the Bernoulli Equation, is the value of interest, the uncertainty of the pressure and temperature measurement are halved before being squared using the principle of partial derivatives. (Coleman & Steele, 1989)

$$U_{vent} = \sqrt{(\tfrac{1}{2}U_{press})^2 + (\tfrac{1}{2}U_{temp})^2} = 1.08\% \qquad (6.7)$$

Note an additional atmospheric pressure term is utilized in the cabin air supply program calculation of the air density for Bernoulli Equation and ideal gas law. This term is manually taken from local weather reports and, therefore has a small unknown uncertainty value associated.

6.2.2.4 Sampling Uncertainty

The three Carbon dioxide analyzers used in experimentation were installed at different times and are similar, but slightly different models. It is important to note when calculating uncertainties, the Gascard NG has an output voltage which extends beyond the 1V range of the DAQ and,

therefore, the 10V range was required. The Gascard NG analyzer was used to measure the inlet air CO_2 concentration. The NOVA and Gascard II analyzers, used to measure sample location of interest and exit concentration, respectively, are used with a 1V DAQ range. Table 6.4 lists the uncertainty value for each of the CO_2 analyzers as well as the required ranges of the DAQ. The Agilent DAQ used for these measurements was located in the chamber enclosure hallway where ventilation air with added heat from the thermal manikins maintained an environmental temperature above 18 °C, so no temperature correction is needed.

Table 6.4 CO$_2$ Analyzer Measurement Uncertainty

Model	Uncertainty	Range
Edinburgh Gascard NG	2% of range (accuracy)	0 to 3000 ppm
	0.3% @ zero 1.5% @span (repeatability)	
Edinburgh Gascard II	2% of range (accuracy)	0 to 3000 ppm
	0.3% @ zero 1.5% @span (repeatability)	
NOVA Analytical 420	50 ppm (accuracy)	0 to 5000 ppm
	0.3% @ zero 1.5% @span (repeatability)	
Agilent 34970a DAQ	0.0040% of reading + 0.0007% of range	1V
	0.0035% of reading + 0.0005% of range	10V

To tabulate uncertainty levels for instrument readings which change throughout experimentation, a value was chosen which represents the least accurate case and applied to all scenarios. The representative CO_2 concentrations and corresponding voltages are summarized in Table 6.5. These values represent a situation where the sampled location receives negligible steady state tracer gas concentrations. This scenario amplifies the importance of instrument accuracy because the sample reading is very close to the environmental CO_2 level being factored out.

Table 6.5 CO$_2$ Analyzer Representative Sample for Uncertainty Calculation

Model	Location	Sample Reading	Voltage
Edinburgh Gascard NG	Inlet	378 ppm	0.516203 V
Edinburgh Gascard II	Outlet	597 ppm	0.366473 V
NOVA Analytical 420	Inside Cabin	384 ppm	0.243481 V

Due to the highly linear nature of these analyzers, the repeatability for the sampling range of interest is taken as a linear interpolation of the zero and span repeatability values for that

particular instrument. These calculated repeatability values are listed for each instrument in Table 6.6. The table also lists a calibration data set r-squared average linearity value for each of the instruments. The details of this calculation can be found in

Table 6.7, where the linearity of each individual calibration data set is calculated and then averaged to a single value per instrument.

Table 6.6 CO2 Analyzer Repeatability and Calibration Linearity

Location	Repeatability	Linearity
Inlet	0.451%	0.0250%
Outlet	0.539%	0.0224%
Inside Cabin	0.392%	0.3629%

Table 6.7 Calibration R-Squared Values

Calibration Date	Inlet	Outlet	Inside
4/21/2010	0.999627	0.999478	0.999962
5/27/2010	0.999309	0.999995	0.985594
6/9/2010	0.999982	0.999978	0.999998
7/8/2010	0.999799	0.999956	1.000000
8/10/2010	0.999676	0.999995	0.999503
10/26/2010	0.999996	0.999517	0.999999
2/22/2010	0.999863	0.999517	0.989542
Average	0.999750	0.999776	0.996371

Equations (6.8) through (6.13) show the calculation of the root means squared error for each of the analyzers using previously calculated uncertainties as well as an associated DAQ uncertainty.

$$U_{inlet} = \sqrt{U_{repeat}^2 + U_{calib}^2 + U_{linear}^2 + U_{DAQ,10V}^2} \tag{6.8}$$

$$U_{inlet} = \sqrt{0.451\%^2 + 2.45\%^2 + 0.0250\%^2 + 0.0132\%^2} = 2.49\% \tag{6.9}$$

$$U_{outlet} = \sqrt{U_{repeat}^2 + U_{calib}^2 + U_{linear}^2 + U_{DAQ,1V}^2} \tag{6.10}$$

$$U_{outlet} = \sqrt{0.539\%^2 + 2.45\%^2 + 0.0224\%^2 + 0.00591^2} = 2.51\% \qquad \text{(6.11)}$$

$$U_{NOVA} = \sqrt{U_{repeat}^2 + U_{calib}^2 + U_{linear}^2 + U_{DAQ,1V}^2} \qquad \text{(6.12)}$$

$$U_{NOVA} = \sqrt{0.392\%^2 + 2.45\%^2 + 0.3629\%^2 + 0.00688\%^2} = 2.51\% \qquad \text{(6.13)}$$

6.2.2.5 Overall Measurement Uncertainty

All previously calculated uncertainty values are summed, using Equation (5.2), into a total measurement uncertainty value for the normalized measurements of the entire experiment. This method was selected over other statistical analyses due to the very small size of the sample population. Presenting an uncertainty value for the measurements is more meaningful than presenting the large confidence interval for the sample in question. Equation (6.14) represents this uncertainty level on a relative basis using the root means squared method of partial derivatives. Note the subscript from Equation (5.2) $measured$ is now $NOVA$, $tracer\ gas$ is now $CO2$, and $vent.air$ is now $vent$.

$$U_N^2 = \left(\frac{\partial N}{\partial C_{NOVA}} U_{NOVA}\right)^2 + \left(\frac{\partial N}{\partial C_{inlet}} U_{inlet}\right)^2 + \left(\frac{\partial N}{\partial V_{CO_2}} U_{CO_2}\right)^2$$
$$+ \left(\frac{\partial N}{\partial V_{vent}} U_{vent}\right)^2 \qquad \text{(6.14)}$$

Each of the partial derivatives in Equation (6.14) is evaluated in Equations (6.15) through (6.18).

$$\frac{\partial N}{\partial C_{NOVA}} = \frac{V_{vent}}{V_{CO_2}} \qquad \text{(6.15)}$$

$$\frac{\partial N}{\partial C_{inlet}} = -\frac{V_{vent}}{V_{CO_2}} \qquad \text{(6.16)}$$

$$\frac{\partial N}{\partial V_{CO_2}} = -\frac{V_{vent}(C_{NOVA} - C_{inlet})}{V_{CO_2}^2} \qquad \text{(6.17)}$$

$$\frac{\partial N}{\partial V_{vent}} = \frac{C_{NOVA} - C_{inlet}}{V_{CO_2}} \tag{6.18}$$

Substituting the Equations (6.15) through (6.18) into Equation (6.14) and dividing the entire expression by N to put the uncertainty of the normalized values in percentage terms yields Equation (6.19).

$$\frac{U_N^2}{N} = \left(\frac{U_{NOVA}}{C_{NOVA} - C_{inlet}}\right)^2 + \left(\frac{U_{inlet}}{C_{NOVA} - C_{inlet}}\right)^2 + \left(\frac{U_{CO_2}}{V_{CO_2}}\right)^2 + \left(\frac{U_{vent}}{V_{vent}}\right)^2 \tag{6.19}$$

Solving for U_N and noting uncertainty is most useful on a percentage basis as well as the fact that that U_{CO2} and U_{vent} have already been calculated on a percentage basis, Equation (6.20) is formed. The uncertainty value is put in terms of percentage because the normalized value has less tangible meaning than percentage. The first two terms under the radical are calculated using sample reading values form Table 6.5 and uncertainties from Equations (6.9) and (6.13).

$$U_{norm} = \sqrt{\left(\frac{U_{NOVA}}{C_{NOVA} - C_{inlet}}\right)^2 + \left(\frac{U_{inlet}}{C_{NOVA} - C_{inlet}}\right)^2 + U_{CO_2}^2 + U_{vent}^2} \tag{6.20}$$

$$U_{norm} = \sqrt{\left(\frac{9.6}{384 - 378} \times 100\%\right)^2 + \left(\frac{9.4}{384 - 378} \times 100\%\right)^2 + 2.90\%^2 + 1.08\%^2} \tag{6.21}$$

$$U_{norm} = 224\% \tag{6.22}$$

This value appears very alarming, but it is important to remember this is a worst case scenario. Nearly all of the uncertainty comes from the fact the sampled tracer gas level is only marginally greater than the environmental level of CO_2. Dividing by this small concentration difference, even for an absolute reading uncertainty of 10 ppm, creates a relative uncertainty of over 200%. For an uncertainty reading more relevant to the majority of data, a similar process is performed in the forward area of the E column of seats. More experimental data was gathered here because this location produced the most interesting results. Table 6.8 presents updated representative concentration levels and associated repeatability and voltage readings.

Table 6.8 Updated CO2 Analyzer Repeatability and Calibration Linearity

Location	Reading	Repeatability	Voltage
Inlet	411	0.464%	0.678677
Inside Cabin	446	0.478%	0.250639

With the new repeatability and voltage readings, Equations (6.8) and (6.12) are replaced with Equations (6.23) and (6.24), respectively.

$$U_{inlet} = \sqrt{0.464\%^2 + 2.45\%^2 + 0.0250\%^2 + 0.0109\%^2} = 2.49\% \tag{6.23}$$

$$U_{NOVA} = \sqrt{0.478\%^2 + 2.45\%^2 + 0.3629\%^2 + 0.0234\%^2} = 2.52\% \tag{6.24}$$

Substituting values from Table 6.8 and Equations (6.23) and (6.24) the updated normalized measurement uncertainty for seat location 4E is shown in Equation (6.26).

$$U_{norm} = \sqrt{\left(\frac{11.2}{446-411} \times 100\%\right)^2 + \left(\frac{10.2}{446-411} \times 100\%\right)^2 + 2.90\%^2 + 1.08\%^2} \tag{6.25}$$

$$U_{norm} = 43.5\% \tag{6.26}$$

This uncertainty value is much more reasonable. Obviously, the uncertainty level will differ slightly from experimental run to run and between seat locations, but this value is representative of a reasonable area around this seat location (4E). The uncertainty value for each normalized reading will generally decrease the closer the sample location is to the injection because the steady state concentration will increase while the inlet environmental concentration remains constant. For this particular tracer gas injection rate, the concentration levels are too low to provide data with much meaning when far from the injection location. Though the uncertainty levels may negate results in the southeast corner of the cabin, the observed values generally adhere to more well behaved, perceivable levels as seen in Figure 5.37.

6.2.3 Statistical Analysis

In addition to stating uncertainty levels, it is important to provide statistical analysis for the data collected. Statistical analysis should be used in context for all data reported in this study since

each sample size is small (three repetitions for all but one group of seat locations which had six). Just as in the previous section, representative locations throughout the cabin are examined so results can be generalized without a need to calculate values for every seat location sampled.

To evaluate a standard deviation for the representative seat locations, a method similar to the one used in the latter half of Section 5.5 is used. A single value average is taken for runs with and without the cart for each experimental run in a particular seat location. The standard deviation of these values was taken separately for runs with and without the cart. Typical standard deviation values ranged from 10 to 50%, but were generally less than 30%. The forward seats of column E, where a larger sample size (six runs) was available, had a standard deviation of less than 25%. The statistical analysis generally agrees with uncertainty values, but it many cases may exceed the uncertainty value. It is important to note the standard deviation would need to be doubled to form a 95% confidence interval, assuming the data has a normal distribution.

Erratic airflow and experimental anomalies are responsible for any discrepancy between uncertainty values and statistical analysis. Discrepancies can also be attributed to other phenomena such as quasi-steady state eddies and other cabin airflow behavior, which cannot be understood simply from this experimental data. It is important, however, to stress the sample size of this study was extremely small so statistically sound data cannot be expected even if experiments were highly predictable.

Increasing the statistical sample size improves the accuracy of the reading, as would be expected. Completing only six experimental runs is not sufficient to statistically verify these results with any degree of certainty for numerical values. To use the numerical data in this study it would be recommended to complete many more experimental repetitions.

Chapter 7 - Summary and Conclusions

As can be seen in the data presented in Chapter 5 - , the beverage cart movement clearly has an effect on tracer gas concentrations in particular locations throughout the cabin. The extent to which this effect could actually transmit a biological or chemical contaminate from one passenger to another is beyond the scope of this paper, but the data clearly shows the transport is a measurable level. Measurable, however, may not be practical in whole-cabin analysis as the peak effect due to cart movement is generally equivalent to the steady state contamination level one row nearer the contamination source in the same column of seats.

The airflow pattern appears to generally hold true to design and essentially evacuate contamination within two rows of the source. However, tangible traces of contamination could be sampled throughout the entire sample area, but effects decayed to marginal levels within five to six rows of the source in aisle seats. As would be expected, seat locations lining either side of the aisle were affected the most by a moving body in that aisle.

Only having a test sample of three leaves the confidence interval of the measurements very broad. This can be further exemplified by examining data from individual test runs for a single seat location located in the electronic appendix. The measurement range of similar run-to-run experiments, in some cases, varies more than the average between runs with and without the cart for the same seat location. Realizing the run-to-run variation can be so large puts the results of these experiments in perspective, but it is important to remember the general consensus for seat locations near the aisle is an increase of up to 10% for readings during compared to before and after the cart movement effect. In real world transportation scenarios this could be an important design scenario to account for.

It would be recommended these studies be used qualitatively for feasibility of transport phenomenon, but using this data numerically to any degree of precision would require building a much more statistically robust data set. It is also important to note, the wake creation in this study examines a worst case scenario in regards to profile area (beverage cart and manikin) and movement speed. The regular cart traverse speed (0.43 m/s) would be fairly quick for a flight attendant to sustain while navigating any meaningful length of the aisle. Additionally, the fast

cart movement speed would be more likely to occur when a passenger was moving the length of the aisle while not laden with a beverage cart and, thus, have a slightly decreased profile.

Chapter 8 - Recommendations

Tying into the statistical analysis of the data, it would be recommended to continue similar experimental tests to solidify the data set for numerical use. The same experimental setup could be used, but it would be beneficial to conduct each experiment many more times.

Additionally, it would also be beneficial to conduct similar experiments utilizing more accurate carbon dioxide analyzers and tracer gas flow controllers. Another, potentially more advantageous option would be to simply increase the tracer gas injection rate. This would effectively reduce the uncertainty the sampling equipment. The steady state CO_2 concentration would also be increased throughout the test cabin so factoring out environmental effects would have less of an impact on uncertainty. In several locations during this phase of experimentation, the tracer gas concentration sampled was so low the normalized value became negative due to instrument inaccuracies.

Studies could also be conducted to determine how far down the cabin aisle the wake effect of a beverage cart could be stretched. This would require running similar tracer gas studies in an elongated version of this eleven row mockup or, ideally, an actual fuselage from a wide-body aircraft with more of the actual ventilation system intact.

References

Air Transportation Center of Excellence (CoE) for Airliner Cabin Environment Research (ACER). (2007). *Transport Project.*

ASHRAE. (2005). *ASHRAE Handbook of Fundamentals.* American Society of Heating Refrigerating and Air-Conditioning Engineers.

ASHRAE. (2007). Aircraft. In *2007 ASHRAE Handbook.* Atlanta: American Society of Heating Refrigerating and Air-Conditioning Engineers.

Beneke, J. (2010). *Small Diameter Particle Dispersion in a Commerical Aircraft Cabin.* Kansas State University, Manhattan.

Bureau of Transportation Statistics. (2011). *2010 Traffic Data for U.S Airlines and Foreign Airlines U.S. Flights.* Washington D.C.: U.S. Department of Transportation.

Coleman, H. W., & Steele, W. (1989). *Experimentation and Uncertainty Analysis for Engineers.* New York: John Wiley & Sons.

Etheridge, D., & Sandberg, M. (1996). *Building Ventilation:Theory and Measurement.* New York: John Wiley & Sons.

FAA. (2008). *Draft Final Technical Report, Contaminant Transport in Airliner Cabin.* Kansas State University. Manhattan: FAA Cooperative Agreement 04-C-ACE-KSU, Institute for Environmental Research.

Frodl, R., & Tille, T. (2006, December). A High-Precision NDIR CO_2 Gas Sensor for Automotive Applications. *IEEE Sensors Journal*, 1697-1705.

Gerencher, C. L. (2010). Research on the Transmission of Disease in Airports and on Aircraft. *Summary of a Symposium. 47*, pp. 15-35. Washington, D.C.: Transportation Research Board of the National Academies.

Kohsiek, W. (2000). *Water Vapor Cross-Sensitivity of Open Path H2O/CO2 Sensors.* Royal Netherlands Meteorological Institute. De Bilt, Netherlands: American Meteorological Society.

Lebbin, P. (2006). *Experimental and Numerical Analysis of Air, Tracer Gas, and Particulate Movement in a Large Eddy Simulation Chamber.* Kansas State University, Manhattan.

Miró, C. R., & Cox, J. (2000, September). Evaluating Aircraft Air Cabin Quality. *ASHRAE Journal*, 12.

O'Donnell A., D. G. (1991, April). Air quality, ventilation, temperature, and humidity in aircraft. *ASHRAE Journal*, 42.

Olsen, H., & Willson, M. (2002, July). Development of the tracer gas method for large bore natural gas engines--Part I:Method Validation. *Journal of Engineering for Gas Turbines and Power, 124*, 678-685.

Padilla, A. (2006). *Experimental Analysis of Particulate Movement in a Large Eddy Simulation Chamber.* Kansas State University, Manhattan.

Shehadi, M. (2010). *Experimental Investigation of Optimal Particulate Sensor Location in an Aircraft Cabin.* Kansas State University, Manhattan.

Shin, H.-S., Lee, l.-K., Ahn, Y.-C., & Yeo, C.-S. (2005). Measurement of Indoor Air Quality for Ventilation with the Existence of Occupants in Schools. *Journal of Mechanical Science and Technology, 19*(4), 1001-1005.

Thibeault, C. (2002, April-June). Airliner Cabin Air Quality. *Occupational Medicine, 17*(2), 279-292.

United Kingdom Accreditation Service. (2007). *The Expression of Uncertainty and Confidence in Measurement.* Feltham: United Kingdom Accreditation Service.

United States Environmental Protection Agency. (2000). *Carbon Dioxide as a Fire Suppressant: Examining the Risks.*

Walkinshaw, D. S. (2010, April). Germs, Flying, and the Truth. *ASHRAE Journal*, 70-73.

Zhang, Y., & Sun, Y. (2005). Experimental Characterization of Airflow in Aircraft Cabins. *ASHRAE Transactions*, *111*, pp. 45-59.

Appendix A - Instrumentation Errors

As in any experimental research, the quality of the results is only as accurate as the precision of the experimenter and instruments used to take measurements. Instrumentation error was an issue which plagued this research from the onset.

A.1 - VFD Noise

Originally, the temperature readings for the cabin air supply program were handled by an FP-RTD-122 module in the National Instruments Field Point system. Since RTD measurements are achieved by measuring the change in resistance of a circuit, a small current needs to be induced on circuit to acquire the resistance measurement. Therefore, the measurement is highly susceptible to stray voltage spikes emanating from other equipment in the experimental facility.

Variable Frequency Drives are used in three locations throughout this experimental setup as well as several additional locations in the same laboratory facility for other experimentation. By design, VFD's constantly adjust the output voltage in attempt to match the AC voltage sine wave at the desired frequency to drive the electric motor. The actual supply voltage provided to the equipment oscillates much more rapidly above and below the AC wave attempting to be achieved. This, in turn, emits very high frequency noise in all electrical circuits in the laboratory facility.

It was discovered the activation of VFD's controlling the air supply and conditioning system caused a shift of up to 10 °C in RTD temperature readings. After supplemental electrical grounding was added to all of these controllers and motors, the temperature signals were still disturbed by VFD operation. In an attempt alleviate this issue, a Rasmi RS 2020-V7 3-phase filter was added to the blower motor VFD as well as a Schaffner FN350-20-29 filter for the heating loop pump VFD. These filters were installed in-line between the VFD and respective motor. A SolaHD SLR-3H-480-3 line reactor, which uses inductive filtering, was also installed between the heating loop pump VFD and building power. Adding filters and a line reactor reduced the signal disturbance, but did not fully remedy the ailment.

After much trial and error, it was discovered the National Instruments Field Point DAQ was the primary culprit of temperature signal disturbance. The system was designed utilizing 50 and 60 Hz noise filters for measurements, but could not filter the high frequency noise generated by the VFDs. A simple solution, which removed all temperature disturbances, was found in switching RTD measurement duties to an Agilent 34970A DAQ unit. The Agilent unit uses a patented Multi-slope III analog-to-digital converter which calculates the measurement using an integration method rather than taking an instantaneous sample as the National Instruments unit did. The period of integration is programmable so it could be custom-tailored to cancel high frequency noise generated by the VFD controllers.

A.2 - Unreliable CO_2 Sampling

Another instrumentation issue which afflicted experimentation was the noise present in signals produced by the carbon dioxide analyzers. In the original configuration the NOVA analyzer handled measurements within the cabin mockup with an additional Gascard II analyzer for each the inlet and outlet CO_2 concentrations. The Gascard II used to sample cabin outlet concentrations was very finicky and would oftentimes produce no signal at all during experimentation.

It was decided to replace this analyzer, but the manufacturer updated the Gascard II model with the new Gascard NG. It was claimed to be a direct replacement, but the new model had a different voltage output range, which necessitated rewriting a bit of the data acquisition program. Once replaced and experimentation had begun again, the Gascard II unit sampling inlet air began generating unreliable results. These issues could be resolved temporarily by power cycling the unit, but would return not long after. Since the measurements generated from the new Gascard NG unit, sampling outlet concentration, were not used in the normalization function, these two analyzers were swapped before the majority of experimentation had been conducted. The Gascard II continued to function for the remainder of experimentation, but would randomly yield unpredictable results.

A.3 - CO$_2$ Analyzer Linear Offset

It was noticed during experimentation, occasionally, the CO$_2$ concentration reported by each of the analyzers did not match even when no tracer gas was being injected. In this situation all air in the system is 100% outdoor air and should have a uniform CO$_2$ concentration. This could not be corrected through recalibration as data remained very similar between calibration data sets for each instrument. It was decided to incorporate an offset to account for the difference in concentration the inlet analyzer and internal cabin analyzer exhibited for each experimental test. The NOVA analyzer was chosen for the base reading because it was the most reliable throughout the entirety of experimentation.

The highly linear nature of the CO$_2$ analyzers allows this offset to be a single concentration value added to each reading from the inlet analyzer. The offset is calculated from measurements recorded during the pre-test scans phase of the experimental procedure outlined in Table 4.1 and Table 4.2. The offset value is calculated while the data is being analyzed in spreadsheet format, after having concentrations calculated using linear regression. Spreadsheets for each run include a "Calibration" tab which houses information about the calibration data, testing date, as well as the calculated linear offset.

The original data acquisition program was set to only record 12 pre-test scans during the first minute of each experiment. Once it was decided an offset value needed to be calculated from these results, this period was extended to 144 scans over 12 minutes since the inlet CO$_2$ analyzer produced fairly noisy readings. The total number of readings available for each the inlet and NOVA analyzers are averaged before the difference is figured for each experimental run.

Appendix B - Guide to Electronic Appendix

The electronic appendix includes data for each experimental run conducted during this study and is located in a file called "Electronic Appendix.zip" included with this thesis. It would be advised to extract this entire archive locally as spreadsheets which summarize data from multiple experimental runs link to the spreadsheets for each respective run. The root folder includes subfolders labeled "7F" and "9F," which correspond to the location of the injection during those experiments. Each of those has subfolders for tests with and without the cart traverse. The "Cart" folder in "9F" has an additional folder for the fast cart movement.

Under each of these folders are subfolders containing results for the Averaged and Transient Inlet data calculation methods. The other folders labeled with seat column names contain the raw data recorded by the data acquisition program. These files use a naming convention similar to (seat column)(1 for front 4 rows or 2 for back four rows of sample).(test run number)-(sampling tree port).xlsx. It may be counterintuitive, but the sampling tree orientation is swapped when sampling the forward and rear four rows of the sample due to physical constraints. Thus, the port locations for the front four rows are in reverse order of the seat location, i.e. file A1.1-1.xlsx corresponds to the first test run in seat location 4A and A1.1-4.xlsx would be for seat 1A. Similarly, A2.3-1.xlsx would be for the third test run in seat 5A and A2.3-4.xlsx for 8A.

Under the folders labeled "Averaged Inlet" and "Transient Inlet" are the analyzed results for each test run per group of four seats. These files use the naming convention (seat locations sampled).(test run number).xlsx. Filenames not including a test run number suffix are the average of all available test runs for the named seat locations.